水研センター研報，第23号，11－90，平成20年
Bull. Fish. Res. Agen. No. 23, 11-90, 2008

博士号論文

A numerical study on the intrusion of Kuroshio water onto the continental shelf of the East China Sea[*1]

Joon-Soo Lee[*2]

Abstract: The Kuroshio, which flows into the East China Sea (ECS) through the east of Taiwan, runs along the continental shelf break, and significantly affects the characteristics of the ECS water in terms of the exchange of heat, salt and nutrients.

The main objectives of this study are to evaluate the contribution of the Kuroshio onto the ECS shelf, and to reveal the possible mechanism of the Kuroshio intrusion. In order to investigate the seasonal pattern of the intrusion from the Kuroshio and the behavior of the intruded Kuroshio water, numerical simulation and passive tracer experiment were executed using RIAM Ocean Model (RIAMOM), which is a 3-dimensional, primitive equation model with a free surface. For the realistic simulation of the ECS circulation, tide effect was considered by parameterization of the M_2 tide, enhancing the background turbulence as vertical eddy diffusivity and viscosity, and increasing the bottom friction where the tidal current is strong.

Preliminary experiment, which released tracers in the Taiwan Strait and east of Taiwan, showed the tracer from the Taiwan Strait was mainly confined at the surface layer shallower than 80 m in summer and water mass originated from the Kuroshio occupied the lower layer. Based on the vertical profile of the tracer, two vertical sections along the 200 m isobath line were determined for the release of tracers: 0～80 m and 80～200 m.

Passive tracer experiment confirmed the region of the main intrusion from the Kuroshio as indicated by previous studies: northeast of Taiwan and west of Kyushu. The total intruded volume transport across the 200 m isobath line was evaluated as 2.74 Sv in winter and 2.47 Sv in summer, while the intruded transport below 80 m was estimated to be 1.32 Sv in winter and 1.64 Sv in summer. The tracer experiments revealed that the east of Taiwan (122 ～ 123°E) is the main entrance of the Kuroshio intrusion onto the ECS shelf, and the intrusion from the Kuroshio to the central part of the shelf area, shallower than 80 m, takes place mainly through the lower layer northeast of Taiwan in summer as well, with a volume transport of 0.19 Sv.

Comparative studies showed several components affecting the intrusion of the Kuroshio across the 200 m isobath line. The intrusion of Kuroshio water onto the shelf was less compared with a case without consideration of tide-induced bottom friction, especially northeast of Taiwan. The variations of the transport from the Taiwan Strait and the east of Taiwan have considerable effects on the intrusion of the Kuroshio onto the shelf.

Momentum balance analysis along 122.58°E northeast of Taiwan, where the Kuroshio mainly intruded onto the shelf area of the ECS, showed that just north of Taiwan it was highly dominated by a geostrophic balance corresponding to surface elevation. In summer, while the northeastward strong current originated from the Taiwan Strait in geostophic balance passes north of 28°N, northward current occurs in the balance of the geostrophic com-

2007年12月10日受理 (Received on December 10, 2007)
[*1] 九州大学審査学位論文（掲載に際し投稿規程に沿って一部修正した）
[*2] 中央水産研究所　〒236-8648　神奈川県横浜市金沢区福浦2-12-4 (National Research Institute of Fisheries Science, 2-12-4, Fukuura, Kanazawa, Yokohama 236-8648, Japan)

ponents and the vertical friction component near the bottom. The northward current at the bottom layer north of 28°N induces the characteristic intrusion of the Kuroshio water onto the shelf area shallower than 80 m.

The passive tracer experiments and the momentum balance analysis revealed that upper water of the Taiwan Warm Current (TWC) is originated from the Taiwan Strait, while deep water of the TWC is derived from the east of Taiwan by means of the bottom Ekman layer flow.

Residence time in the Yellow Sea was estimated in both cases with and without consideration of tide effect by the tracer experiments which released the tracer at the inflow open boundaries. In the case with consideration of tide, the residence time was 5.3 years and 4.7 years for inclusion and exclusion of the Bohai Sea, respectively. Meanwhile, in the case without consideration of tide, the results showed remarkable decrease of the residence time to be 2.6 years and 1.7 years, respectively. The results emphasize that the consideration of tide effect is indispensable to the numerical simulation in the Yellow and East China Seas.

Keywords: intrusion of Kuroshio water, East China Sea, outflow from the Taiwan Strait, tide parameterization, bottom Ekman layer flow

---

Contents

Chapter 1. Introduction

The East China Sea (ECS) is a marginal sea, surrounded by Korea, Japan, China, and Taiwan. The ECS has a vast continental shelf and is bordered by the Okinawa Trough with a maximum depth exceeding 2000 m (Fig. 1.1). The cold, fresh shelf water is distributed on the continental shelf, and the warm, saline Kuroshio water occupies the area around the shelf water.

The most dominant current in ECS, the Kuroshio,

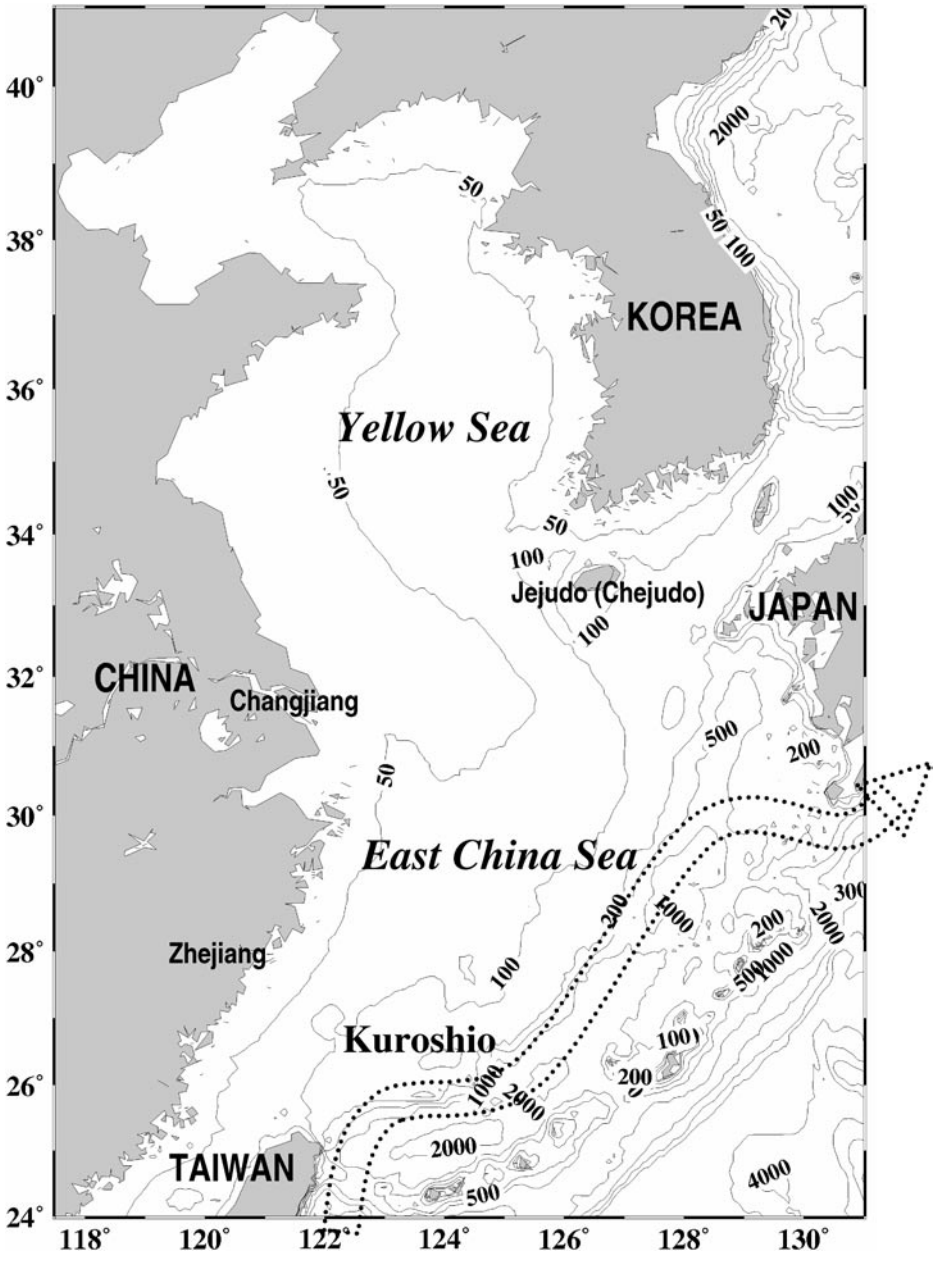

Fig. 1.1 Bathymetry of the Yellow and East China Seas and path of the Kuroshio. (pp.1)

is one of the major western boundary currents in the world ocean, and is defined as a distinct current from just north of the place where the North Equatorial Current is separated into two branches offshore east of the Philippines to the east of Japan where the current veers away from land (Nitani, 1972). The Kuroshio, which runs northward along the east coast of the Luzon and Taiwan, enters the ECS at the northeast of Taiwan, turns eastward by the steep topography along the continental shelf break of ECS, and flows out through the Tokara Strait. In this procedure, which the Kuroshio flows into the ECS and runs along the continental shelf break, the characteristics of the ECS water are greatly affected by the exchange of heat, salt, and nutrients between the Kuroshio water and the shelf water. For several decades, a lot of researchers have paid attentions to these roles of the Kuroshio on the ECS, and discussed actively about several issues such as origin of the Taiwan Warm Current and the Tsushima Warm Current, upwelling and intrusion of the Kuroshio, eddy motion, and generation of internal wave.

As a method to study the interaction between the Kuroshio water and the shelf water, in-situ observations have been widely used for a long time. Recently, satellite observations provide consistent global coverage of the ocean. However, the former has limitations of temporal and spatial resolutions, and the latter is basically confined to the surface. For this reason, numerical methods have come into use in recent years as a powerful and effective method to understand the overall system of the ocean, and several studies using numerical models have improved our understanding of the exchange process in the ECS. Seung (1999) considered the dynamics of the shelfward intrusion of the oceanic upper water using a simple geostrophic adjustment model. He found that the sea level difference moves the front shelfward through a barotropic effect, while the density difference increases the width of the front through a baroclinic effect. Recently, using a triply nested ocean model with a maximum resolution of 1/18°, Guo *et al.* (2003) explained the seasonal change of the veering latitude of the Kuroshio southwest of Kyushu by the JEBAR (joint effect of baroclinicity and bottom relief) term of the vorticity equation, which is the interaction between the baroclinicity and bottom topography. With the same model, Guo *et al.* (2006) evaluated the temporal and spatial variations of the Kuroshio onshore flux across the shelf break of the ECS in terms of a depth-averaged volume transport vector. They discussed the effect of the Ekman transport and the change in density field on the Kuroshio onshore flux. Isobe and Beardsley (2006) estimated the onshore cross-frontal transport at the shelf break of the ECS using the FVCOM (Finite Volume Coastal Ocean Model), which has finer resolution and resolves the complex bottom topography. They simulated frontal waves excited near the location where the bottom topography changes abruptly and also evaluated the onshore transport by passive tracer experiments, mainly focusing on the role of frontal waves.

In this study our major concern is shelfward net transport from the Kuroshio. Chen and Wang (1999) have already discussed the importance of the subsurface Kuroshio water as a nutrient source. The net transport along the 200 m isobath line, which was discussed by Guo *et al.* (2006), is significant for the volume transport budget itself. However, the shelfward net transport from the Kuroshio is important as a supply of nutrients for primary production from the viewpoint of the ecosystem.

In order to investigate the shelfward intruded Kuroshio water, numerical model experiments are executed for various cases, and the intrusion process from the Kuroshio onto the continental shelf of the ECS is examined. This study reveals a seasonally varying spatial intrusion pattern of the Kuroshio across the 200 m isobath line of the ECS and calculated the net volume transport of the shelfward Kuroshio water using passive tracer experiments. In addition, the Kuroshio branch current east of Taiwan is considered, which was not included in the numerical experiment of Isobe and Beardsley (2006). Furthermore, the tide effect is also examined. As a final step, mechanisms of the Kuroshio intrusion are discussed.

General descriptions about several major issues on the ECS are given in Chapter 2 as a background. Chapter 3 contains overall explanations about numerical model. A simple box model is also examined in Chapter 3 for error test of volume

transport estimation using passive tracer. Chapter 4 deals with the pattern of the Kuroshio intrusion by the numerical model experiment. The intrusion mechanisms of the Kuroshio onto the ECS shelf are described by means of the analysis of momentum balance and the case studies in Chapter 5. Finally, Chapter 6 summarizes the results of this study and concludes with further discussion for a future study.

Chapter 2. Background

2.1 Kuroshio Intrusion

As the Kuroshio flows northward along the eastern coast of Taiwan, it faces the steep topography northeast of Taiwan. The main axis of the Kuroshio turns to east along the shelf break, but some of it crosses the isobath line mainly at the upper layer. The Kuroshio intrusion northeast of Taiwan has long been reported by a lot of researchers (e.g., Mao *et al.*, 1964; Inoue *et al.*, 1975; Fan *et al.*, 1980; Chern and Wang, 1990; Chern *et al.*, 1990; Lin *et al.*, 1992; Liu *et al.*, 1992a; Liu *et al.*, 1992b; Hsueh *et al.*, 1992; Tang and Yang, 1993; Chuang and Liang, 1994). Especially, Liu *et al.* (1992b) confirmed the topography-induced upwelling of the Kuroshio subsurface water, and showed it to be a year-round upwelling.

Concerning the intrusion mechanism, using an idealized barotropic model, Chern and Wang (1990) explained that the thermal wind effect, associated with the strong upwelling along the shelf break, drives part of the nearshore Kuroshio subsurface water flows into the shelf area at north of Taiwan. In addition, analyzing the moored current meter data, they reported the existence of the Kuroshio intrusion below 60 m with strength about 10 ~ 20 cm/s both in summer and winter season, and proposed the Kuroshio intrusion as a major source of the cool and saline water above the southern ECS shelf.

Qiu and Imasato (1990) showed a schematic view of surface flow pattern in the ECS derived from the long-term GEK observations (1953~1984) and confirmed the Kuroshio intrusion as a branch current northeast of Taiwan. They further argued that the planetary beta effect and the existence of Taiwan Island are two indispensable conditions for the formation of the Kuroshio branch current, and the branch current is reinforced by topographic Rossby waves induced by the repeated crossing of the Kuroshio over the continental slope, executing several case studies of a barotropic potential vorticity equation model.

Liu *et al.* (1992a) suggested that the winter northeast monsoon induces the increase of potential energy near the shelf break due to the rise of isopycnal, so that the northward Kuroshio intrusion is intensified by releasing potential energy.

Unlike the intrusion mechanism by the Kuroshio itself, Chern and Wang (1992) suggested that the variation of the Kuroshio intrusion is closely correlated with the outflow from the Taiwan Strait. Based on the wind data and the hydrography observations over the Taiwan Strait and northeast of Taiwan on July and August 1988, they argued that the outflow from the strait has a strong influence on the spreading of the upwelled water.

Meanwhile, Chuang and Liang (1994) suggested that cooling rather than direct wind forcing may be the major cause for triggering the observed winter intrusion event, analyzing the observation results that one month after the wind pattern changed from southerly to northeasterly at mid-September 1992, the massive Kuroshio intrusion occurred at mid-October.

However, the past researches of the Kuroshio intrusion northeast of Taiwan were mainly confined to the southern ECS close to Taiwan, so that more studies are necessary about the effects over the whole ECS, the spreading patterns of the intruded water, the seasonal variations of the intrusion, and so on.

2.2 Taiwan Warm Current (TWC)

The TWC was named by Mao *et al.* (1964) because of its high temperature characteristics in winter compared with that of the southward coastal current. It flows to the north all the year round between the 50 m to 100 m isobaths, even during strong northerly winds in winter. (Su *et al.*, 1990; Guan, 1994)

Prior to the explanation about its origin, it needs to understand the current in the Taiwan Strait. Calculating the sea-level difference between Macao

and Takao (southwest of Taiwan), Wrytki (1961) explained that the monsoon is the primary force causing current variation due to the shallowness of the shelf and rather strong consistent winds in this area (from Chuang, 1986), southwestward in winter and northeastward in summer. However, direct current measurement in winter showed the existence of northward current against the northerly wind (Chung, 1985, 1986; Huang *et al.,* 1994; Guan, 1994; Liang *et al.,* 2003). Using long-term moored current meter, Chuang (1985, 1986) suggested that the permanent source exists at the southern end of the Taiwan Strait that drives the steady flow to the north regardless of season, and the northward mean flow is modulated by the seasonal wind field. Huang *et al.* (1994) explained that, in winter, the current is southwestward only in the western coastal region of the Taiwan Strait and in other regions the current is mainly northeastward, except under a strong northeasterly monsoon which makes the current at the upper layer turn southwestward temporarily. Recently, based on the shipboard Acoustic Doppler Current Profiler (sb-ADCP) measurements during 1991 ~ 2000, Liang *et al.* (2003) concluded that the currents in the Taiwan Strait flows primarily in a northward direction, except for the southward current near the coast of Mainland China.

Returning to the origin of the TWC, Mao *et al.* (1964) argued that the TWC is a Kuroshio branch originated from the northeast of Taiwan where the shelf intrusion by Kuroshio takes place by hydrographic studies. Inoue (1975) supported this concept by the bottom drifter observation at the north of Taiwan. However, after the observation of "against the wind" northward current in winter, TWC was recognized as a current from the Taiwan Strait. Beardsley *et al.* (1985) showed a schematic view of the TWC which runs out of the Taiwan Strait and flows northeastward toward the Korea/Tsushima Strait (K/T Strait) inshore of the Kuroshio. Further, Fang *et al.* (1991) argued the Taiwan-Tsushima-Tsugaru Warm Current System driven by the sea level difference.

On the other hand, Su *et al.* (1994) argued that the large scale pressure field impressed on the ECS by Kuroshio and shelf-intrusion of the Kuroshio are two main driving forces for the TWC. They showed distinct winter and summer patterns of TWC: In winter, a part of intruded Kuroshio mainly forms TWC, however in summer, the water from the Taiwan Strait occupies the upper layer and the Kuroshio subsurface water spreads over the southern ECS along the bottom layer. Recently, Zhu *et al.* (2004) suggested that the TWC in winter is originated from the Taiwan Strait as an episodic feature. On the contrary, Chen and Sheu (2006) reported that most of the TWC in wintertime originates in the Kuroshio, which moves onto the ECS shelf northeast of Taiwan.

After all, clear understanding about the variation of the current from the Taiwan Strait could be the key to elucidate the origin of TWC. When it comes to the throughflow transport in the Taiwan Strait, Wyrtki (1961) suggested it as ~ 1 Sv northward in summer and a little smaller than 1 Sv southward in winter, and Fang *et al.* (1991) estimated the transport as 1 Sv northward in winter and 3.1 Sv northward in summer. Hu *et al.* (2005) suggested 1.74 Sv in winter and 3.32 Sv in summer. In recent years, several researches using shipboard ADCP (sb-ADCP) or bottom-mounted ADCP (bm-ADCP) have provided more reliable results. Wang *et al.* (2003) estimated the volume transport from the empirical formula using the sb-ADCP for 2.5 years and the along-strait wind data. They suggested 0.9 Sv northward in winter and 2.7 Sv in summer. Teague *et al.* (2003) analyzed the currents observed by four bm-ADCPs in the Taiwan Strait from October to December in 1999, and concluded ~ 0.14 Sv in this winter season. Lin *et al.* (2005) showed the detailed variation in winter season using the same data with Teague *et al.* (2003). The transport varied from −5 to 2 Sv with a mean value of 0.12 ± 0.33 Sv. Jan *et al.* (2006) calculated the throughflow transports in January and February 2001 as −0.15 Sv and −0.03 Sv respectively by three bm-ADCPs, and in addition, May 1999, August 1999, March 2000 and June 2000 as 2.02, 2.34, 1.61 and 1.87 Sv respectively by sb-ADCP.

However, long term observations of throughflow transport in the Taiwan Strait were scarce due to rough sea conditions in winter monsoon and intensive fishing activities. So, the volume transport through the Taiwan Strait and the origin of the

TWC are still under debate.

2.3 Tsushima Warm Current (TSWC)

The Tsushima Warm Current flows northward west of Kyushu toward south of Korean Peninsula and enters the Korea/Tsushima Strait (K/T Strait). It has been debated for a long time about the origin of the TSWC whether the TSWC is a branch current separated from the Kuroshio or not, since Uda (1934) showed a simple schematic view of the ECS currents.

Many researchers have suggested that the TSWC was separated from the Kuroshio west of Kyushu and flows to the K/T Strait. (Nitani, 1972; Huh, 1982; Lie and Cho, 1994; Hsueh *et al.*, 1996; Lie *et al.,* 1998)

On the other hand, Beardsley *et al.* (1985) showed a schematic view of the ECS circulation, which regarded the TSWC as an extension of the TWC. Fang *et al.* (1991) also explained that the TWC was continued to the TSWC.

In recent years, solving the vertically integrated vorticity equation diagnostically, Isobe (1999a) explained that the Taiwan-Tsushima Warm Current System exists in almost seasons, however the system breaks down in autumn due to the positive vorticity inducing the cross-isobath transport: the Ekman term east of Taiwan and the JEBAR term west of Kyushu. He estimated about 66 % of volume transport of the TSWC is originated from the Kuroshio in autumn crossing the shelf edge of the ECS. In a different manner using a JODC temperature dataset from 1961 to 1990, Isobe (1999b) showed the monthly map of the horizontal heat transport describing the existence of the Taiwan-Tsushima Warm Current System at least from April to August.

2.4 Yellow Sea Warm Current (YSWC) and Cheju Warm Current (CWC)

In relation with the TSWC, it has been known that a part of it, named the Yellow Sea Warm Current (YSWC), flows into the Yellow Sea through west of Jejudo (Chejudo), and transports warm and saline water to the Yellow Sea (Uda, 1934; Nitani, 1972; Beardsley *et al.,* 1985). However, analyzing hydrography data, satellite-tracked drifter trajectories and satellite infrared images, Lie *et al.* (2001) revealed that the YSWC is not a persistent mean flow but an intermittent northwestward current induced by strong northerly wind bursts.

Instead, Lie *et al.* (1998) defined the clockwise circulation around Jejudo (Chejudo) as the Cheju Warm Current (CWC). Lie *et al.* (2000) further confirmed that the year-round existence of the CWC west of Jejudo (Chejudo) and in the Jeju Strait (Cheju Strait) with current speeds of 5 to 40 cm/s. Chang *et al.* (2000) estimated the volume transport through the Jeju Strait (Cheju Strait) from the ADCP measurements to be 0.37 Sv in March to 0.66 Sv in August and revealed that it has a low-frequency fluctuation along the strait with a period near 37 days. Pang *et al.* (2003) also estimated the transport through to vary from 0.3 Sv to 0.6 Sv. They suggested that barotropic component of the transport is 0.2 Sv corresponding to 5 cm/s and baroclinic component ranges from 0.1 Sv in winter to 0.4 Sv in summer.

The CWC joins to the TSWC after passing through the Jeju Strait (Cheju Strait), and mainly flows into the western channel of K/T Strait.

2.5 Changjiang Diluted Water (CDW)

The Changjiang River is one of the largest rivers in the world with a mainstream length of 6,300 km and is the main source of fresh water input into the ECS. Its volume transport amounts to 0.03 Sv on average with maximum about 0.06 Sv in summer and 0.01 Sv in winter. Changjiang diluted water (CDW), formed by the mixing of the Changjiang river runoff with the ECS water, contains various terrigenous materials and has significant effects on the marine ecosystem of the ECS. In recent years, active researches have been done with regard to the Changjiang river, because the ECS is now faced with various environmental problems caused by the increase of human activities and construction of the Three Gorges Dam (For example, harmful algal blooms).

The CDW is generally confined to the Chinese coast in winter, when northerly wind is prevail. In summer, it flows northeastward toward Jeju (Cheju) Island in the form of patches of low-salinity water with thickness about 10 to 15 m (Lie *et al.,* 2003). Recent studies suggested that the movement of the

CDW depends largely on the wind system (Chang and Isobe, 2003, Chang and Isobe, 2005). In addition, Matsuno *et al.* (2006) suggested that the vertical transport from the bottom layer is an important mechanism for the dispersion process of the CDW

2.6 Nutrients from the Kuroshio

It has been known for many years that the Kuroshio contributes nutrients to the ECS (Liu *et al.,* 1992b; Ito *et al.,* 1994; Chen *et al.,* 1995; Gong *et al.,* 1995; Chen *et al.,* 1998; Chen *et al.,* 1999; Liu *et al.,* 2000; Chen, 2005). Since the Kuroshio originates from the subtropical and tropical regions with low near-surface nutrient contents, if only near-surface Kuroshio water moved onto the shelf, the water would not contribute much to the high productivity of the ECS (Chen *et al.,* 1999). However, as already reported, the nutrient-rich Kuroshio subsurface water upwells onto the shelf, and roles the major source of nutrients on the ECS continental shelf (Liu *et al.*, 1992; Chen *et al.*, 1995; Chen and Wang, 1998). The nutrient-rich Kuroshio subsurface water is mainly from the North?Pacific Intermediate Water (NPIW) or from the nutrient-rich South China Sea Intermediate Water (SCSIW, Chen, 1996; Chen and Huang, 1996; Chen, 2005).

The reason why the Kuroshio contains the nutrient-rich SCS water is related with the water exchange in the Luzon Strait. The Luzon strait is located between the Taiwan and the Luzon Island, and it connects the SCS with the open Pacific Ocean. When the Kuroshio flows northward along the eastern Philippine coast, it encounters the Luzon strait at the northern tip of the Luzon Island. And, it forms a loop current or a warm eddy entering the SCS, or passes the Strait without intrusion into the SCS, as reviewed by Hu *et al.* (2000). Though the exact behavior of the Kuroshio at the Luzon strait and the northeast of SCS still remains not clear, the path of the Kuroshio at the Luzon Strait seems to be affected by the monsoon winds with maximum intrusion in winter (e.g., Shaw and Chao, 1994). While, in the deeper layer from 350 m to 1350 m, as reported by Chen and Huang (1996), Chen and Wang (1998), and Chen (2005), SCSIW flows out through the Luzon Strait and joins the Kuroshio.

Chen and Wang (1999) emphasized the importance of the Kuroshio intrusion, concluding that the upwelled sub-surface Kuroshio water supplied about 70 % of phosphorus (P) and about 50 % of nitrogen (N) to the ECS shelf. Liu *et al.* (2000) also estimated the cross-shelf nutrient flux by the observation of the flow field and the chemical hydrography north of Taiwan in winter and in summer. They concluded that the volume transport of the subsurface Kuroshio intrusion is 0.59 Sv in winter and 0.83 Sv in summer, and reported that the nutrients input from the Kuroshio was more than double those from the Taiwan Strait in summer.

2.7 Kuroshio Meandering or eddy motions on the ECS shelf break

At the location where the Kuroshio flows along the continental shelf break, it is known that the frontal eddy plays an important role in the intrusion from the Kuroshio. James *et al.* (1999) summarized wavelengths, periods, and downstream phase speeds of propagating Kuroshio meanders reported in the previous researches. The meanders of the Kuroshio in the ECS typically have horizontal scales of 100 ~ 375 km, periods of 7 ~ 23 days, and downstream phase speeds of 8 ~ 28 km/day (Sugimoto *et al.,* 1988; Qiu *et al.,* 1990; Ichikawa and Beardsley, 1993; James *et al.,* 1999). The detailed three-dimensional structure of the Kuroshio frontal eddy along the shelf edge of the ECS was revealed by Yanagi *et al.* (1998), who showed the nutrient transport across the shelf edge via the frontal eddy motion. On the other hand, Isobe *et al.* (2004) focused on the intrusion of shelf water into the Kuroshio subsurface layer due to the eddy motion.

2.8 Tide, internal tide, internal wave, and small scale motions

Tides in the Yellow and the East China Seas (YECS) have been investigated by a number of researchers using two or three-dimensional numerical models assuming homogeneous density (An, 1977; Choi, 1980; Choi, 1990; Kang *et al.,* 1991; Kang *et al.,* 1998; Guo and Yanagi, 1998). Recently, Lee and Beardsley (1999) investigated the residual circulation using three-dimensional coastal ocean model, and founded stratified tidal rectification intensifies the residual currents at the front and

at the top of the bottom boundary layer over the sloping bottom. Kang *et al.* (2002) also considered the effect of stratification using two-layer tidal model, and revealed that seasonal stratification has noticeable effects on the tides in terms of varying current shear, frictional dissipation, and barotropic energy flux.

The tidal flow in a stratified ocean can produce nonlinear internal waves by the interaction with topography, and the internal waves play an important role in the transfer of energy from tides to ocean mixing. The semi-diurnal tide is strong in the East China Sea and tidal currents of cross-shelf direction is dominant (Larsen *et al.,* 1985), so that the semi-diurnal internal tides can take place in conjunction with inclined topography. Using linear generation model for internal tides, Baines (1982) indicated that the East China Sea is the area with the largest internal tidal energy production. Actually, internal tides have been observed on the continental shelf break of the East China Sea. Kuroda and Mitsudera (1995) showed some evidences of internal tides, using an USV (Underwater Sliding Vehicle) and ADCP, and suggested the generation mechanism of internal tides.

From several researches, it was reported that there are not only internal-tides but also internal waves of higher frequency. Matsuno *et al.* (1997) suggested that high frequency internal waves would be generated around the lower part of the lower thermocline near the shelf break. Han *et al.* (2001) showed that vertical mixing generated by high frequency internal waves produces ageostrophic density current around the lower thermocline, which can intrude the Kuroshio water into the shelf-water or the shelf-water into the Kuroshio water. Recently, Matsuno *et al.* (2005) found large values of the turbulent energy dissipation rate just above the bottom of the shelf and around the thermocline near the shelf break, and suggested the possible propagation of the vertically high wave number internal tides along the characteristic ray. Episodes of high frequency internal waves were also observed in the northern ECS by Lee *et al.* (2006), and the internal waves lasted approximately 3 hours and influenced the whole water column. Meanwhile, by using the SAR images, Liu *et al.* (1998) analyzed the rank-ordered packets of internal solitons propagating shoreward from the edge of the continental shelf northeast of Taiwan and simulated them by numerical model. Hsu *et al.* (2000) further suggested that the generation mechanisms of complicated internal waves northeast of Taiwan are associated with the tide and the upwelling, which is induced by the intrusion of the Kuroshio across the continental shelf. They also showed the merging of two wave packets due to nonlinear wave-wave interaction, which were generated from the islands near the southwest tip of Korea Peninsula by the collision of the Korea coastal current and the semi-diurnal tides in summer.

Chapter 3. Model description

The RIAMOM (RIAM Ocean Model), which was developed in the Research Institute for Applied Mechanics in Kyushu University, is a 3-dimensional, primitive equation ocean model with a free surface. It employs a spherical coordinate horizontally with a staggered Arakawa B-grid and a z-coordinate vertically. As a previous study using RIAMOM, You and Yoon (2004) simulated the circulation of the Pacific Ocean including the ECS, and supported the existence of the Ryukyu current which is a northeastward current along the Pacific side of the Ryukyu Islands with a subsurface core at 500～600 m. Recent studies using RIAMOM have shown good performance of ocean simulation (e.g., Lee *et al.*, 2003; Hirose *et al.,* 2005).

In this chapter, detailed explanations about the equation sets and the numerical model are given.

3.1 Fundamental equations and approximations

With several assumptions and approximations, the model solves the Navier-Stokes equation for an incompressible Newtonian fluid, together with supplemental equations: the mass conservation equation, advection-diffusion equations for temperature and salinity. The governing equations for flow and tracer in Cartesian coordinates are expressed in vector form as follows.

$$\frac{D\mathbf{u}}{Dt} + 2\Omega \times \mathbf{u} = -\frac{1}{\rho}\nabla p - \mathbf{g} + \nu\nabla^2\mathbf{u}$$

Momentum equation (3.1)

$\nabla \cdot \mathbf{u} = 0$ Mass conservation equation (3.2)

$\frac{DC}{Dt} = \kappa \nabla^2 C$ (C is a tracer such as θ or S)

Advection-Diffusion equation (3.3)

where t is time, **u**= (u,v,w) velocity, p pressure, ρ density of fluid, Ω angular velocity of the Earth (or rotating frame), **g** acceleration due to gravity of magnitude g, ν the kinematic viscosity, κ the diffusivity, θ potential temperature, and S salinity.

As mentioned above, the equations already assumed the incompressibility of fluid, and the property of Newtonian fluid that the viscous stress is proportional to the velocity shear. In addition, several standard approximations are used to simplify the governing equations.

1. Boussinesq approximation which means density differences are sufficiently small to be neglected, except in the terms where it is multiplied by g, i.e., a buoyancy term. So, density is regarded as a constant except in terms multiplied by g of the vertical momentum equation. Thus, the pressure gradient terms in the horizontal momentum equation are expressed by the perturbation pressure. This approximation also includes the incompressibility of the fluid.
2. Hydrostatic approximation by the scale analysis representing the motion of horizontal scale is large enough compared with the vertical scale. It assumes the vertical pressure gradient to be balanced by the forcing due to buoyancy excess, so that all the vertical acceleration terms except a buoyancy term and a pressure gradient term is omitted in the vertical momentum equation.
3. Similar to the molecular viscosity, eddy viscosity is also regarded to be proportional to the product of turbulent speed and path length. Since horizontal velocity tends to be much larger than vertical velocity, horizontal eddy viscosity and vertical eddy viscosity are separated into A_h and A_z. Besides, A_h has the same value in the x and y momentum equations. This also applies to eddy diffusivity.
4. Salt and heat diffusivities are taken as equal, considering diffusion is mainly accomplished by turbulence much larger than molecular diffusion.
5. Atmospheric pressure is not considered.

3.2 Coordinates transformation

The fluid motion is considered as the motion on the spherical polar coordinates (λ, ϕ, r), where λ is longitude, ϕ latitude, and r radial distance. Arbitrary point (x, y, z) is expressed as ($r\cos\lambda\cos\phi$, $r\sin\lambda\cos\phi$, $r\sin\phi$) using λ, ϕ, r in Cartesian coordinates. Now, the scale factor (h_λ, h_ϕ, h_r) is applied to change the dimension between Cartesian and Spherical coordinates when transforming. In addition, another assumption and approximation is applied.

1. The earth is a perfect sphere with radius R (6370 km)
2. Thin shell approximation since the depth of the ocean on the earth is much smaller than the Earth's radius. So, R+z of the curvature term when transforming the coordinates is approximated as R
3. The coordinate z is defined by $z=r-r_0$, which means the distance measured upward from the sea-level geopotential surface (r_0).
4. Some terms involving w in the horizontal momentum equations are neglected except vertical advection term, on the basis of scale analysis.

With these assumptions, the equation sets are expressed in spherical coordinates form, as follows.

The horizontal momentum equations are

$$\frac{\partial u}{\partial t} + L(u) - \left(2\Omega + \frac{u}{R\cos\varphi}\right) v\sin\varphi = -\frac{1}{\rho_0 R\cos\varphi}\frac{\partial p'}{\partial \lambda} - \frac{g}{R\cos\varphi}\frac{\partial \eta}{\partial \lambda} + F_\lambda \quad (3.4)$$

$$\frac{\partial v}{\partial t} + Lv + \left(2\Omega + \frac{u}{R\cos\varphi}\right) u\sin\varphi = -\frac{1}{\rho_0 R}\frac{\partial p'}{\partial \varphi} - \frac{g}{R}\frac{\partial \eta}{\partial \varphi} + F_\varphi \quad (3.5)$$

$$F_\lambda = A_h\left(\nabla^2 u - \frac{u}{R^2\cos^2\varphi} - \frac{2\sin\varphi}{R^2\cos^2\varphi}\frac{\partial v}{\partial \lambda}\right) + A_v\frac{\partial^2 u}{\partial z^2} \quad (3.6)$$

$$F_\varphi = A_h\left(\nabla^2 v - \frac{v}{R^2\cos^2\varphi} + \frac{2\sin\varphi}{R^2\cos^2\varphi}\frac{\partial u}{\partial\lambda}\right) + A_v\frac{\partial^2 v}{\partial z^2} \tag{3.7}$$

The advection () and Laplacian () operators are defined by,

$$L(\mu) = \frac{1}{R\cos\varphi}\frac{\partial}{\partial\lambda}(\mu u) + \frac{1}{R\cos\varphi}\frac{\partial}{\partial\varphi}(\mu v\cos\varphi) + \frac{\partial}{\partial z}(\mu w) \tag{3.8}$$

$$\nabla^2\mu = \frac{1}{R^2\cos^2\varphi}\frac{\partial^2\mu}{\partial\lambda^2} + \frac{1}{R^2\cos\varphi}\frac{\partial}{\partial\varphi}\left(\cos\varphi\frac{\partial\mu}{\partial\varphi}\right) \tag{3.9}$$

The vertical momentum equation is simplified into the hydrostatic equation

$$p(z) = \rho_0 g(z+\eta) + \int_0^z(\rho-\rho_0)dz \tag{3.10}$$

The advection-diffusion equations for potential temperature and salinity are

$$\frac{\partial\theta}{\partial t} + L\theta = K_h\left[\frac{1}{R^2\cos^2\varphi}\frac{\partial^2\theta}{\partial\lambda^2} + \frac{1}{R^2\cos\varphi}\frac{\partial}{\partial\varphi}\left(\cos\varphi\frac{\partial\theta}{\partial\varphi}\right)\right] + K_v\frac{\partial^2\theta}{\partial z^2} \tag{3.11}$$

$$\frac{\partial S}{\partial t} + LS = K_h\left[\frac{1}{R^2\cos^2\varphi}\frac{\partial^2 S}{\partial\lambda^2} + \frac{1}{R^2\cos\varphi}\frac{\partial}{\partial\varphi}\left(\cos\varphi\frac{\partial S}{\partial\varphi}\right)\right] + K_v\frac{\partial^2 S}{\partial z^2} \tag{3.12}$$

Density is calculated by an adaptation of the UNESCO equation of state revised by Mellor (1991).

$$\rho = \rho(\theta, S, p) \tag{3.13}$$

Finally, the mass conservation equation is

$$\frac{1}{R\cos\varphi}\frac{\partial u}{\partial\lambda} + \frac{1}{R\cos\varphi}\frac{\partial}{\partial\varphi}(v\cos\varphi) + \frac{\partial w}{\partial z} = 0 \tag{3.14}$$

The mass conservation equation is used to diagnose vertical velocity.

3.3 Mode-splitting technique and vertically integrated equations

Since the model considers the variation of surface elevation without rigid-lid approximation, the external gravity wave, which is the fastest wave with $c=\sqrt{gH}$, is generated at the surface. In order to avoid the numerical instabilities, Courant-Friedrichs-Levy (CFL) condition must be satisfied, and it requires a very short time step and thus large computing time. However, it is generally unnecessary to obtain results with such a high temporal resolution. So, a mode-splitting technique, which separates the external mode for the calculation of external gravity wave from the basic equation sets, is adopted to save the computing time. The external mode equations are obtained from the vertical integration of the momentum equations and the mass conservation equation. The vertically integrated continuity equation is changed to the free-surface equation with conditions of $z=\eta$ at the free surface and w=0 at bottom. The vertically integrated equations in spherical coordinates are given by,

$$\frac{\partial\overline{u}}{\partial t} + \overline{Lu} + \overline{L'u'} - \left(2\Omega + \frac{\overline{u}}{R\cos\varphi}\right)\overline{v}\sin\varphi = -\overline{\frac{1}{\rho_0 R\cos\varphi}\frac{\partial p'}{\partial\lambda}} - \frac{g}{R\cos\varphi}\frac{\partial\eta}{\partial\lambda} + \overline{F_\lambda} \tag{3.15}$$

$$\frac{\partial\overline{v}}{\partial t} + \overline{Lv} + \overline{L'v'} + \left(2\Omega + \frac{\overline{u}}{R\cos\varphi}\right)\overline{u}\sin\varphi = -\overline{\frac{1}{\rho_0 R}\frac{\partial p'}{\partial\varphi}} - \frac{g}{R}\frac{\partial\eta}{\partial\varphi} + \overline{F_\varphi} \tag{3.16}$$

$$\overline{F_\lambda} = \frac{\tau^\lambda}{\rho_0 H} - \frac{\tau_B^\lambda}{\rho_0 H} + A_h\left(\nabla^2\overline{u} - \frac{\overline{u}}{R^2\cos^2\varphi} + \frac{2\sin\varphi}{R^2\cos^2\varphi}\frac{\partial\overline{v}}{\partial\lambda}\right) \tag{3.17}$$

$$\overline{F_\varphi} = \frac{\tau^\varphi}{\rho_0 H} - \frac{\tau_B^\varphi}{\rho_0 H} + A_h\left(\nabla^2\overline{v} - \frac{\overline{v}}{R^2\cos^2\varphi} + \frac{2\sin\varphi}{R^2\cos^2\varphi}\frac{\partial\overline{u}}{\partial\lambda}\right) \tag{3.18}$$

$$\frac{\partial\eta}{\partial t} = -\frac{1}{R\cos\varphi}\frac{\partial\overline{u}(H+\eta)}{\partial\lambda} - \frac{1}{R\cos\varphi}\frac{\partial(H+\eta)\overline{v}\cos\varphi}{\partial\varphi} \tag{3.19}$$

3.4 Numerical schemes

In this model, the "slant advection" effect is considered in order to represent the vertical advection effect of the horizontal momentum at the bottom topography as correctly as possible (Ishizaki and Motoi, 1999). As an advection scheme for tracers, the "modified split QUICK (MSQUICK) scheme (Webb *et al.*, 1998)" was adopted. In

addition, the use of "partial step topography" facilitated a more realistic simulation near the bottom. The horizontal eddy viscosity and diffusivity were calculated using the Smagorinsky formula with a coefficient of 0.2. The vertical coefficients of eddy viscosity and diffusivity were calculated by solving the turbulent kinetic energy equation (Noh *et al.*, 2002).

The tide effect was parameterized by enhancing the background turbulence as vertical eddy diffusivity and viscosity and by increasing the bottom friction where the tidal current is strong. As the M2 tide is dominant over the ECS shelf, the amplitude of the M_2 tidal current was used for the parameterization of the tide effect.

The increased vertical eddy diffusivity due to the M_2 tide was calculated using the Munk-Anderson scheme, which depends on the Richardson number (Munk and Anderson, 1948):

$$K_z = K_o/(1+\sigma Ri)^p \tag{3.20}$$

$$Ri = \frac{N^2}{(\partial U/\partial z)^2} \tag{3.21}$$

where σ and p are coefficients, assigned the value 3.33 and 1.5 respectively, K_o is the maximum diffusivity, $1.0\times10^{-3}\mathrm{m^2s^{-1}}$, and is the Richardson number.

The vertical shear of the horizontal velocity in the Richardson number was replaced by James' (1977, 1978) method (see also Lee *et al.*, 2006):

$$\left(\frac{\partial U}{\partial z}\right)^2 = \frac{1}{2}\left(\frac{A}{H-z}\right)^2 \tag{3.22}$$

where N is the Brunt-Väisälä frequency, H is the water depth, and $A=C_d^{\frac{1}{2}}V_t/k$. C_d is the bottom drag coefficient, 0.0025, k is the von Kármán constant, 0.41, and is the amplitude of the M2 tidal current obtained from the NAO.99Jb model (Matsumoto *et al.*, 2000).

The vertical eddy viscosity due to the M_2 tide was calculated by the James' (1978) method, as follows:

$$A_z = A_o \Big/ \left(1+\frac{p\sigma Ri}{p-1}\right)^{p-1} \tag{3.23}$$

where A_o is the maximum viscosity and it is assumed that $A_o=K_o$, following James (1978).

The Richardson number is given by the same equation as (3.21). The enhanced vertical eddy diffusivity and viscosity due to the M_2 tide were simply superposed on those calculated by the Noh scheme (Noh *et al.*, 2002).

Lee *et al.* (2000) showed the effectiveness of the linear bottom friction given by Hunter's formula (1975) in the ECS. In order to consider the enhanced bottom friction due to the tidal stress, a linear-type bottom friction formulated by Hunter (1975) was adopted instead of a quadratic bottom friction:

$$\tau_{b\lambda} = \rho_o C_d \kappa u_b \tag{3.24}$$

$$\tau_{b\varphi} = \rho_o C_d \kappa v_b \tag{3.25}$$

where $\tau_{b\lambda}$ and $\tau_{b\phi}$ are the zonal and meridional components of the bottom frictional stress, respectively. ρ_o is the sea water density, C_d is the bottom drag coefficient (0.0025), κ is the coefficient of the linear bottom friction, and u_b, v_b, are the model velocity at the bottom in the zonal and meridional directions, respectively.

The linear bottom friction coefficient, κ, was given by time averaging the quadratic bottom friction term in the presence of strong tidal currents. In this study we applied a linear bottom friction coefficient used by Lee *et al.* (2000).

$$\kappa = 1.23\sqrt{(\overline{u_t})^2+(\overline{v_t})^2} \tag{3.26}$$

where $\overline{u_t}$ and $\overline{v_t}$ represent the depth-averaged M_2 tidal velocity in the zonal and meridional directions, respectively. The zonal and meridional components of the M_2 tidal current for the tide parameterization were obtained from the NAO.99Jb model (Matsumoto *et al.*, 2000).

3.5 Model test run (Error test for calculation of volume transport using box model)

Finite difference schemes have fundamental errors such as truncation error. Though MSQ scheme for tracer advection effectively suppresses the spurious tracer extrema than centered scheme, it still has some problems of computational dispersion and numerical diffusion. So, before the

tracer experiment in the ECS model, a simple box model using RIAMOM is tested in this section for error estimation of volume transport calculation using the passive tracer (Fig. 3.1a). The box model has 10 vertical grids (z-direction) with 10 m vertical spacing in Cartesian coordinates, and 50 × 50 horizontal grids (x, y-direction) with horizontal grid spacing of 18.53 km, corresponding to the distance of 1/6° in the meridional direction on the earth's surface. In order to exclude the variation of the current induced by the earth's curvature and angular velocity, x-direction velocity is fixed to a constant positive value in the whole model domain, and y, z-direction velocities are set to 0 throughout all the simulation time. The constant velocity in the x-direction is calculated from the volume transport through inflow boundary and the vertical area. Six velocity cases in the x-direction are tested: 5.74, 11.48, 17.22, 22.96, 28.70, 34.44 cm/s correspond to 5, 10, 15, 20, 25, 30 Sv, respectively.

Tracer release positions are set in the inflow boundary along the y-direction (Fig. 3.1b) and in the middle line of the y-direction along the x-direction (Fig. 3.1c). The former estimates the error along the current direction and the latter in the lateral direction. In conjunction with these two different release positions, another two cases, with or without diffusion, are executed for the respective former cases of different release position. For the With-Diffusion cases, the horizontal and vertical eddy diffusivities are fixed to 442.358 cm^2/s and 456.706 cm^2/s, which were annually averaged in the shallow area west of 123°E from the results of preliminary experiment in Chapter. 4. After all, with the combination of current velocity, release position, and diffusion effect, total 24 cases are calculated, and

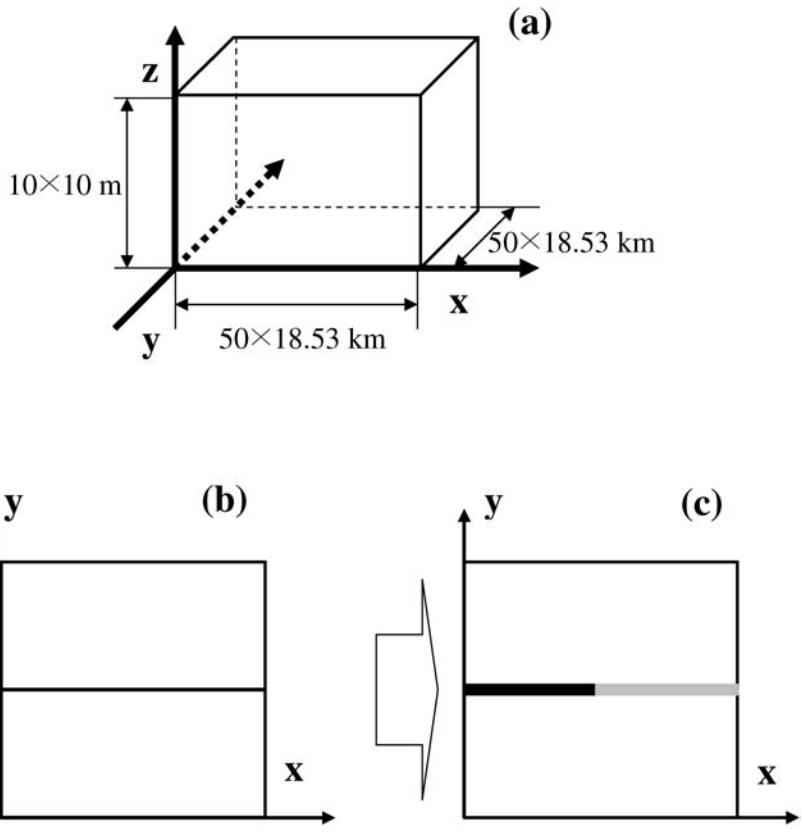

Fig. 3.1 (a) Box model has 10 vertical grids with 10 m vertical spacing, and 50×50 horizontal grids with horizontal grid spacing of 18.53 km (a). Tracer release positions are set in the inflow boundary along the y-direction (b) and in the middle line of the y-direction along the x-direction. (c). Thick black lines are release positions with concentration of 100, and thick gray line fixes to 0. (pp.21)

Table 3.1 Calculated volume transports using tracer for each case with fixed volume transports. A case and B case denote that the release positions are parallel to y-direction (Fig. 3.1b) and x-direction (Fig. 3.1c). (pp.22)

	With-Diffusion [Sv]		Without-Diffusion [Sv]	
Volume Transport [Sv = 10^6 m^3/s]	A case	B case	A case	B case
5	5.134	0.065	5.101	0
10	10.219	0.065	10.202	0
15	15.314	0.065	15.302	0
20	20.412	0.065	20.403	0
25	25.511	0.065	25.504	0
30	30.610	0.065	30.605	0

the results are summarized in Table 3.1. Though the volume transports estimated from the tracer experiment were slightly overestimated about 2 % of the real transport in both with and without diffusion, the error was not so large. In addition, the false advection of tracer across the current was not occurred. The table shows that the inclusion of the diffusion for the estimation of the volume transport is trivial, but the volume transports are calculated just from the advection term of advection-diffusion equation in the study (Without-Diffusion).

3.6 Model domain and boundary conditions

The model region (Fig. 3.2) covers the entire Yellow and East China Seas. The horizontal resolution is 1/6° and the number of vertical levels is 41 with a minimum depth of 10 m and a maximum depth of 2000 m (Table 3.2). We increased the vertical resolution near the sea surface. From the surface to a depth of 300 m, there are 23 vertical levels with 5 to 20 m spacing. The bottom topography is derived by the horizontal averaging of the Jtopo30 dataset from the Marine Information Research Center of the Japan Hydrographic Association (www.mirc.jha.or.jp/products /JTOPO30/). In spite of the high resolution, the Jtopo30 dataset only covers the eastern part of 120°E, so the Etopo5 dataset (NGDC, www.ngdc.noaa.gov/mgg/global/relief/ETOPO5/) is used for the remainder. The bottom topography of the model region is shown in Fig. 3.2. The Taiwan Strait, the east of Taiwan, the Tokara Strait, and the K/T Strait are the main open boundaries. The southeastern boundary along the Ryukyu Islands is closed.

Many scientists have suggested different volume transports through the Taiwan Strait, depending on the measuring time and position. The result of Wang *et al.* (2003) is used as an inflow volume transport of a control case for this study and the transport through the Taiwan Strait is set to 0.9 Sv in winter and 2.7 Sv in summer. Wang *et al.* (2003) estimated the volume transport from the empirical formula using the shipboard ADCP for 2.5 years and the along-strait wind data. Transports are interpolated as a sinusoidal curve. The seasonally varying transport east of Taiwan has a maximum of 24 Sv in summer with a weaker secondary maximum in winter, and a minimum of 20 Sv in fall (Lee *et al.*, 2001). They estimated the volume transport from a sea level difference time series, a 7-year dataset from 1989 to 1996, between Ishigaki island in Japan and Keelung in Taiwan. The outflow transport of the K/T Strait varies monthly and is estimated from sea level differences, a 37-year dataset from 1965 to 2001, between Hakata and Busan (Takikawa and

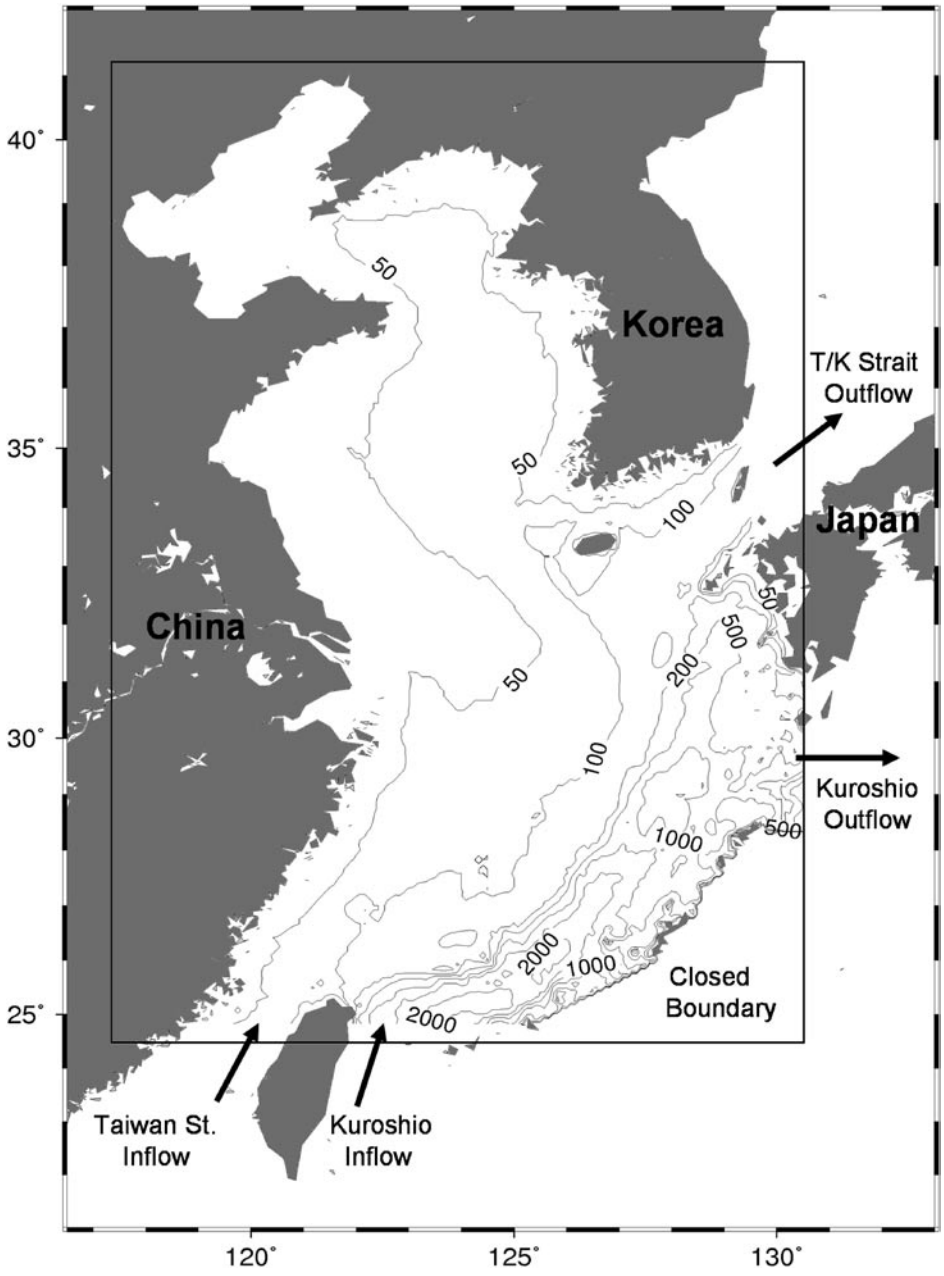

Fig. 3.2 Model domain and boundaries. (pp.22)

Yoon, 2005). The average volume transport through the eastern and western channels is 2.6 Sv.

The remnants of the inflow transport flow out through the Tokara Strait. Fig. 3.3 shows the monthly variations of the volume transport through the Taiwan Strait, the east of Taiwan, and the K/T Strait. The density, derived from the temperature and salinity at each inflow boundary, determined the vertical geostrophic velocities using the thermal wind relation. The calculated geostrophic velocities are adjusted to meet the volume transports specified at the open boundaries. The inflow temperature and salinity were obtained from the climatology data of the World Ocean Atlas 2001 (WOA01) with a 1/4° grid resolution (Boyer *et al.,* 2002; Stephens *et al.,* 2002).

The heat flux at the sea surface was calculated using the Barnier method (Barnier *et al.,* 1995). The model heat flux appears as the sum of a climatological flux and a correction term proportional

Table 3.2 Layer thickness and depth used in the model. Δz is layer thickness and z is depth. (pp.22)

Levels	Δz [m]	z [m]
1~6	5	30
7~13	10	100
14~23	20	300
24~33	40	700
34~38	80	1100
39	200	1300
40	200	1500
41	500	2000

to the difference between the climatological sea surface temperature and the model surface temperature,

$$Q_{NET}(T_S) = Q_{NET}(T_S^{C\lim}) + \left(\frac{\partial Q_{NET}}{\partial T}\right)_{T_S^{C\lim}} (T_S^{C\lim} - T_S) \tag{3.28}$$

where $Q_{NET}(T_S^{C\lim})$ is the climatological flux, $T_S^{C\lim}$ is the climatological sea surface temperature, and T_S is the model surface temperature.

The heat flux was evaluated with a combination of the Southampton Oceanography Centre (SOC) climatological heat flux (Grist and Josey, 2003) and the sea surface temperature of the WOA01 climatology dataset with a relaxation time scale of ten days. The sea surface salinity was restored at the surface grid using the WOA01 climatology dataset. We adopted the monthly mean sea surface wind field which was computed from the weather

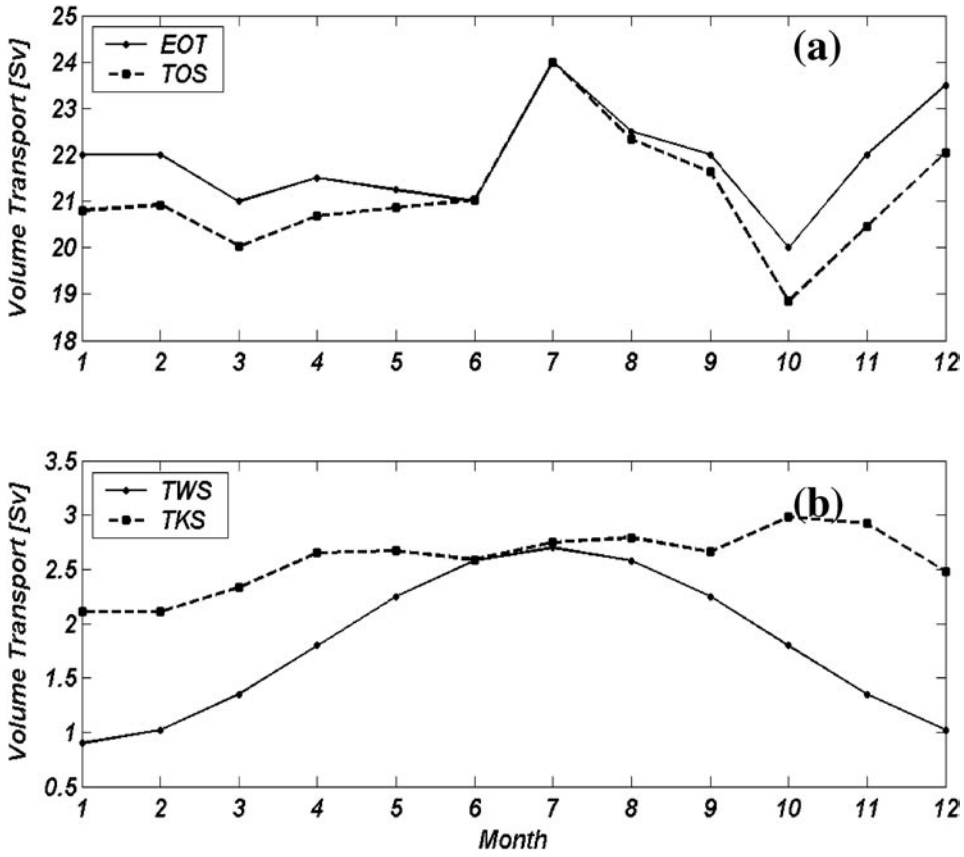

Fig. 3.3 Monthly value of the volume transports through (a) the east of Taiwan (EOT: solid line), the Tokara Strait (TOS: dashed line), (b) the Taiwan Strait (TWS: solid line), and the Korea/Tsushima Strait (TKS: dashed line). (pp.23)

Table 3.3 Names of experiments and cases. (pp.24)

Name of Experiment		Name of case	Section
Tracer Experiment	Preliminary Experiment	Case. A, B	4.3
	Experiment 1 (Exp. 1)	Case. 1	4.4
	Experiment 2 (Exp. 2)	Case. 1 ~ 8	5.2
	Experiment 3 (Exp. 3)	Case. C, D	5.4
Momentum balance analysis		Case. 1, 2	5.3

charts for 1978 ~ 1995 (Na and Seo, 1998), and converted it into wind stress using the Large and Pond (1981) surface drag coefficient formulation.

The model was initialized from rest with zero sea level elevation and with an annual mean temperature and salinity taken from the WOA01 dataset. All forcing and boundary inputs were provided by monthly data and linearly interpolated to the model time step. After a spin up time of six years, passive tracers were released. A detailed explanation of passive tracer experiments is given in Section 4.4.1. Names of experiments and cases are summarized in Table 3.3

Chapter 4. Intrusion pattern of Kuroshio water

4.1 Introduction

The intrusion pattern of Kuroshio water is investigated by the passive tracer experiments in this chapter. Section 4.2 confirms a validation of the model, and describes the general features of the ECS. In the Preliminary Experiment, section 4.3, the tracer distribution released from the Taiwan Strait is discussed (Case. A) and that from the east of Taiwan (Case. B). Section 4.4 describes the results of a control case. The control case, labeled Case. 1 (Experiment 1), sets tracer release positions along the local sections of the 200 m isobath line and adopts the boundary conditions described in the previous Chapter.

This chapter emphasizes the importance of the Kuroshio intrusion east of Taiwan showing winter and summer intrusion patterns. When it comes to the seasonal variation, Hur *et al.* (1999) pointed out that the oceanographic season in the ECS lags the meteorological season slightly. They defined four seasons based on the monthly T-S diagram: spring from April to June, summer from July to September, autumn from October to December, and winter from January to March. In this study, the seasonal variation is discussed on the basis of this criterion, and the modeled winter and summer cases are represented by the results of February and August, respectively.

4.2 General features of the current field and comparison with the vertical section in the PN-line

Fig. 4.1 shows that the time variations of spatially-averaged (0 ~ 200 m) kinetic energy, temperature, and salinity during a six-year spin up of a control case. It represents that the model reached a statistical equilibrium after a spin up of about six years. The monthly averaged current distribution of the control case after a spin up is shown in Fig. 4.2. In order to verify the validation of current field, the model results are compared to previous studies.

Researchers have suggested a schematic view of the current system based on observations using ADCPs, current meters, and satellite tracked drifters. Fang *et al.* (1991) analyzed historical current meter data above the continental shelf of the ECS and obtained similar northeastward current patterns for four seasons. More detailed current patterns of the ECS in summer were shown by Katoh *et al.* (1996a, 1996b, 2000) using four round-trip ADCP surveys. Katoh *et al.* (1996a,

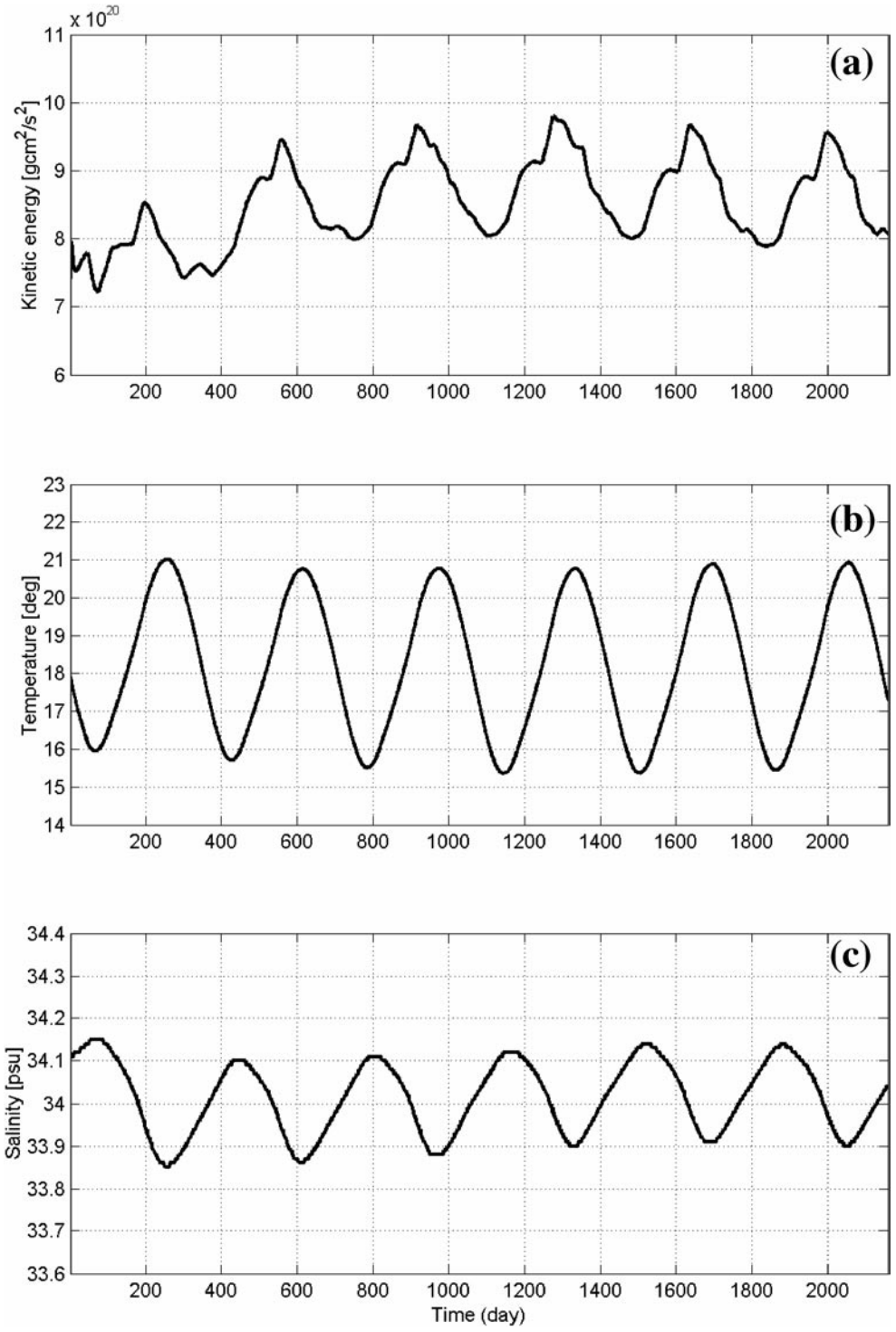

Fig. 4.1 Time variations of spatially-averaged (0∼200 m) kinetic energy (a), temperature (b), and salinity (c) during a six-year spin up. (pp.25)

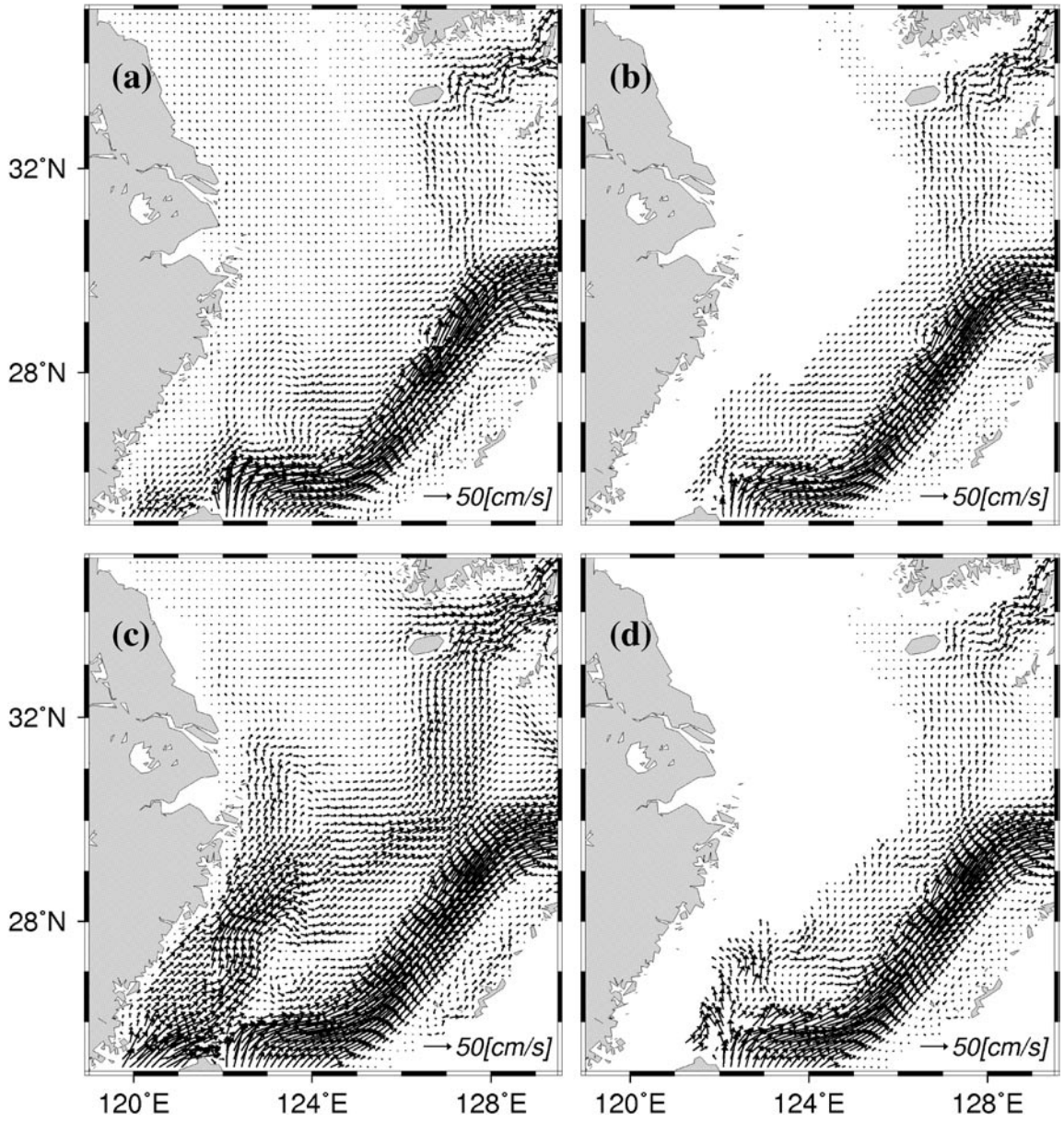

Fig. 4.2 Surface (2.5 m) and deeper layer (85 m) velocity fields of the seventh year of the control case (Case.1) in the ECS: (a) surface velocity field in winter, (b) deeper layer velocity field in winter, (c) surface velocity field in summer, (d) deeper layer velocity field in summer. (pp.25)

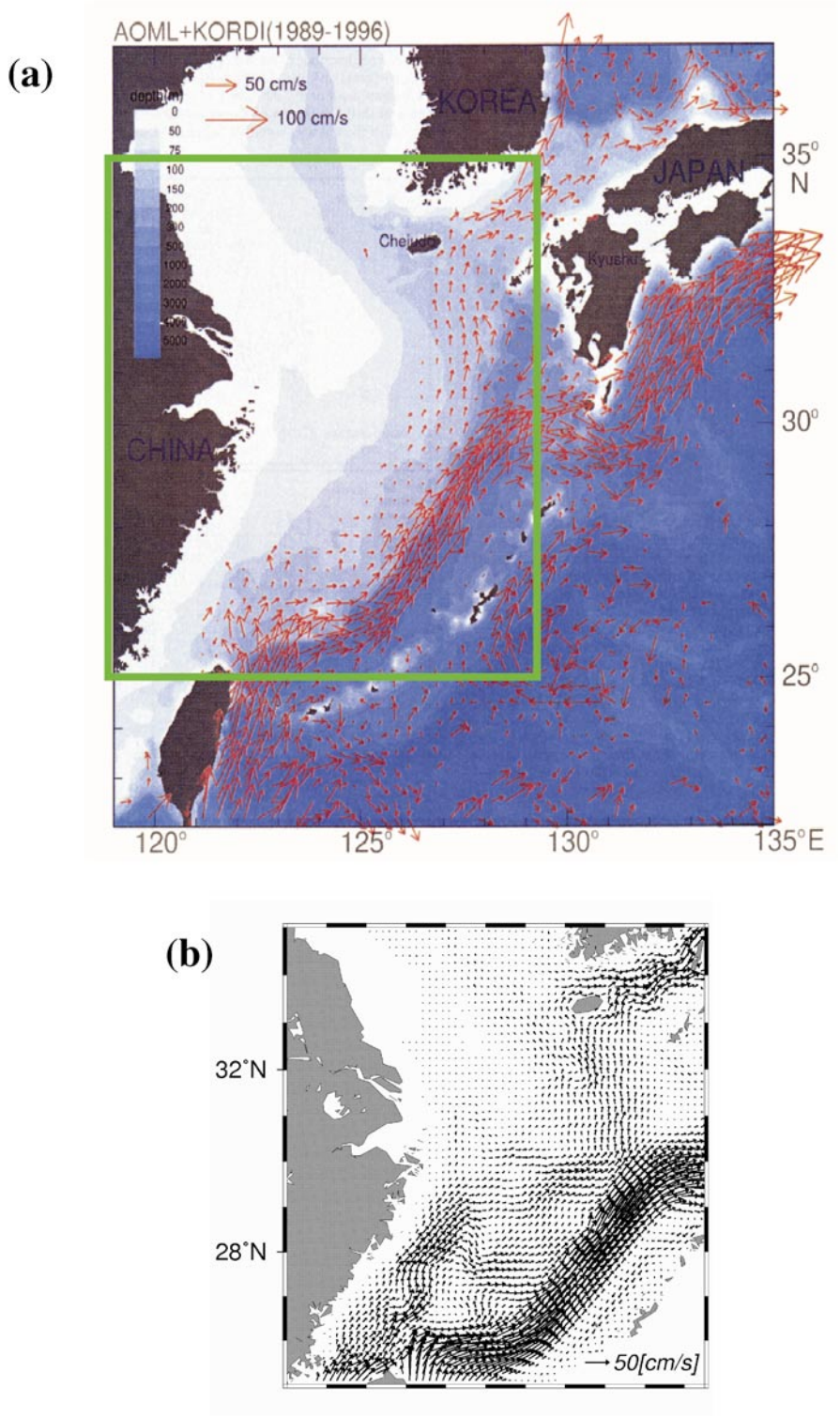

Fig. 4.3 Current field estimated from surface drifter trajectories deployed at 15～50 m depth (after Lie *et al.*, 1998) and annual-mean surface current field (15～50 m) obtained by the model results of the seventh year. (pp.26)

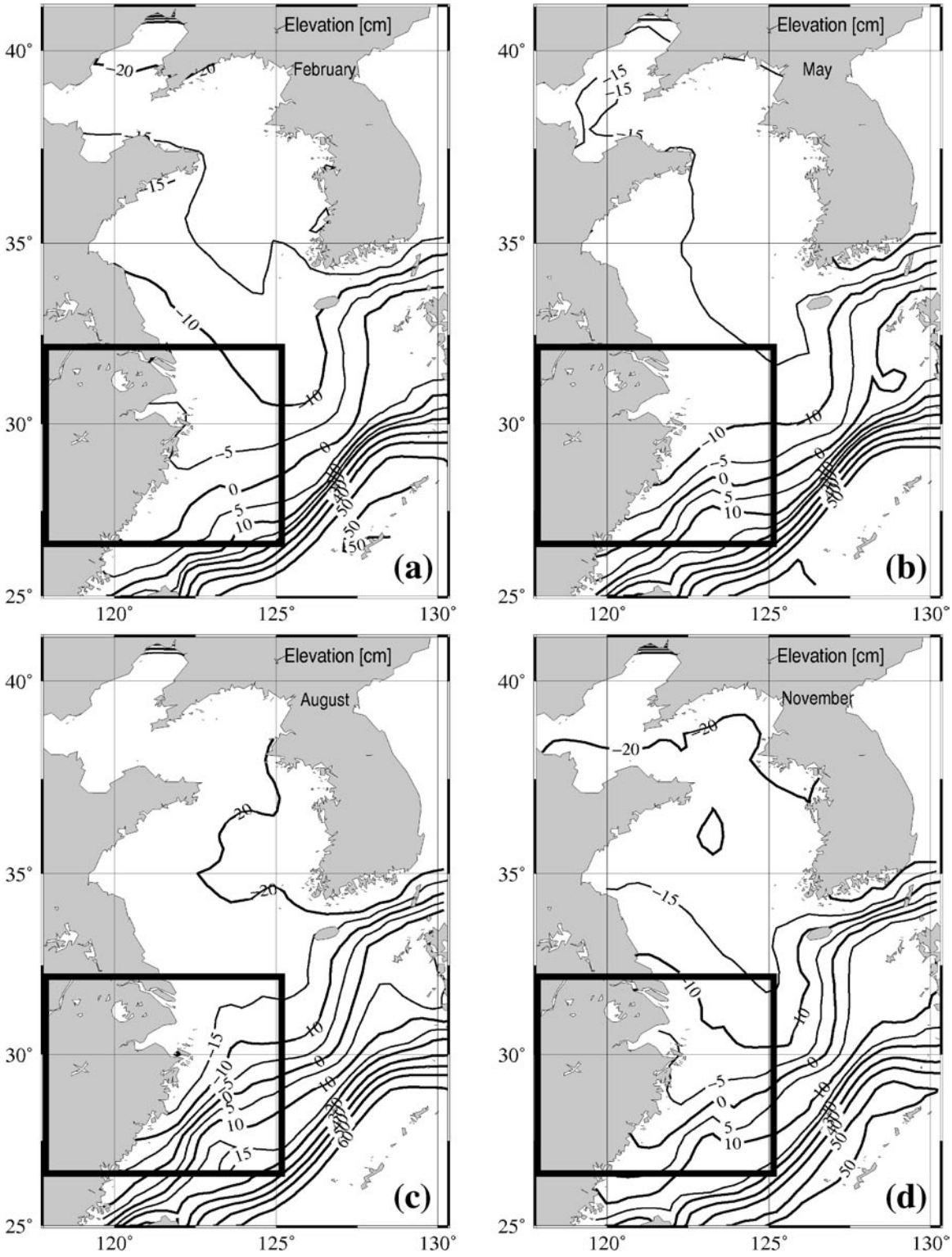

Fig. 4.4 Modeled sea surface elevation fields: (a) winter, (b) spring, (c) summer, and (d) autumn. Patterns of seasonal variation inside the box agree well with those by Yanagi *et al.* (1997). (pp.26)

1996b) presented detailed current structures west of Kyushu and the eastern continental shelf margin of the ECS, respectively. Moreover, Katoh *et al.* (2000) showed current distributions in the southern ECS where the outflow from the Taiwan Strait flows northeastward along the coast of China, and the Kuroshio branch current flows northward east of Taiwan with the anti-cyclonic eddy on its right. Lie *et al.* (1998) showed the separation of the Tsushima Warm Current from the Kuroshio by composite trajectories of 172 drogued drifters (Fig. 4.3a).

Fig. 4.3b shows an annual mean of surface current field averaged in the same depth (15～50 m) with Fig. 4.3a calculated by Lie *et al.* (1998). The model results of the seventh year successfully simulated the well-known currents such as the Kuroshio, the outflow from the Taiwan Strait, and the Kuroshio branch current. The surface elevation after a spin up (Fig. 4.4) also represents a good agreement with the estimated distribution from altimetric data (Fig. 4.5) by Yanagi *et al.* (1997), especially on the western ECS shown by rectangular boxes where might be affected by the Kuroshio.

The PN line in the ECS is a regular section observed by the Nagasaki Marine Observatory, and it provides a good measure for the model validation in the ECS. Fig. 4.6 shows the modeled temperature, salinity, and along-shelf velocity fields in winter and in summer at the PN line. The temperature and salinity fields are similar to those of Oka and Kawabe (1998), Fig. 4.7, seasonally averaged during 1988 to 1994, especially in summer, by displaying the

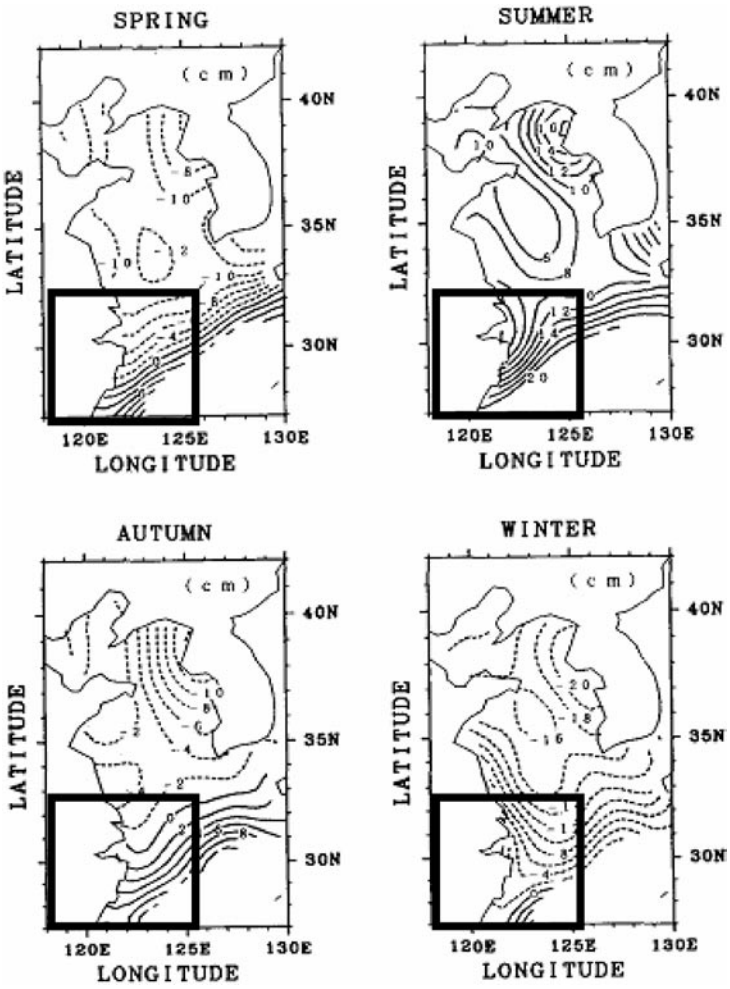

Fig. 4.5 Seasonal variation of sea surface dynamic topography estimated from altimetric data. (after Yanagi *et al.*, 1997) (pp.26)

same extent of intrusion range and thickness. The profiles of the along-shelf velocity component also show well the structure of the Kuroshio in the ECS. Although the maximum velocity is smaller than the observation, the velocity field around the Kuroshio and near the shelf-break matches well with those of Oka and Kawabe (1998).

Through comparison of the model results with the surface current distributions, the surface elevation, and the PN-line observations by previous studies, it is confirmed that the model simulates well the circulation in the ECS and the vertical density field around the shelf break. Based on the validation of model, the results of the tracer experiments will be described.

4.3 Preliminary Experiment (Case. A, B — released from the Taiwan Strait and the east of Taiwan)

In order to investigate the behavior of the outflow

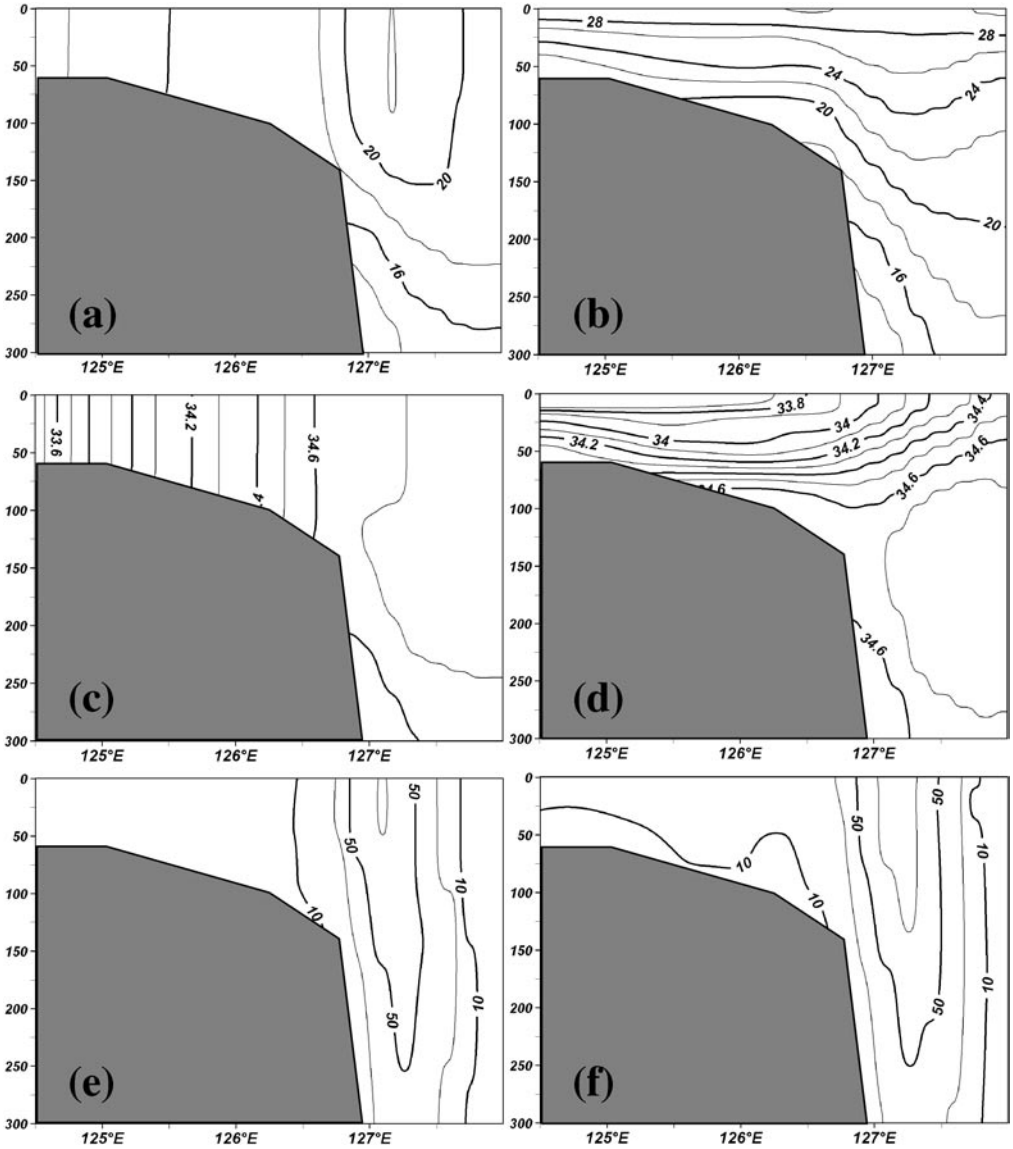

Fig. 4.6 Cross-sections of temperature [℃], salinity, and along-shelf velocity [cm/s] along the PN-line for the modeled control case in winter and in summer: (a) temperature profile in winter, (b) temperature profile in summer, (c) salinity profile in winter, (d) salinity profile in summer, (e) along-shelf velocity in winter, (f) along-shelf velocity in summer. Thin solid line represents a middle value between two thick solid lines. (pp.26)

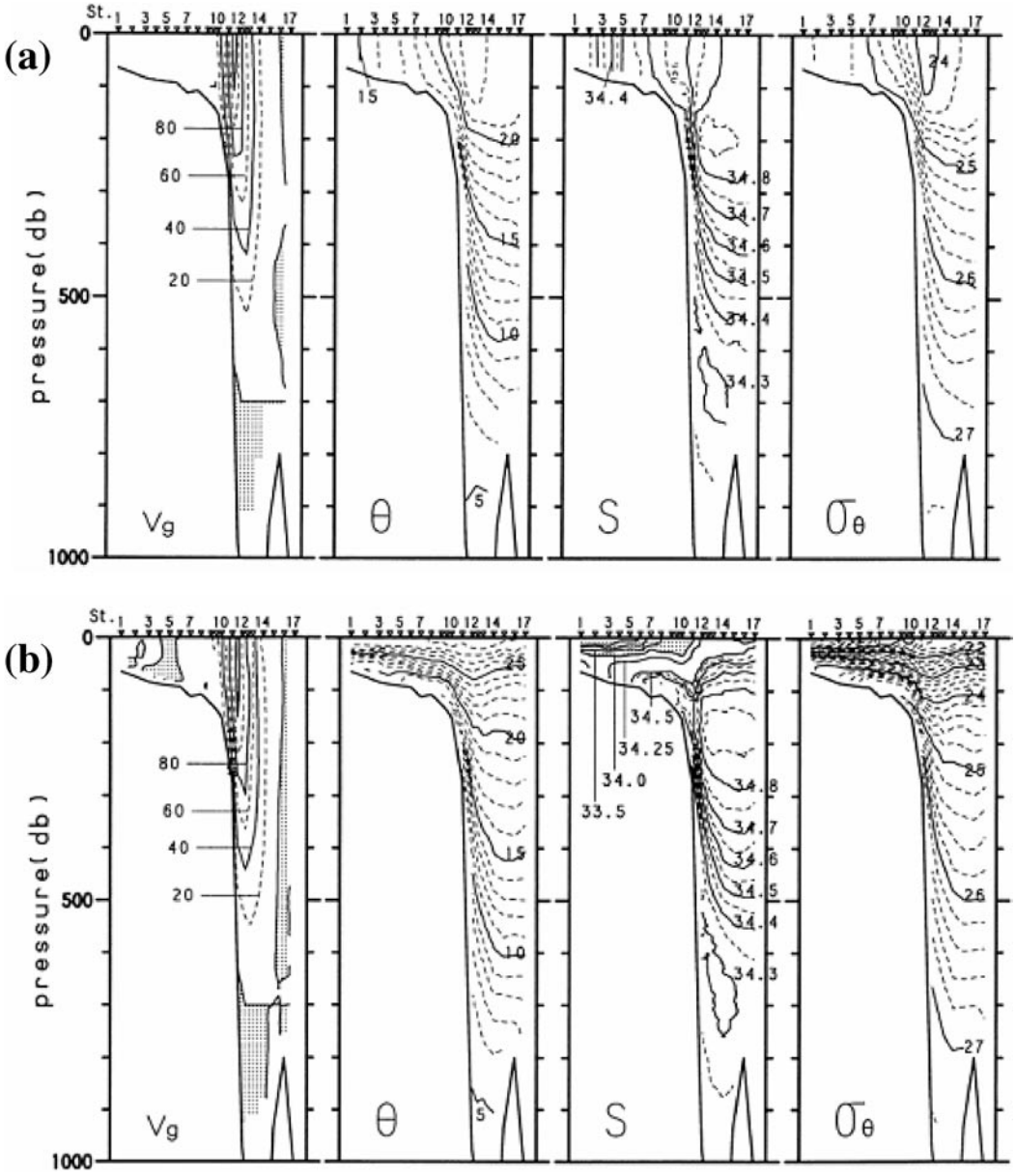

Fig. 4.7 Distributions of geostrophic velocity (Vg) (cm/s), potential temperature (θ) (℃), salinity (S) and potential density ($\sigma\theta$) at the PN line in winter (a), summer (b), averaged during 1988～94 (after Oka and Kawabe, 1998). (pp.26)

from the Taiwan Strait, the tracer was deployed for six years through the Taiwan Strait after a spin up time of six years. The concentration of the tracer was set to 100 and released into the model domain in which the initial concentration was entirely zero. The tracer concentration was governed by the same advection-diffusion equation that determined the temperature and salinity. No surface or bottom flux of the tracer was applied.

At the central part of the ECS, concentration of the tracer, which originated from the Taiwan Strait, reached a converged state having regular seasonal variation in the third year after deployment (not shown here). Results of the sixth year after the release of the tracer were analyzed and it is presented as the preliminary study, as a similar experiment was already carried out by Guo *et al.* (2006).

Fig. 4.8 shows the vertical profile of the tracer concentration which is horizontally averaged at

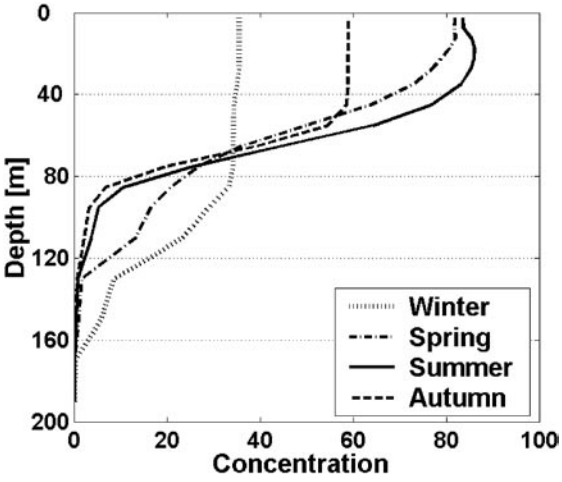

Fig. 4.8 Vertical profile of the averaged tracer concentration in the Preliminary Experiment. The tracer is horizontally averaged at the area where the water depth ranges from 100 m to 200 m along the shelf break at the west of 127°E. (pp.27)

the area where the water depth ranges from 100 m to 200 m along the shelf break. The area was selected since it was expected to be a boundary between the outflow from the Taiwan Strait and the Kuroshio. The tracer from the Taiwan Strait is mainly distributed in the upper part of the shelf. The average tracer concentration falls to about 10 percent in the summer at the depth of 80 m. Taking into account the fact that the depth of the Taiwan Strait is less than 60 m, the summer season with strong stratification by surface heating and relatively weak wind stress allows the water from the Taiwan Strait to be confined to just the upper layer. For simplicity, the vertical section along the 200 m isobath line was divided into an upper layer (0～80 m) and a lower layer (80～200 m). Based on this vertical partition, the Kuroshio intrusion pattern is investigated.

The horizontal distributions of the tracers at depths of 2.5 m and 85 m are shown in Fig. 4.9. In winter, surface cooling and strong wind stress induce vigorous vertical mixing, making the water column homogeneous. The tracer from the Taiwan Strait is distributed in nearly the same area at the surface (2.5 m) and at a deeper layer (85 m). However, different patterns emerge in summer. With the increased inflow transport from the Taiwan Strait, the tracer from the Taiwan Strait covers the surface of the ECS widely. Unlike the surface, concentration of the tracer is reduced remarkably at the deeper layer (85 m). Because the model inflow boundaries are not only the Taiwan Strait but also east of Taiwan, the deeper layer, where showed a low concentration of the tracer from the Taiwan Strait, was filled with the tracer from east of Taiwan (Fig. 4.10).

This experiment cannot give us clear information regarding the location of the vigorous intrusion, how much transport flows into the shelf area of the ECS from the Kuroshio, where the intruded Kuroshio water flows to, and so on. To answer these questions, Experiment 1 was carried out.

4.4 Tracer Experiment 1 (Case.1 — released from a 200 m-line: Control case)

4.4.1 Description of passive tracer experiments

In order to investigate the behavior of the Kuroshio water intruded onto the ECS shelf, the release position was set along the 200 m isobath line. The release position was divided into five local sections of 1 degree interval from 122°E to 127°E and one additional section from 127°E to 128.5°E. Moreover, each local section was divided into two vertical sections: upper layer (0～80 m) and lower layer (80～200 m).

The passive tracers were independent of each other but they moved in the same current field. A tracer which flowed down with the Kuroshio outside of the 200 m isobath line could intrude across other local sections along the 200 m line. To prevent this contamination by the same tracer from outside, when tracers were released along a certain local section, the concentration of tracers along the other local section and from 128.5°E to Kyushu Island on the 200 m isobath line was fixed to 0. The tracers were deployed separately for 30 days through the local sections of the 200 m isobath line. The 30 days were selected for the time that the tracers did not arrive at the K/T Strait. In this way, four seasonal cases were simulated. After a spin up time of six years, four sets of models were ready for the tracer experiments of the seventh year. With the additional calculations of 1 month for a winter case, 4 months for a spring case, 7 months for a summer case, and 10 months for an autumn, the tracers were released

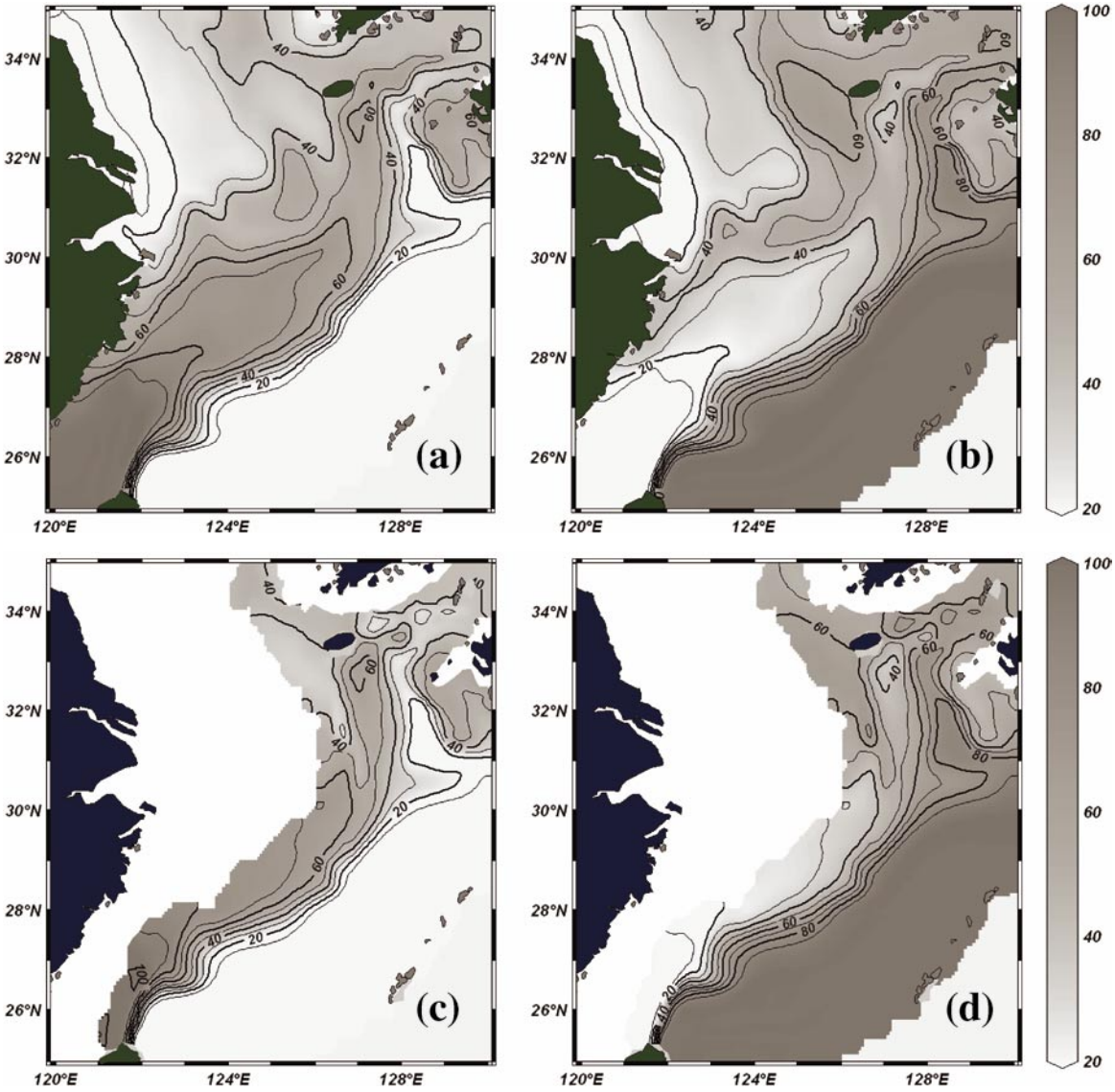

Fig. 4.9 Winter distributions of the tracers in the Preliminary Experiment: surface distributions (2.5 m) of the tracers released from the Taiwan Strait (a) and the east of Taiwan (b). subsurface distributions (85 m) of the tracers released from the Taiwan Strait (c) and the east of Taiwan (d). (pp.28)

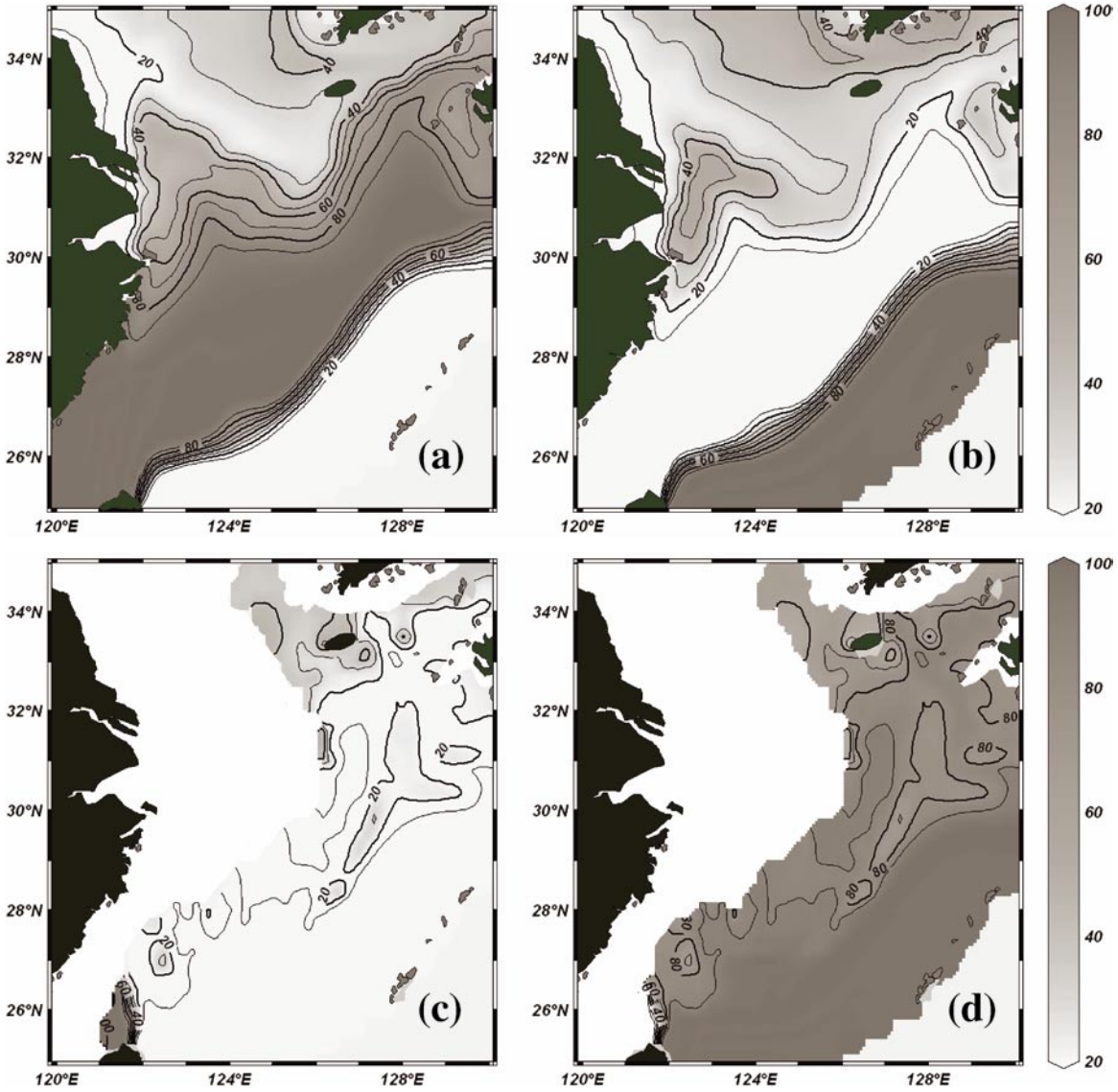

Fig. 4.10 Summer distributions of the tracers in the Preliminary Experiment: surface distributions (2.5 m) of the tracers released from the Taiwan Strait (a) and the east of Taiwan (b). subsurface distributions (85 m) of the tracers released from the Taiwan Strait (c) and the east of Taiwan (d). (pp.28)

on the first day of February for the winter case, May for spring, August for summer, and November for autumn. To show the horizontal distribution of intruded water, a vertically integrated mass was used.

The vertically integrated mass is expressed as follows.

$$\int_V C \cdot dV \tag{4.1}$$

where C is the concentration of the tracer from 0 to 100, and V is volume of each grid including the tracer. The unit is [km^3].

The intruded volume transport across the 200 m line could be calculated by the time derivative of the total amount of water including the passive tracer as demonstrated by Isobe and Beardsley (2006).

$$\frac{\partial}{\partial t}\left(\int_V \frac{C}{100} dV\right) \tag{4.2}$$

Calculating the volume transport using the tracer, the diffusions can lead to the wrong estimation of volume transport, especially regarding the tracer released from the local sections. So, for the calculation of the volume transport, the motion of tracer was set to be affected only by the advection, unlike Isobe and Beardsley (2006). Detailed behavior of the tracer is also shown using the same tracer governed only by the advection in the Tracer experiment 1 and 2. Meanwhile, in the Preliminary experiment and Tracer experiment 3, the tracer is considered to be governed by the advection-diffusion equation like temperature and salinity.

4.4.2 Behavior of the tracer intruded onto the ECS shelf

Fig. 4.11 shows horizontal distributions of intruded tracer through the upper 80 m and below 80 m in winter and summer. The outer thick solid line represents the value of 300 [km^3], which is about 10 % of maximum value. The unit of the vertically integrated tracer, [km^3], is omitted. The contour increments are 600. The value of 1500 is also represented by the thick solid line.

To specify the intrusion pattern of the control case, the detailed spatial distribution of the intruded tracer through each local section below 80 m was investigated (Fig. 4.12). Each contour that is depicted by the different types of line represents the value of 300, the same with the outer thick solid line of Fig. 4.11. Fig. 4.12 clearly shows the region of the main intrusion as indicated by previous studies: northeast of Taiwan (e.g., Chen *et al.,* 1994; Tang *et al.,* 1999; Tang *et al.,* 2000) and west of Kyushu (e.g., Lie and Cho, 1994; Lie *et al.,* 1998; Hsueh *et al.*, 1996). The intrusion from the Kuroshio in the central part of the 200 m line (124 ~ 127°E) is confined to the outer continental shelf. A large difference between winter and summer is seen in the distribution of the tracer intruded through 122~123°E. In winter, the tracer is limited south of 28°N, and extends eastward, while in the summer a part of the tracer intrudes northward into the shallow area. Where does the Kuroshio water intruded through 122 ~ 123°E flow to in winter and summer? There is a need to investigate the spatial variability of the intruded tracer with time. An additional experiment was executed at the end of a spin-up. The tracers were released for 90 days to show the behavior of each intruded tracer. To represent the behavior in each season, the tracers were released one month faster than in Fig. 4.11 and Fig. 4.12: the first day of January for the winter case and that of July for summer.

Fig. 4.13 shows the spatial distributions of the intruded tracer through the upper 80 m and below 80 m in winter and summer. The snapshot results of the tracer distribution were taken with a time interval of ten days. In winter, the pattern of the tracer extension is quite similar in both cases (Fig. 4.13a and Fig. 4.13b). The tracer intruded northeast of Taiwan (122 ~ 123°E) and flows northeastward along the shelf edge. In summer, its distribution is quite different (Fig. 4.13c and Fig. 4.13d). First, the intruded tracer in the upper layer does not flow to the Korea/Tsushima (KT) Strait (Fig. 4.13c). The tracer cannot flow across the 29°N line. Unlike the upper layer, the tracer intruded through the lower layer below 80 m northeast of Taiwan (Fig. 4.13d). The tracers are divided into two major routes: along the shelf and along the small valley in the western ECS. A circle in the center indicates the concentration of the tracer is relatively low because

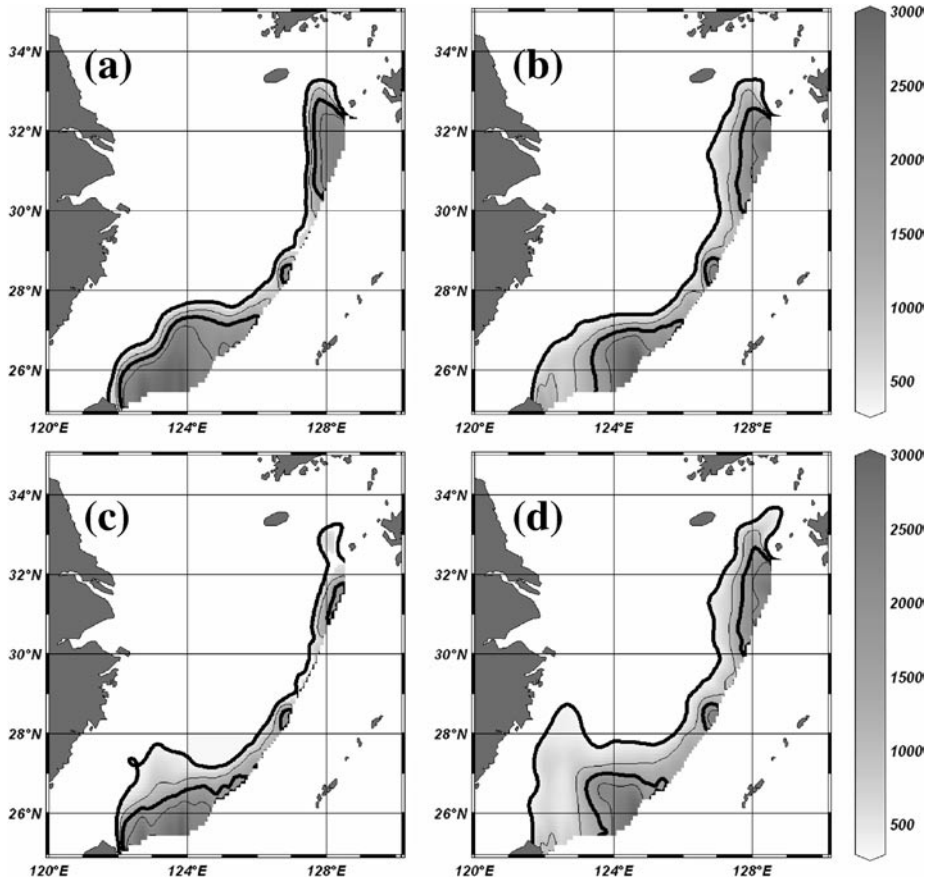

Fig. 4.11 Horizontal distributions of intruded tracer through the upper 80 m and through the below 80 m in winter and summer (Case. 1): the tracers (a) released from 0～80 m in winter, (b) released from 80～200 m in winter, (c) released from 0～80 m in summer, (d) released from 80～200 m in summer. The unit of the vertically integrated tracer, [km^3], is omitted. (pp.30)

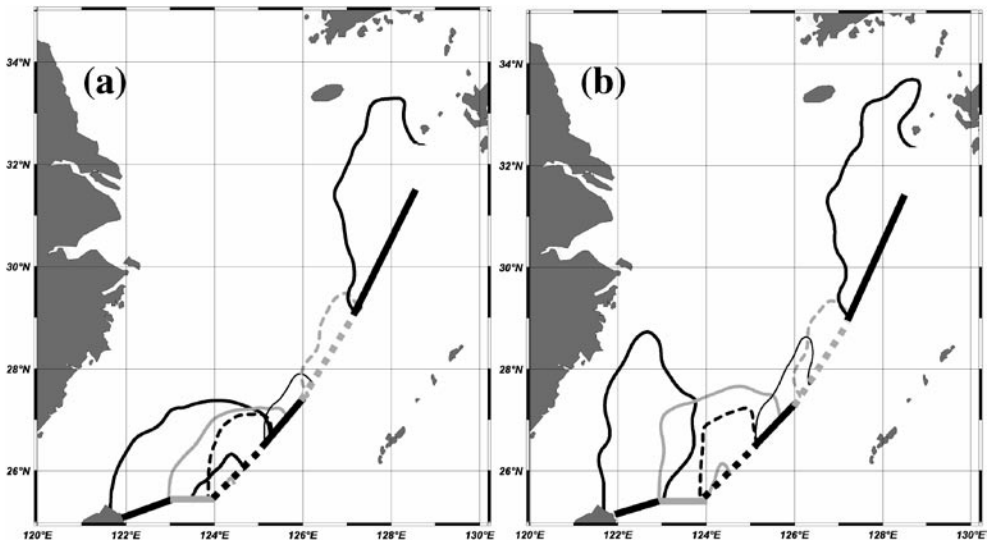

Fig. 4.12 Detailed spatial distribution of the intruded tracer through each local section after 30 days from the release at the 200 m isobath line below 80 m: (a) in winter and (b) in summer. The thick solid or dashed lines with black or gray color along 200 m isobath line represent release positions. The color and shape of the contour lines are matched with those of the line representing the release positions along 200 m isobath line. (pp.30)

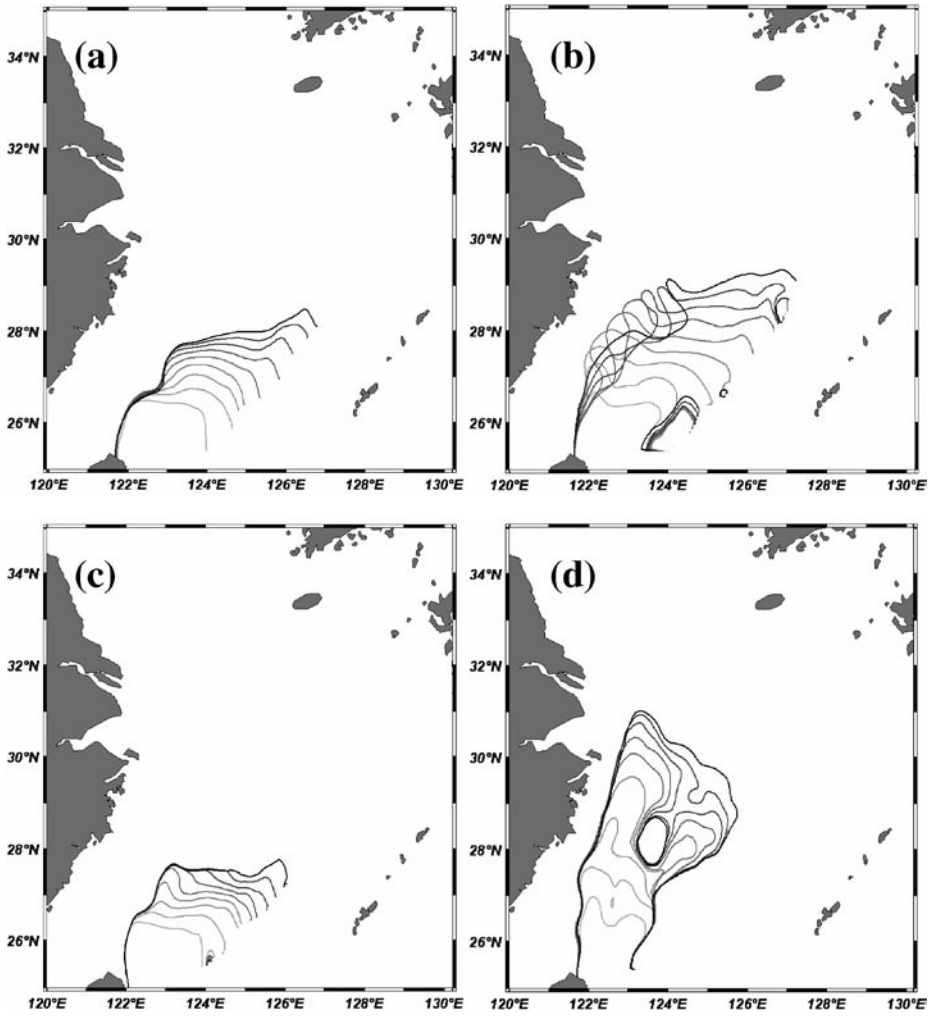

Fig. 4.13 Spatial variability of the intruded tracer through 122°E ~123°E with a time interval of 10 days. The color of line is darkened with time: the tracers (a) released from 0~80 m in winter, (b) released from 80~200 m in winter, (c) released from 0~80 m in summer, (d) released from 80~200 m in summer. (pp.31)

of the local topography bump. It takes about three months to reach the central part of ECS.

Kuroshio water which intruded through the lower layer of 122~123°E in the summer extended into the central part of the ECS. To examine other intrusions through different locations of the 200 m isobath line, the tracers intruded through the lower layer of 123~124°E and 124~125°E in the summer were described. As shown in Fig. 4.14, the intruded Kuroshio water through the lower layer of 123~124°E flows down along the shelf edge, and the Kuroshio water through the lower layer of 124~127°E did not extend far, and remained mainly near the intrusion area of the shelf break. The Kuroshio water through the lower layer of 127~128.5°E flowed into the K/T Strait. As a result, the intruded Kuroshio waters across the 200 m isobath line east of 123°E is not shown here, they also did not extend into the central part of ECS.

The seasonal distribution of the tracer (Fig. 4.11) and its extension (Fig. 4.13) show similar patterns to the schematic view of water mass distribution classified by Su *et al.* (1994) using the hydrographic data (Fig. 4.15). Especially, the summer intrusion through the lower layer below 80 m northeast of Taiwan (Fig. 4.13d) supports the distribution of the

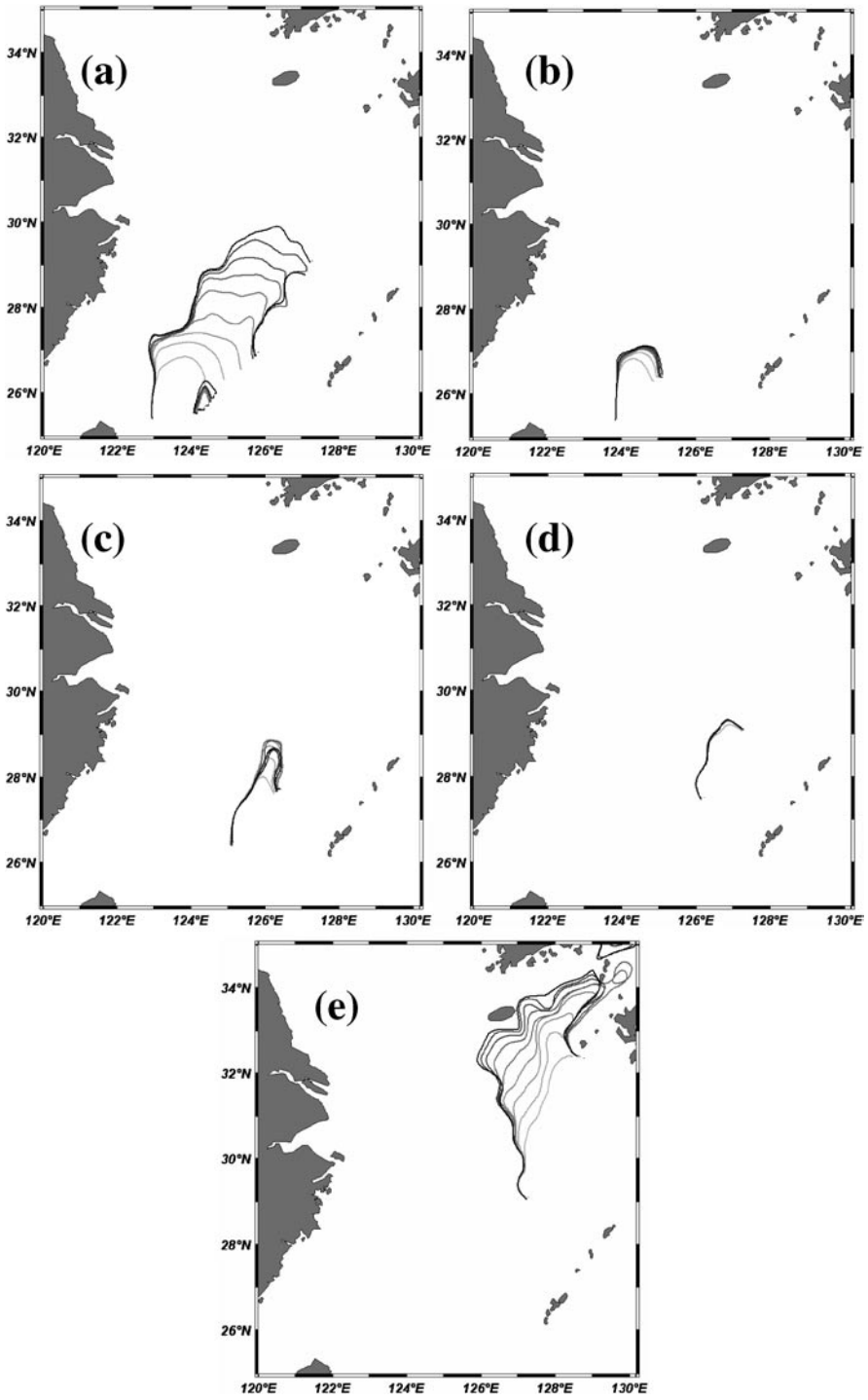

Fig. 4.14 Spatial variability of the intruded tracer (a) through 123°E ~124°E, (b) 124°E ~125°E, (c) 125°E ~126 °E, (d) 126°E ~127°E, and (e) 127°E ~128.5°E at the 200 m isobath line with a time interval of 10 days. The color of the line is darkened with time. (pp.32)

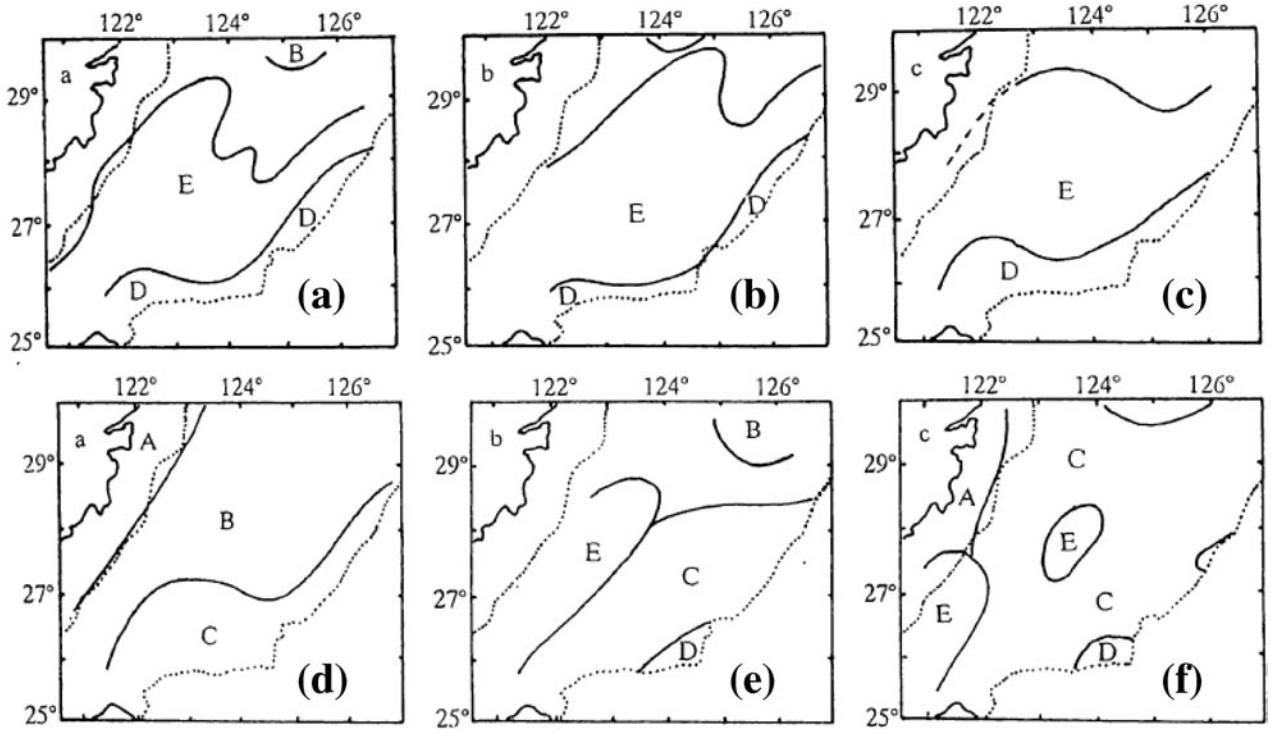

Fig. 4.15 Water mass distributions at the 30 m depth over the ECS shelf for (a) spring of 1988, (b) summer of 1984, and (c) autumn of 1988; Water mass distributions near the bottom of the ECS shelf for (d) winter of 1984/1985, (e) spring of 1988, and (f) summer of 1984. A, Coastal water; B, Winter shelf water; C, Kuroshio subsurface water; D, Kuroshio surface water; E, Taiwan Strait water. (after Su *et al.* 1994) (pp.32)

Kuroshio subsurface water (C in Fig. 4.15f). The observation results reported in Katoh *et al.* (2000) also lead to the existence of a northward current northeast of Taiwan in summer. As shown in Fig. 4.16, the high salinity water (> 34.6 psu) detected by CTD observation can be evidence that the intruded Kuroshio water is distributed below 70 m even at the mouth of the small valley on the western ECS, 28°N and 123°E.

Although there is no current data near the small valley, the observed current data of the southern region, near 27°N and 123°E, show a northward current of about 10～20 cm/s exists at a depth of 70 m, the upper part of the high salinity water in Fig. 4.16b. If there is a northward current about 10～20 cm/s from the northeast of Taiwan, it takes 19～38 days from 25°N to 28°N as a straight line distance, which agrees well with the modeled time scale of one month depicted by Fig. 4.13d. This suggests that the intruded Kuroshio water can have an influence on the central ECS sufficiently through the lower layer in summer.

4.4.3 Volume transport of the Kuroshio intrusion

In order to specify the Kuroshio intrusion, the quantitative value of the Kuroshio intrusion through the local sections was calculated. Table 4.1 shows the value of the intruded volume transport through 80～200 m and 0～200 m, including seasonal variations. The annual average of the Kuroshio intrusion is about 2.62 Sv and the intrusion increased in autumn and in winter, and decreased in spring and summer. However, the ratio of the transport through 80～200 m to that of 0～200 m was clearly increased in the summer (66.4 %) compared with the winter value (48.2 %).

In the previous section, it is shown that the intrusion into the central part of ECS mainly occurs through the lower layer of 122 ～ 123°E in summer. The question arises "How much of the

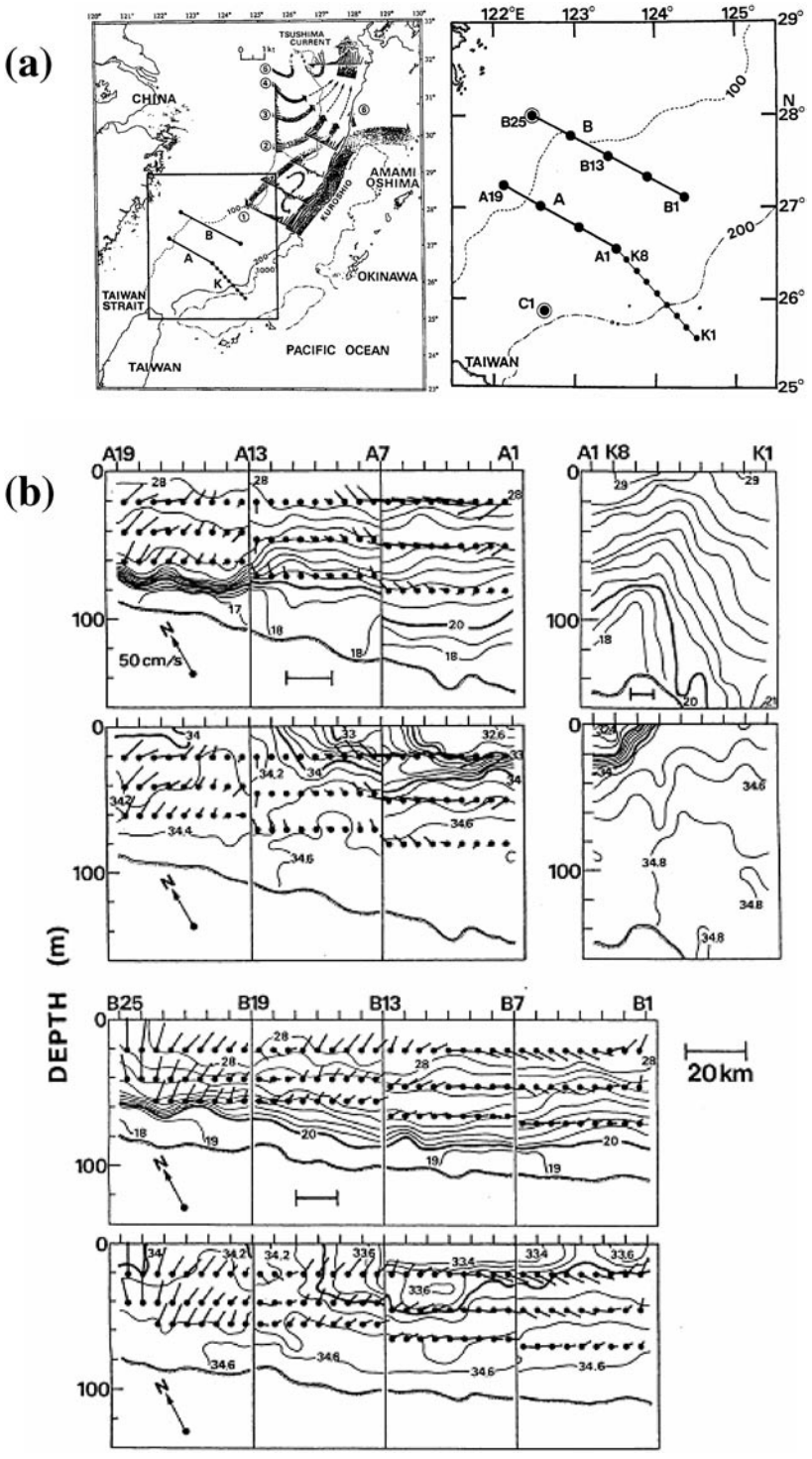

Fig. 4.16 (a) CTD and shipboard ADCP observation lines executed on July 19～30, 1995 (b) vertical distributions of temperature and salinity along transects A, B, and K, together with the diurnally averaged flows from ADCP. (after Katoh *et al.*, 2000) (pp.32)

Table 4.1 Intruded total volume transport through 80～200 m and 0～200 m of the total and local sections for Case. 1, including seasonal variations (Win = winter; Spr = spring, Sum = summer, Aut = autumn). S.A and A.A mean seasonal averaged and annual averaged volume transport, respectively. The volume transport unit is Sv (Sverdrup: 1 Sv = 10 m^6/sec). "Ratio" denotes the ratio of the volume transport through 80～200 m to that through 0～200 m. (pp.33)

		122 °E ~123 °E				123 °E ~127 °E				127 °E ~128.5 °E				Total			
		Win	Spr	Sum	Aut	Win	Spr	Sum	Aut	Win	Spr	Sum	Aut	Win	Spr	Sum	Aut
80~200	S.A	0.41	0.38	0.45	0.32	0.42	0.67	0.72	0.74	0.49	0.46	0.47	0.48	1.32	1.51	1.64	1.54
[m]	A.A	0.39				0.64				0.48				1.5			
0~200	S.A	1.34	0.94	1.05	1.05	0.54	0.82	0.88	1.08	0.86	0.67	0.54	0.71	2.74	2.43	2.47	2.84
[m]	A.A	1.1				0.83				0.7				2.62			
Ratio	S.A	30.6	40.4	42.9	30.5	77.8	81.7	81.8	68.5	57	68.7	87	67.6	48.2	62.1	66.4	54.2
(%)	A.A	36.1				77.5				70.1				57.7			

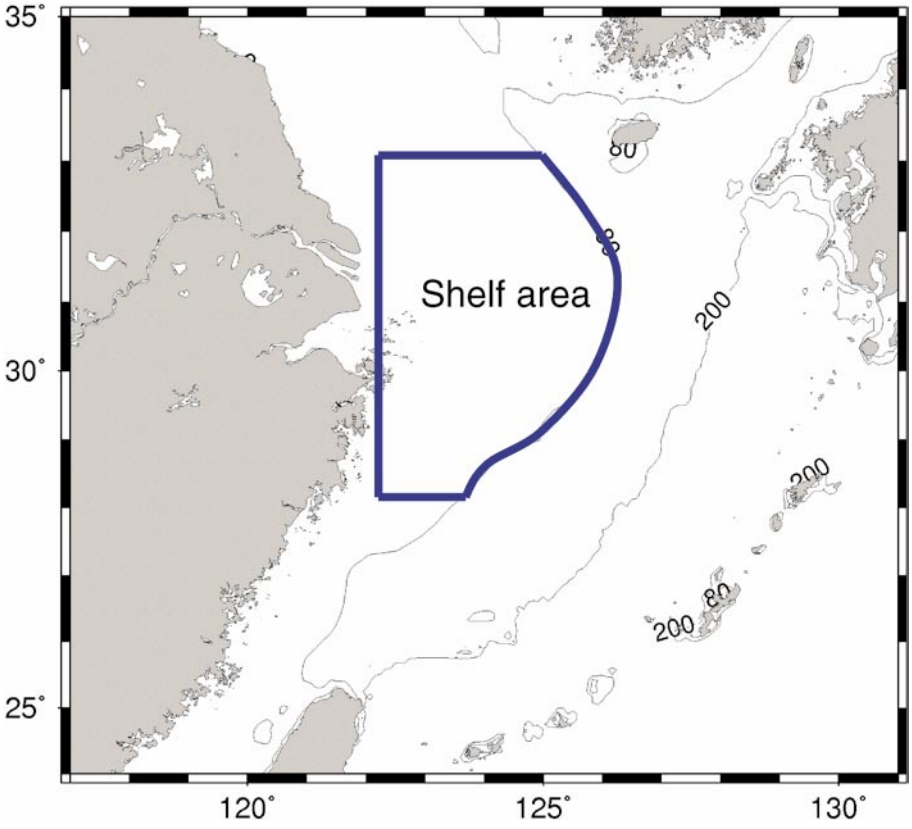

Fig. 4.17 In order to evaluate the volume transport in the central part of ECS, the central part of ECS is defined as the "shelf area". (pp.33)

Kuroshio originated water flows into the central part of ECS?". To evaluate the volume transport in the central part of ECS, the central part of ECS is defined as the "shelf area" (Fig. 4.17). The shelf area in this paper is defined as the area shallower than 80 m south of 33°N, north of 28°N, and east of 122°E. After the previous tracer experiment for one month in summer, in which the tip of the intruded tracer reached the southern edge of the shelf area, the tracer is continuously released at the 200 m isobath line of 122 ~ 123°E for another month. The volume transport of intruded Kuroshio water into the shelf area is calculated by the tracer intruding into the shelf area for one month, with the same method used in the previous section. In this way, the volume transport of the intrusion into the shelf area is calculated for four seasons: 0 Sv for winter, 0.2 Sv for spring, 0.19 Sv for summer, and 0.08 Sv for autumn. This result indicates that the intrusion of Kuroshio water into the shelf area starts in the spring and ends in autumn. The volume transport of the Kuroshio intrusion in summer, 0.19 Sv, is approximately three times the volume transport in summer from the Changjiang River, 0.06 Sv, signifying the intruded Kuroshio water through the lower layer of 122~123°E can transport a great deal of nutrients to the shelf area as well as heat and salt in the summer season.

4.5 Summary

In this Chapter, the intrusion of the Kuroshio onto the ECS shelf was investigated using 3-D numerical model. The model successfully simulated the main current patterns in the ECS: the Kuroshio, the current from the Taiwan Strait, the Tsushima Warm Current. Comparison with the vertical section in the PN line also showed the validation of the model.

After a spin up time of six years, passive tracer experiments were executed using passive tracers which were governed by the same advection-equation that determined the temperature and salinity (Preliminary experiment), or governed only by the advection (Tracer experiment 1). Preliminary experiment, which released tracers at the inflow boundaries, showed that the tracer from the Taiwan Strait and the east of Taiwan were approximately divided into two layers near the depth of 80 m in summer, and water mass originated from the Kuroshio widely distributed at the lower layer. In order to investigate the main intrusion region from the Kuroshio, and its seasonal behavior, Experiment 1 was carried out, releasing the respective tracers into two vertical and five horizontal sections along the 200 m isobath line. The passive tracer experiment revealed that the main intrusion from the Kuroshio takes place east of Taiwan and west of Kyushu, as reported by previous studies. Because the intruded Kuroshio water at the west of Kyushu flows northward and most of it enters the K/T Strait, it can be concluded that the east of Taiwan (122 ~ 123°E) is the main entrance of the Kuroshio intrusion onto the ECS shelf.

The Kuroshio intrusion east of Taiwan shows large seasonal variation. In winter, the tracer released at both layers (0 ~ 80 m and 80 ~ 200 m) just intrudes up to south of 28°N at the north of Taiwan, while the tracer released at the lower layer intrudes farther northward and flows into the small valley on the western ECS in summer. The Kuroshio intrusion across the 200 m isobath line takes place all year round, but the intrusion into the shelf area shallower than 80 m only starts in spring and ends in autumn.

Chapter 5. Mechanism of the Kuroshio intrusion

5.1 Introduction

The Kuroshio, which flows northward along the eastern coast of Taiwan, collides a steep topography east of Taiwan, and changes its direction as a result of geostrophic adjustment. In this procedure, some of it intrudes into the ECS and gives a considerable effect on the ECS shelf area such as supply of nutrients much greater than the river input, as estimated by Chen and Wang (1999). Northeast of Taiwan, the Kuroshio Edge Exchange Processes (KEEP) project of Taiwan (1989 ~ 2000) has contributed to understanding the Kuroshio intrusion and the current pattern, and some papers related to the project are already reviewed in Chapter 2.

As for the intrusion of the Kuroshio east of Taiwan, some mechanisms are suggested in the previous studies: planetary beta effect and the

existence of Taiwan Island (Qiu and Imasato, 1990), wind effect (Chao, 1990), topography and thermal wind effect of the shelf break upwelling (Chern and Wang, 1990), incidence angle and the depth of shelf-break (Hsueh *et al.,* 1992), increase of potential energy by upwelling (Liu *et al.,* 1992), cooling effect (Chuang and Liang, 1994), geostrophic adjustment of the Kuroshio due to the loss of the steep wall of the Taiwan coast (Su *et al.* 1994).

Since Sarkisyan and Ivanov (1971) introduced the concept of "Joint Effect of Baroclinicity and Relief (JEBAR) term" which is derived from the vertical integration of vorticity equation, it had been regarded as a strong tool for the theoretical and diagnostic interpretation of ocean circulation. Introducing this diagnositic tool, in recent years, Isobe (1999a) and Guo *et al.* (2006) explained the main mechanism of the Kuroshio intrusion northeast of Taiwan by JEBAR term and Ekman term in the vorticity equation of the vertically averaged flow. They considered the JEBAR term as a forcing term to generate the velocity fields. Meanwhile, Mertz and Wright (1992) and Pohlmann (1999) explained the JEBAR term as a correction term rather than a forcing term. Chen (2004) reported that maximum and minimum of the JEBAR distribution on the ECS shelf correlates well with shelf break or strait where strong currents exist, and emphasized that the JEBAR plays an important role in the depth-averaged vorticity balance along shelf break and strait where the JEBAR is much larger by two orders of magnitude than other vorticity terms, while it plays a minor role in shallow shelf waters.

In this chapter, in a different manner, the mechanisms of the Kuroshio intrusion is investigated by several model case studies and momentum balance analysis.

5.2 Tracer Experiment 2

5.2.1 Effect of tide (Case.1, 2)

Case.1 is a control case, which was executed by the boundary conditions explained in Chapter 2. For Case.2, the same boundary conditions was used but without consideration of the tide effect. The viscosity and diffusivity by tidal motion was not included and a quadratic bottom friction with the bottom drag coefficient of 0.0025 was used in Case.2.

Volume transports of the Kuroshio intrusion for Case.1 and Case.2 are shown in Fig. 5.1. Considering the effect of the M_2 tide, the intrusion from the Kuroshio across the 200 m isobath line was considerably decreased. As shown in Fig. 5.1b and 5.1c, the decrease of the Kuroshio intrusion mainly occurred east of Taiwan (122 ~123°E). Fig.

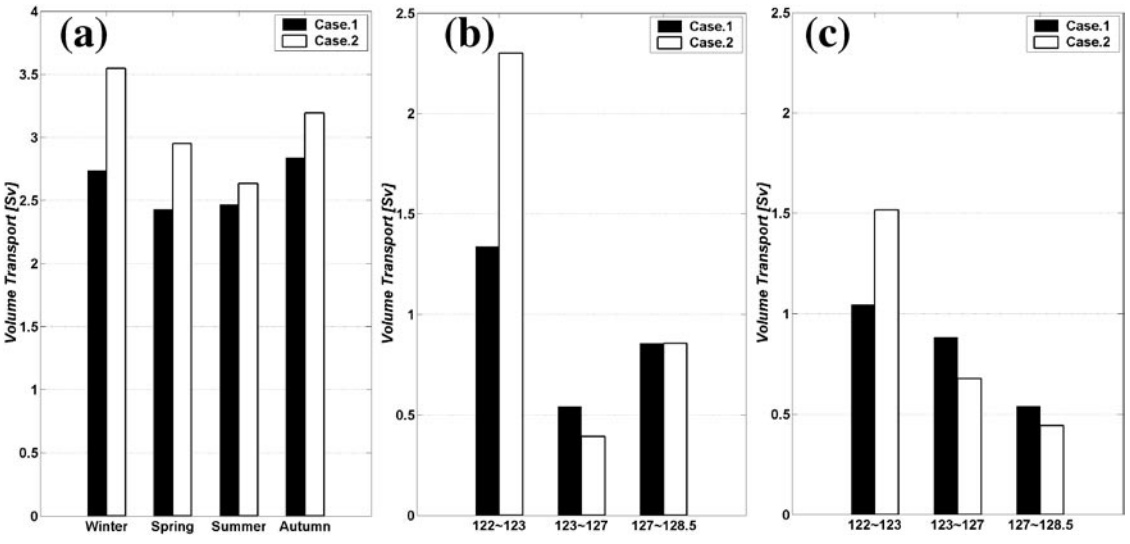

Fig. 5.1 Seasonal variation of the total intruded volume transport through the whole depth of the 200 m line (a), the transport through the local section in winter (b) and in summer (c) for Case.1 and Case.2. (pp.37)

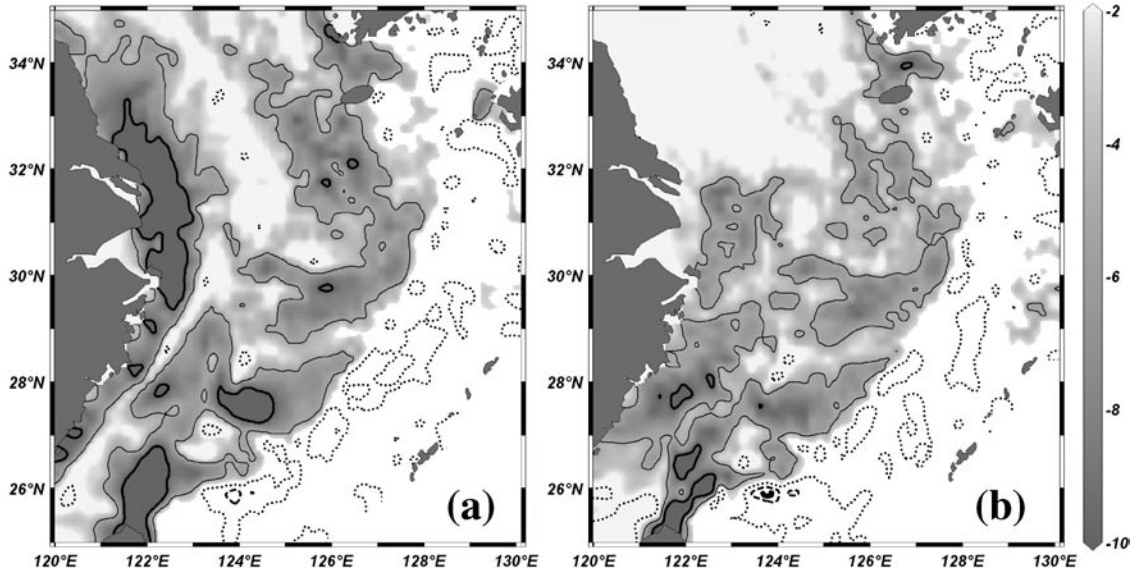

Fig. 5.2 Difference of velocity at the bottom layer (Case.1 minus Case.2): (a) in winter, (b) in summer. The unit is [cm/s] and the negative value indicates that bottom velocity at which Case.1 is smaller than that of Case.2. The thick solid line represents a contour of −10 cm/s, the thin solid line −5 cm/s, the dotted line 0 cm/s, and the thick dashed line 5 cm/s. (pp.37)

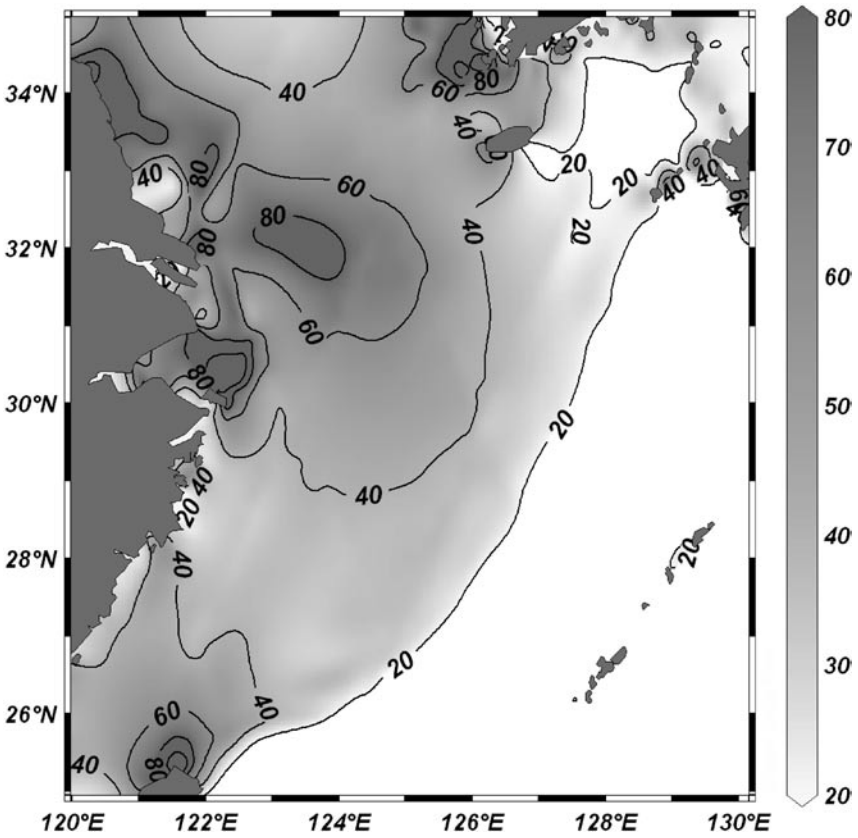

Fig. 5.3 Amplitude of the M_2 tidal current calculated by the NAO.99Jb model (Matsumoto *et al.*, 2000) (pp.37)

5.2 shows the difference of velocity in the bottom layer between Case.1 and Case.2. The velocity near the bottom mainly decreased on the shelf region, and the decreased velocity amounts to ~ 10 cm/s northeast of Taiwan. The strong M_2 tidal current east of Taiwan (Fig. 5.3) intensified the vertical viscosity, vertical diffusivity, and the bottom friction.

On the other hand, at the central part of the shelf break, 123 ~ 127°E, the intrusion increased slightly in Case.1. This is due to the velocity of the M_2 tidal current near the shelf break at 123 ~ 127°E which is smaller than the background current using the quadratic bottom friction in Case.2.

As for the intrusion into the shelf region in Case.2, the volume transport of the intrusion into the shelf area was calculated for four seasons: 0 Sv for winter, 0.24 Sv for spring, 0.21 Sv for summer, and 0.09 Sv for autumn. Although slightly larger than Case.1, these values are not very different compared with the estimated transports in Case.1. The reason is explained in the section 5.3.2.

5.2.2 Effect of transport from the Taiwan Strait (Case.3, 4, 5, 6)

Volume transport from the Taiwan Strait has been disputed by many researchers. In this study, the result of Wang *et al.* (2003) was adopted: the maximum transport (2.7 Sv) in July and the minimum (0.9 Sv) in January. To investigate the effect of transport from the Taiwan Strait, four cases (Case.3, 4, 5, 6) were compared. Based on the boundary conditions of the control case (Case.1), Case.3, 4 increased the volume transport from the Taiwan Strait by as much as 0.7 Sv, while, Case.5, 6 decreased 0.7 Sv through the whole year. The variation components of each transport were maintained, and the average transport was increased (or decreased). The inflow transport from the east of Taiwan had the same value for all cases.

Case.3 (Case.5) set the increased (decreased) transport to flow out through the K/T Strait, and Case.4 (Case.6) set the increased (decreased) transport to flow out through the Tokara Strait, respectively. Fig. 5.4 shows the transport through the Taiwan Strait, the K/T Strait, and the Tokara Strait for each case.

It is obvious that the inflow through the Taiwan Strait causes outflow through the K/T Strait or the Tokara Strait. However, it is not yet clear how much the increased or decreased transport from the Taiwan Strait affects the K/T Strait or the Tokara Strait. We assumed four extreme cases in which the increased transport totally affects the K/T Strait (Case.3) or the Tokara Strait (Case.4), and the decreased transport totally affects the K/T Strait (Case.5) or the Tokara Strait (Case.6). The difference in transport from the Taiwan Strait between Case.3, 4 and Case.5, 6 is 1.4 Sv, however, as shown in Fig. 5.5 (a), the difference of the intrusion from the Kuroshio region is smaller than that, especially in summer. This result shows that the intrusion from the Kuroshio is not totally controlled by the net transport between the Taiwan Strait and K/T Strait, leading to conclude that the evaluation of the intruded transport from the Kuroshio is important to understand the nutrient supply from the Kuroshio into the ECS.

In spite of the large transport difference from the Taiwan Strait, the intrusion below 80 m did not change greatly except during winter. This proves the transport from the Taiwan Strait mainly affects the intrusion only from the upper layer of the Kuroshio region, except during winter.

5.2.3 Effect of transport from east of Taiwan (Case.7, 8)

Lee *et al.* (2001) suggested that the seasonal cycle of the Kuroshio transport east of Taiwan is controlled by a combination of local along-channel wind forcing and Sverdrup forcing over the Philippine Sea. As a control case (Case.1), the result of Lee *et al.* (2001), which has seasonal variations of the transport of 24 Sv in summer and a minimum transport of 20 Sv in fall, was adopted for the volume transport east of Taiwan. And, in order to clarify the effect of the transport variation of the Kuroshio, two cases (Case.7, 8) were compared. On the basis of the volume transport for Case.1, Case.7 (Case.8) increased (decreased) the volume transport from east of Taiwan by as much as 1.6 Sv. The inflow transports from the Taiwan Strait for Case.7 and Case.8 were the same as Case.1, and the outflow volume transport through the Tokara Strait increased (decreased) as much as the increased

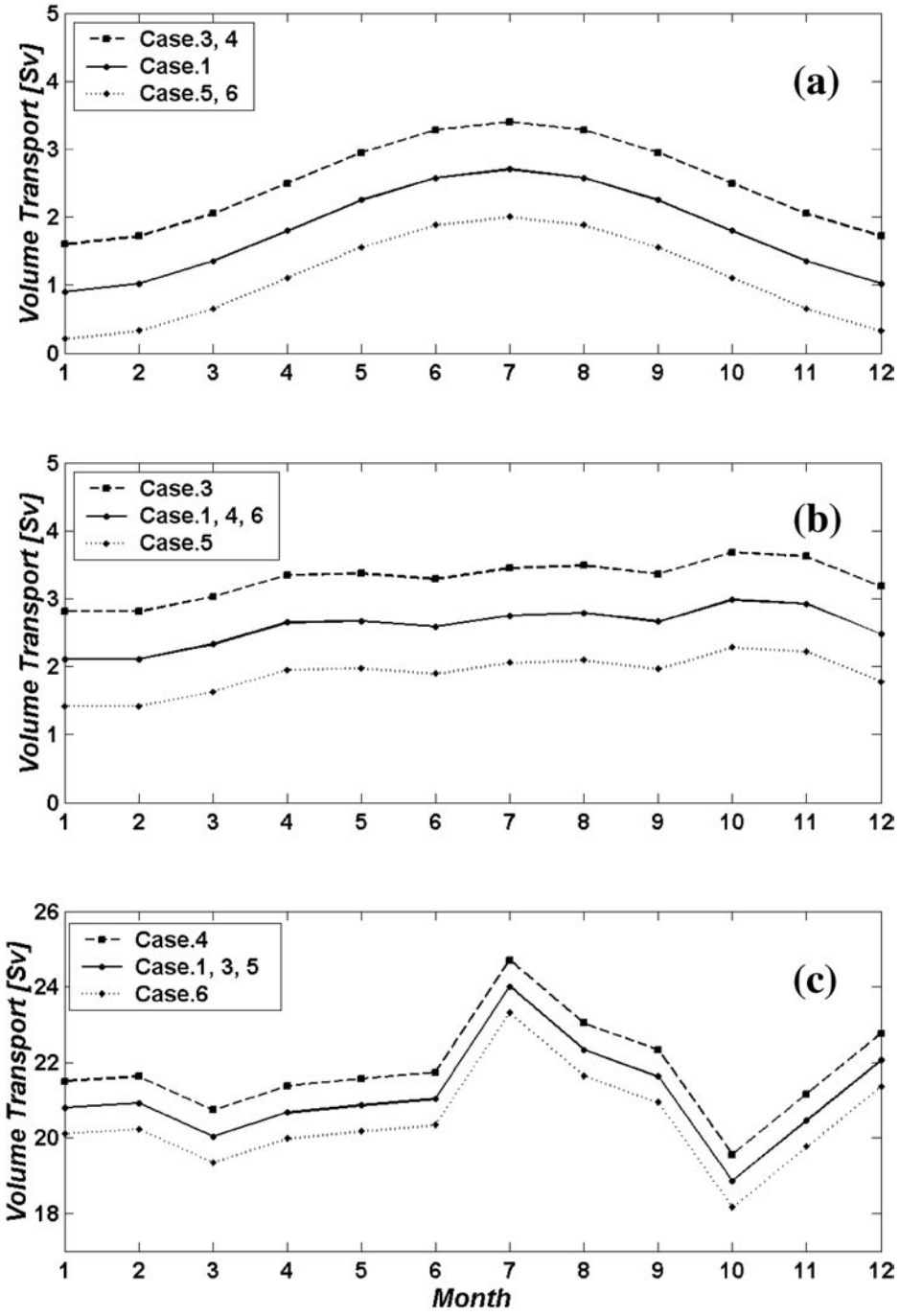

Fig. 5.4 Monthly value of each volume transport through (a) the Taiwan Strait, (b) the K/T Strait, and (c) the Tokara Strait for Case.1, 3, 4, 5, 6 (pp.38)

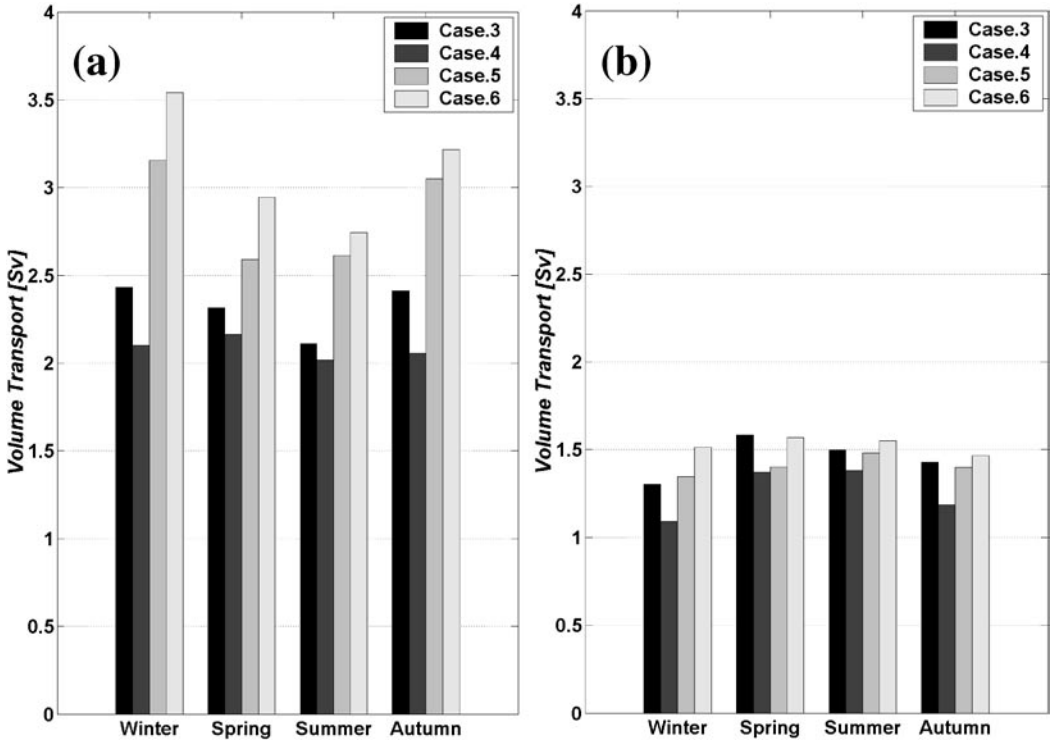

Fig. 5.5 Seasonal variation of the total intruded volume transport through the whole depth of the 200 m line (a), and through 80~200 m (b) for Case.3, 4, 5 ,6 (pp.39)

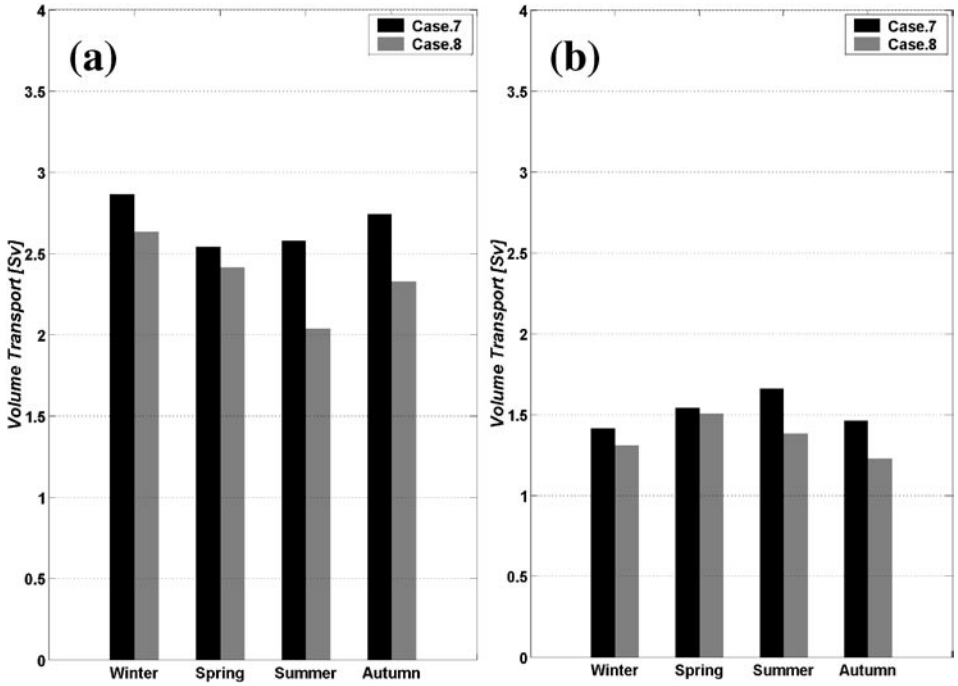

Fig. 5.6 Seasonal variation of the total intruded volume transport through the whole depth of the 200 m line (a), and through 80~200 m (b) for Case.7, 8 (pp.39)

(decreased) volume transport from east of Taiwan.

Fig. 5.6 shows the volume transport of the Kuroshio intrusion through 0 ~ 200 m and 80 ~ 200 m for each case. When the transport from east of Taiwan was increased, the intrusion from the Kuroshio also increased. With the inflow difference of 3.2 Sv from east of Taiwan for Case.7 and Case.8, the Kuroshio intrusion changed ~10% of the inflow difference (~0.4 Sv on an average).

5.3 Momentum balance analysis

5.3.1 Description of the experiment

The model produces dynamically balanced results, so that it can be used to examine the terms that make up the individual components of the momentum equation. These terms control the momentum balance and, hence, account for spatial and temporal variations of the current field. This section deals with the momentum balance by comparing both cases including and excluding the tide effect (Case.1 and Case.2) of the seventh year, i.e. the first year after a spin up time of six years. The temporal variations of each component in the momentum equations are investigated along the line of 122.58°E from 25°N to 29.5°N, which represented the dominant seasonal variations of the Kuroshio intrusion pattern as shown in the previous Chapter (Fig. 4.12). Each component of the momentum equation was daily averaged for a year after a spin up time of six years. The components are explained by acronyms in the momentum equations on the Cartesian form.

$$\underbrace{\frac{\partial u}{\partial t}}_{} = \underbrace{-\left(u\frac{\partial u}{\partial x}+v\frac{\partial u}{\partial y}\right)}_{\text{SHADU}} \underbrace{-w\frac{\partial u}{\partial z}}_{\text{SWU}} \underbrace{+fv}_{\text{USCO}} \underbrace{-\frac{1}{\rho_0}\frac{\partial p'}{\partial x}}_{\text{PSX}} \underbrace{-g\frac{\partial \eta}{\partial x}}_{\text{PNX}} \underbrace{+A_h\left(\frac{\partial^2 u}{\partial x^2}+\frac{\partial^2 u}{\partial y^2}\right)}_{\text{USDIF}} \underbrace{+A_z\left(\frac{\partial^2 u}{\partial z^2}\right)}_{\text{WDIFU}} \quad (5.1)$$

$$\underbrace{\frac{\partial v}{\partial t}}_{} = \underbrace{-\left(u\frac{\partial v}{\partial x}+v\frac{\partial v}{\partial y}\right)}_{\text{SHADV}} \underbrace{-w\frac{\partial v}{\partial z}}_{\text{SWV}} \underbrace{-fu}_{\text{VSCO}} \underbrace{-\frac{1}{\rho_0}\frac{\partial p'}{\partial y}}_{\text{PSY}} \underbrace{-g\frac{\partial \eta}{\partial y}}_{\text{PNY}} \underbrace{+A_h\left(\frac{\partial^2 v}{\partial x^2}+\frac{\partial^2 v}{\partial y^2}\right)}_{\text{VSDIF}} \underbrace{+A_z\left(\frac{\partial^2 v}{\partial z^2}\right)}_{\text{WDIFV}} \quad (5.2)$$

This equation states that current accelerations are driven by the balance between horizontal advection (SHADU, SHADV), vertical advection (SWU, SWV), Coriolis force (USCO, VSCO), pressure gradient force by density field (PSX, PSY), pressure gradient force by surface elevation (PNX, PNY), horizontal friction (USDIF, VSDIF), and vertical friction (WDIFU, WDIFV). In addition, the term "GEOX" and "GEOY" are used to distinguish from the ageostrophic components.

$$\text{GEOX} = \text{PNX} + \text{PSX} + \text{USCO} \quad (5.3)$$

$$\text{GEOY} = \text{PNY} + \text{PSY} + \text{VSCO} \quad (5.4)$$

Based on the component analysis, the mechanisms of the Kuroshio intrusion are analyzed.

5.3.2 Momentum balance analysis

A horizontal line for momentum balance analysis along 122.58°E is represented by thick solid line in Fig. 5.7. Fig. 5.8 to 5.11 show the temporal variations of the daily averaged momentum terms at the depth of 2.5, 22.5, 45, and 85 m, respectively. X-axis indicated the time in days, and y-axis is the latitude. The shading and contour lines are presented in units of m/s^2. The figures shows that the most dominant terms are pressure gradient by surface elevation and Coriolis terms, which are mainly balancing in both x and y momentum equations (zonal and meridional directions of momentum equation). In addition, dominant seasonal variations are seen south of 26°N and from 27°N to 29°N. The maximum or minimum values of the pressure gradient terms appeared near the 200 days, i.e., July, when the volume transport from the Taiwan Strait reaches the maximum value.

For easy understanding, the values of respective terms in summer (thick solid line) and in winter (thin solid line) are presented on the same scale from Fig. 5.12 to Fig. 5.15 for the depth of 2.5,

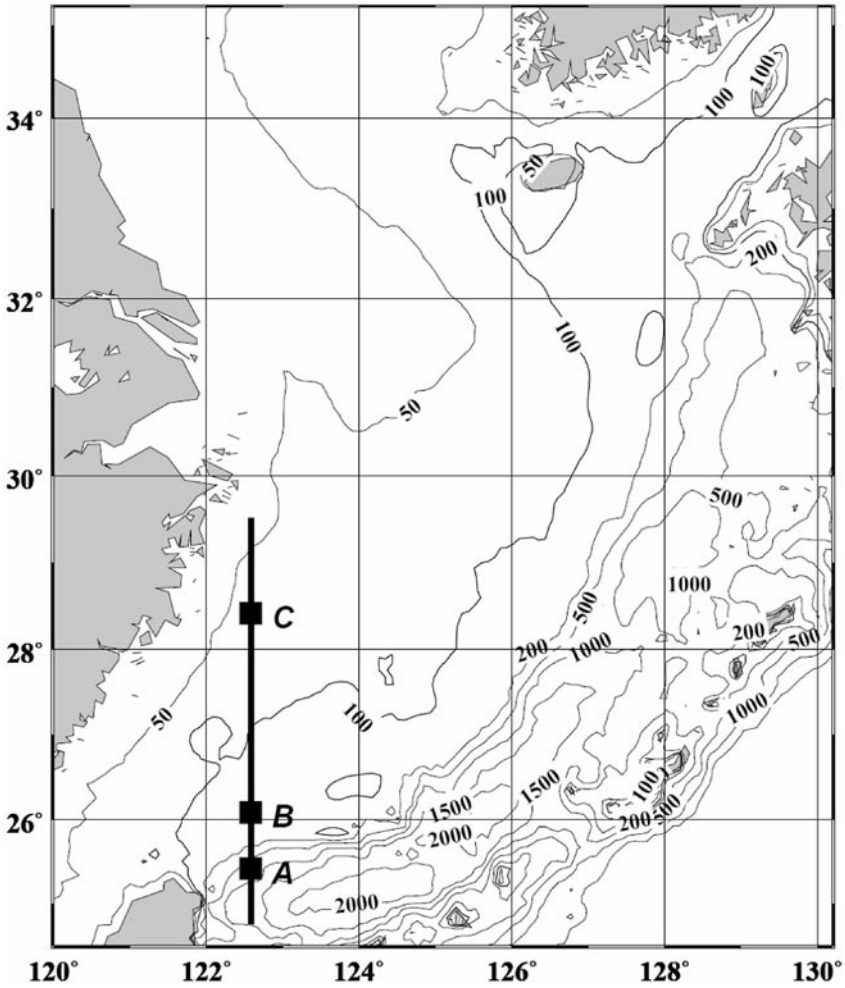

Fig. 5.7 A line and three points for momentum balance analysis along 122.5°E. (pp.41)

22.5, 45, and 85 m, respectively. The horizontal axis denotes latitude and the vertical axis magnitude of terms in units of m/s^2. East of Taiwan near 25°N, the Kuroshio flows northward balancing negative pressure gradient term by surface elevation (PNX) and positive Coriolis terms (USCO) in the x-momentum equation (zonal direction), which means inflow of a geostrophic current into the ECS. Large values of PNX and USCO also appear north of 27°N in summer. In the y-momentum equation (meridional direction), the large positive value of pressure gradient term (PNY) appears around 25~26°N in all year round and 28°N just in summer.

These figures indicates that the momentum balance along 122.58°E northeast of Taiwan was highly dominated by a geostrophic balance between the pressure gradient by surface elevation (PNX, PNY) and the Coriolis terms (USCO, VSCO). Momentum balance analysis at three points in Fig. 5.7 (point A, B, C) show clearer signs on the behavior of the Kuroshio. Point A is the place where the Kuroshio is forced to turn eastward by curved topography (Fig. 5.16a), point B some of the Kuroshio upwells over the steep topography (Fig. 5.16b), and point C the Kuroshio water intrudes onto the shelf area north of 28°N in the summer season (Fig. 5.16c). The magnitude of ageostrophic components (GEOX, GEOY) are mainly balanced with the vertical friction term induced by the wind stress at the surface layer (2.5 m depth) of all points. However, other momentum components become significant at respective places, i.e., point

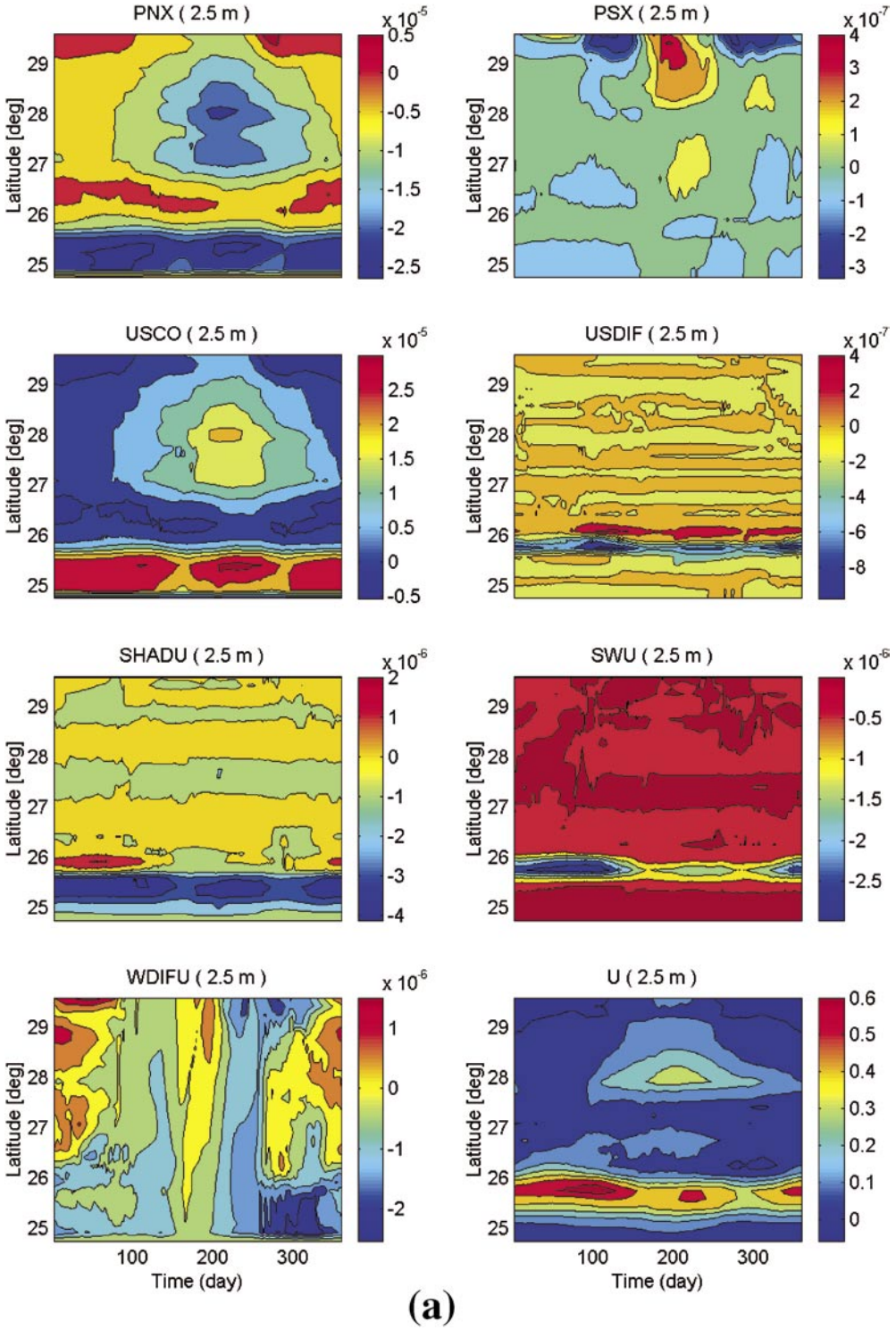

Fig. 5.8 Momentum components (units: m/s^2) and velocity (units: m/s) along 122.58°E at 2.5 m depth (a) in the x-direction and (b) in the y-direction of momentum equation. (pp.41)

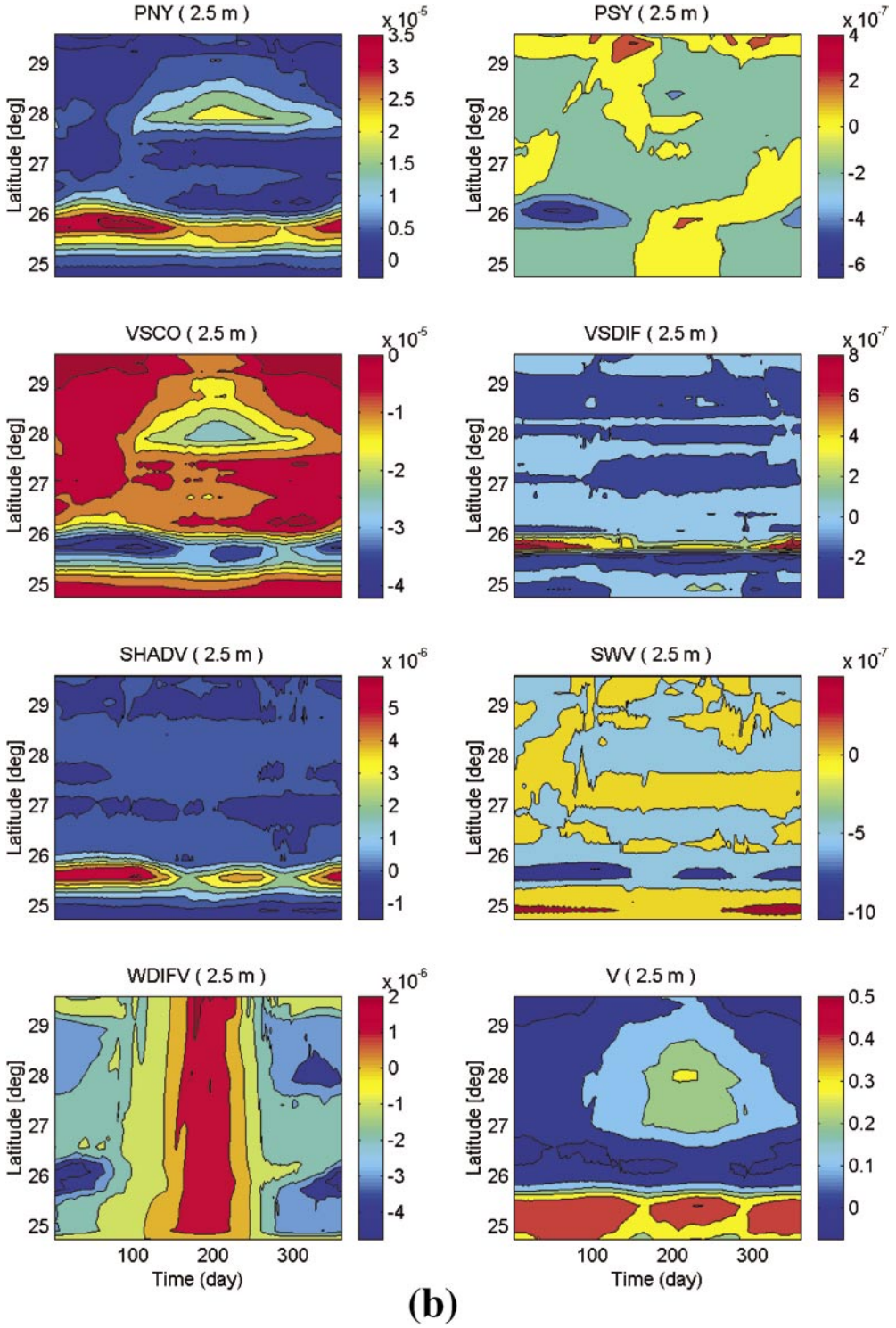

Fig. 5.8 (Continued)

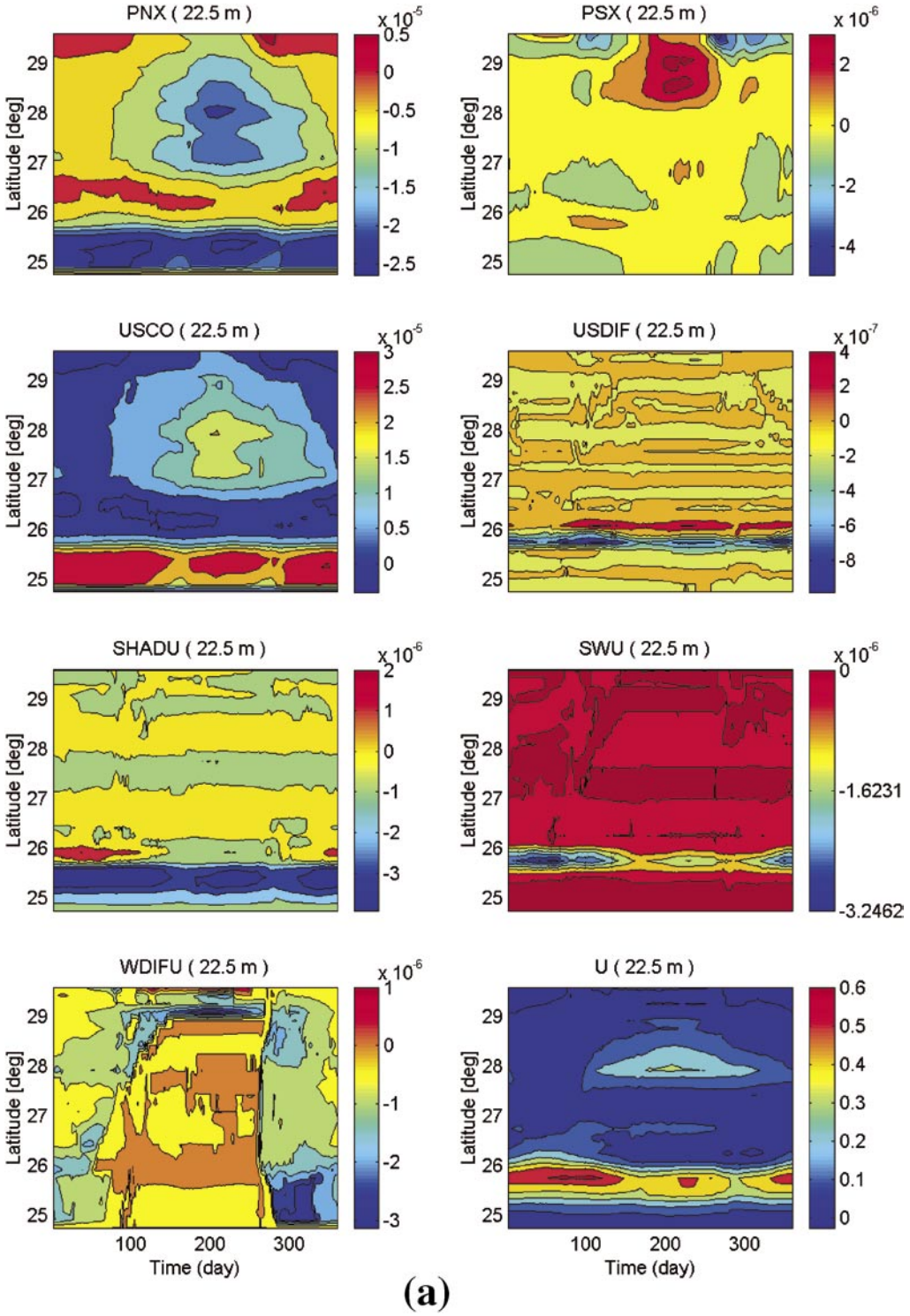

Fig. 5.9 Momentum components (units: m/s^2) and velocity (units: m/s) along 122.58°E at 22.5 m depth (a) in the x-direction and (b) in the y-direction of momentum equation. (pp.41)

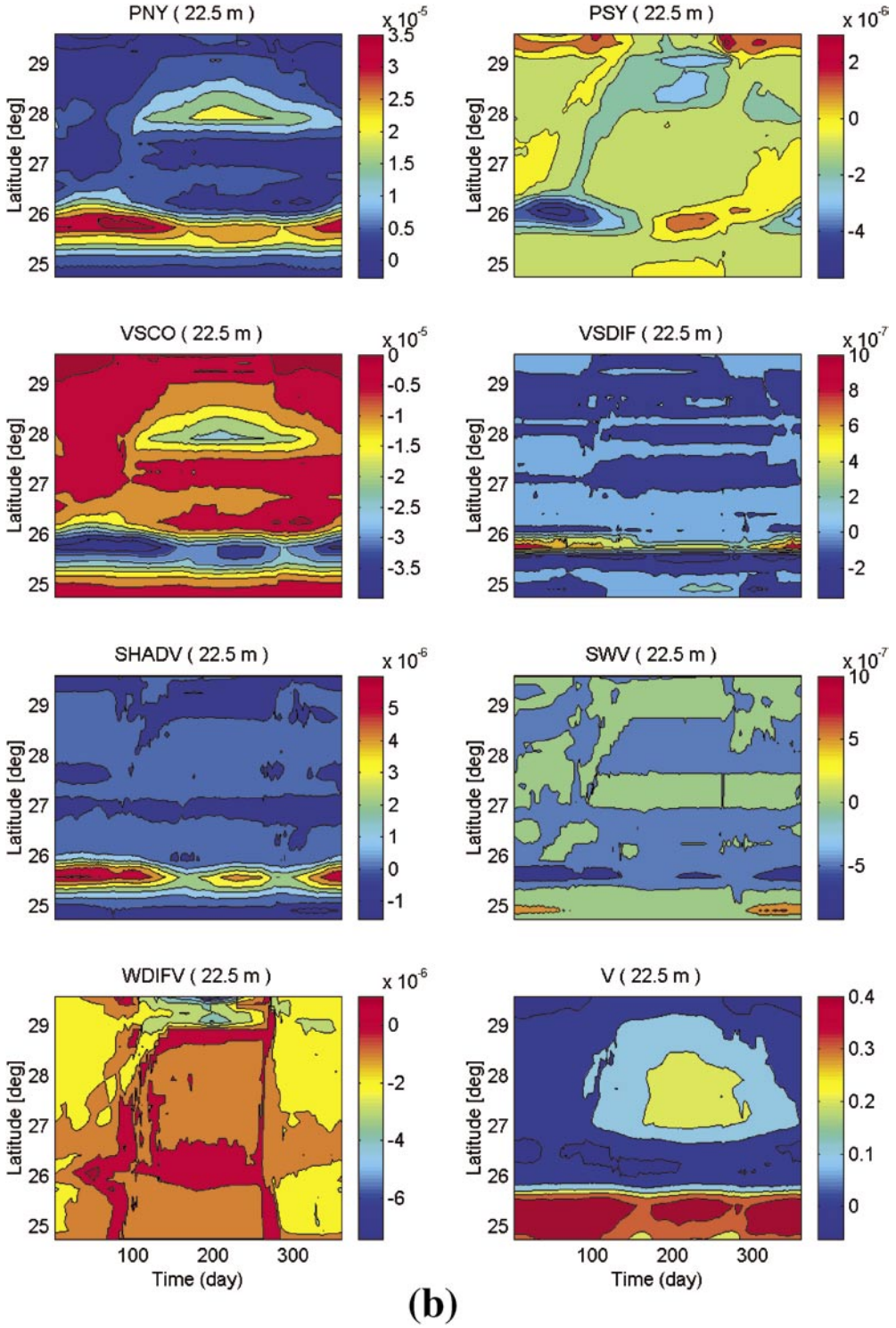

Fig. 5.9 (Continued)

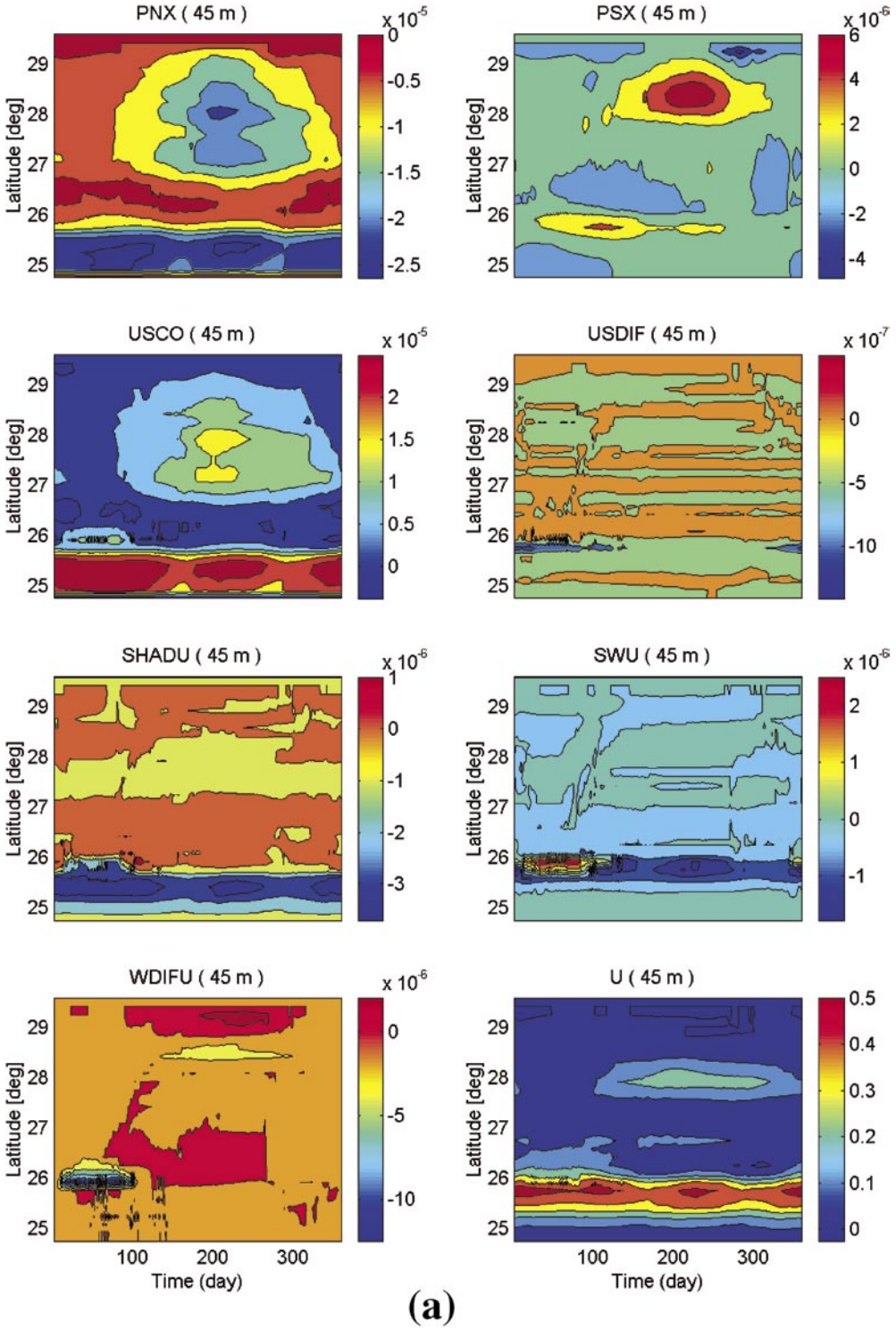

Fig. 5.10 Momentum components (units: m/s^2) and velocity (units: m/s) along 122.58°E at 45 m depth (a) in the x-direction and (b) in the y-direction of momentum equation. (pp.41)

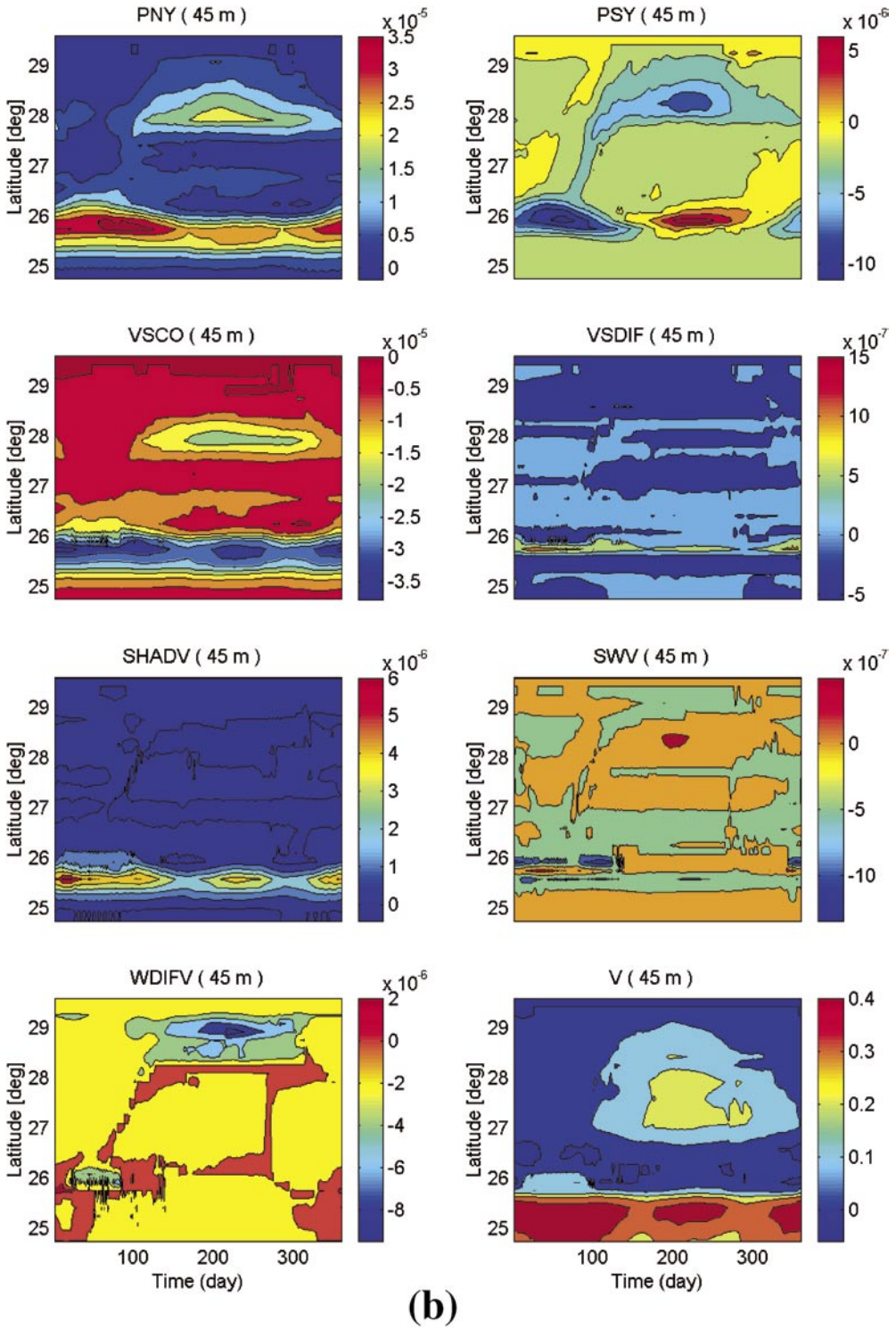

Fig. 5.10 (Continued)

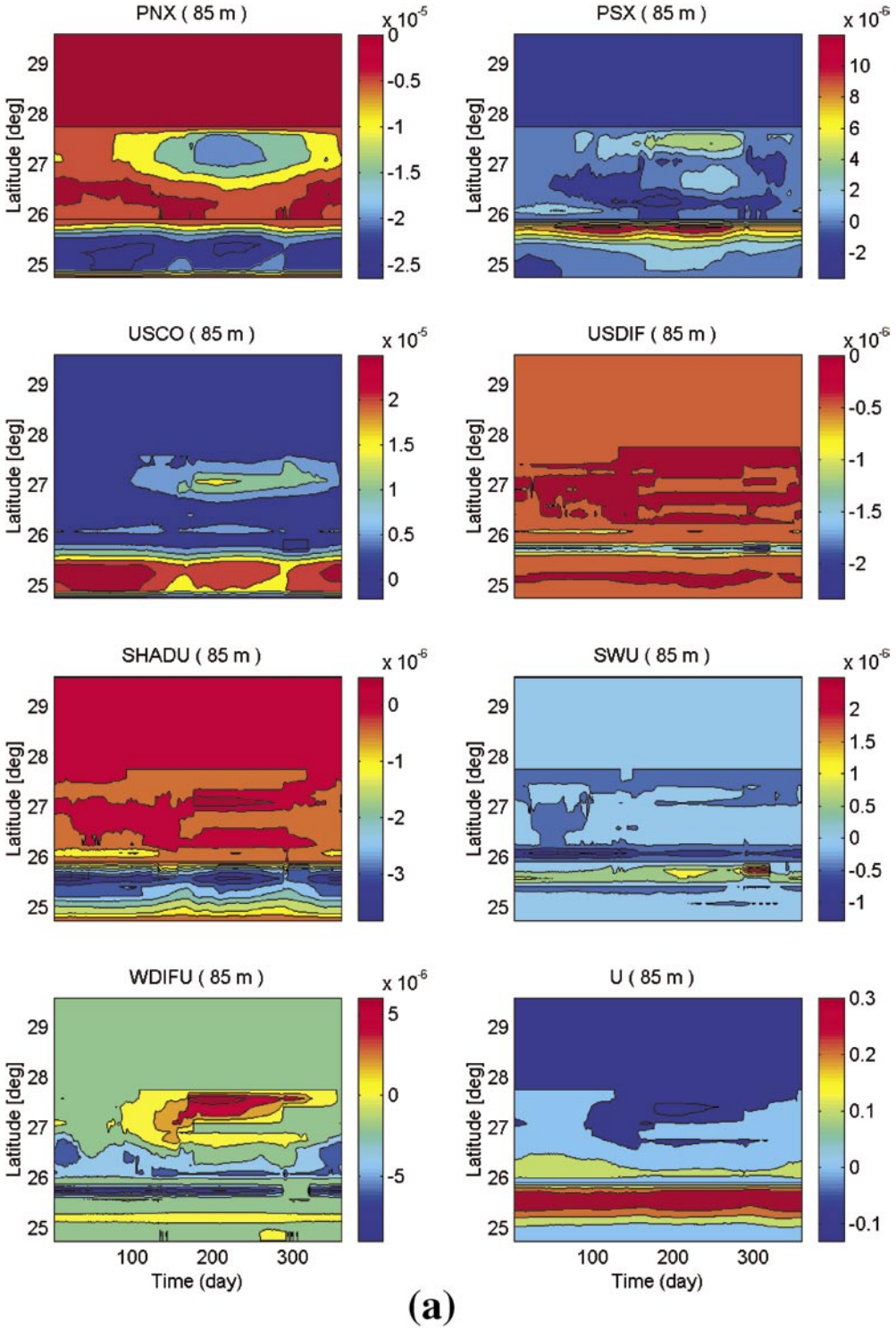

Fig. 5.11 Momentum components (units: m/s^2) and velocity (units: m/s) along 122.58°E at 85 m depth (a) in the x-direction and (b) in the y-direction of momentum equation. (pp.41)

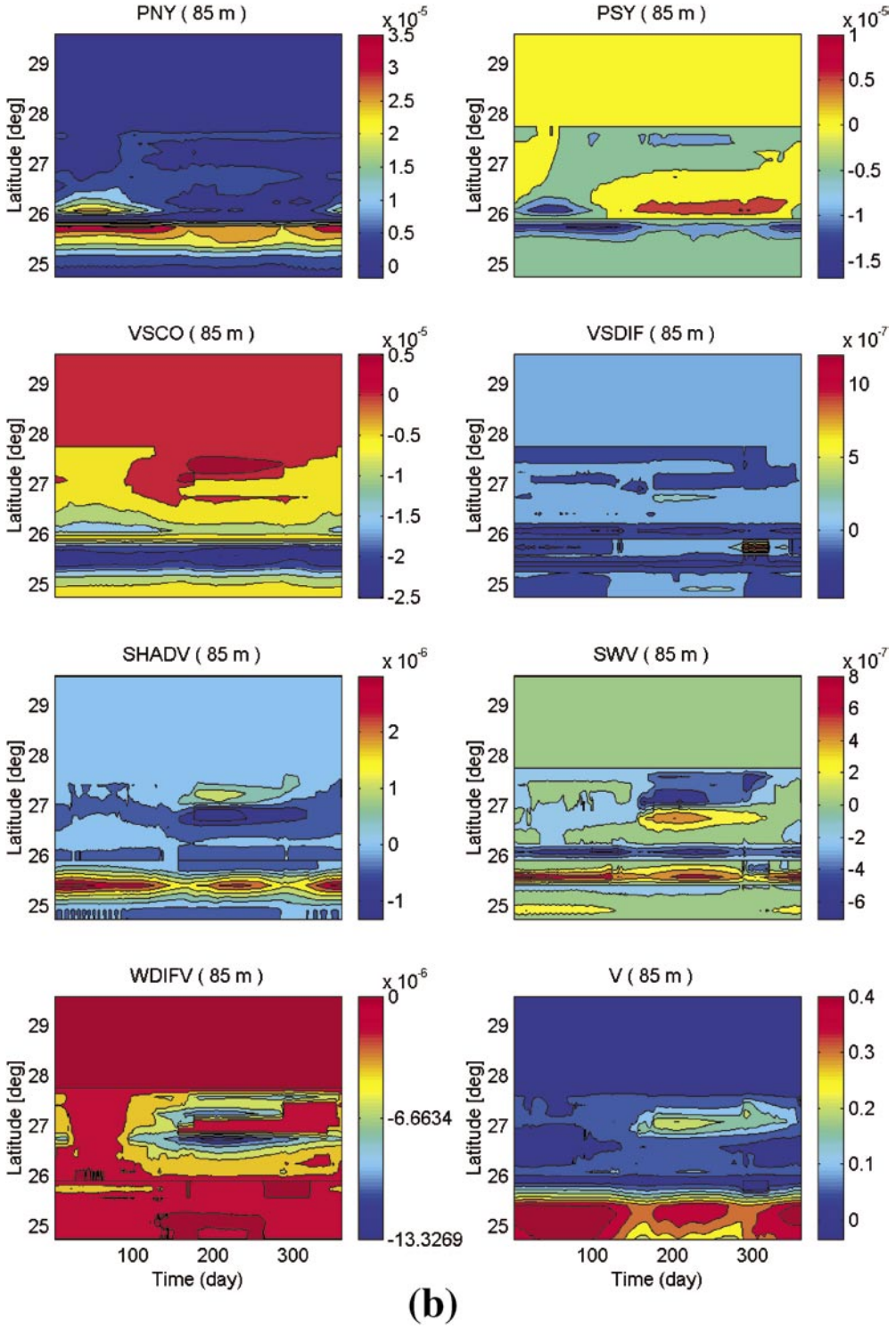

Fig. 5.11 (Continued)

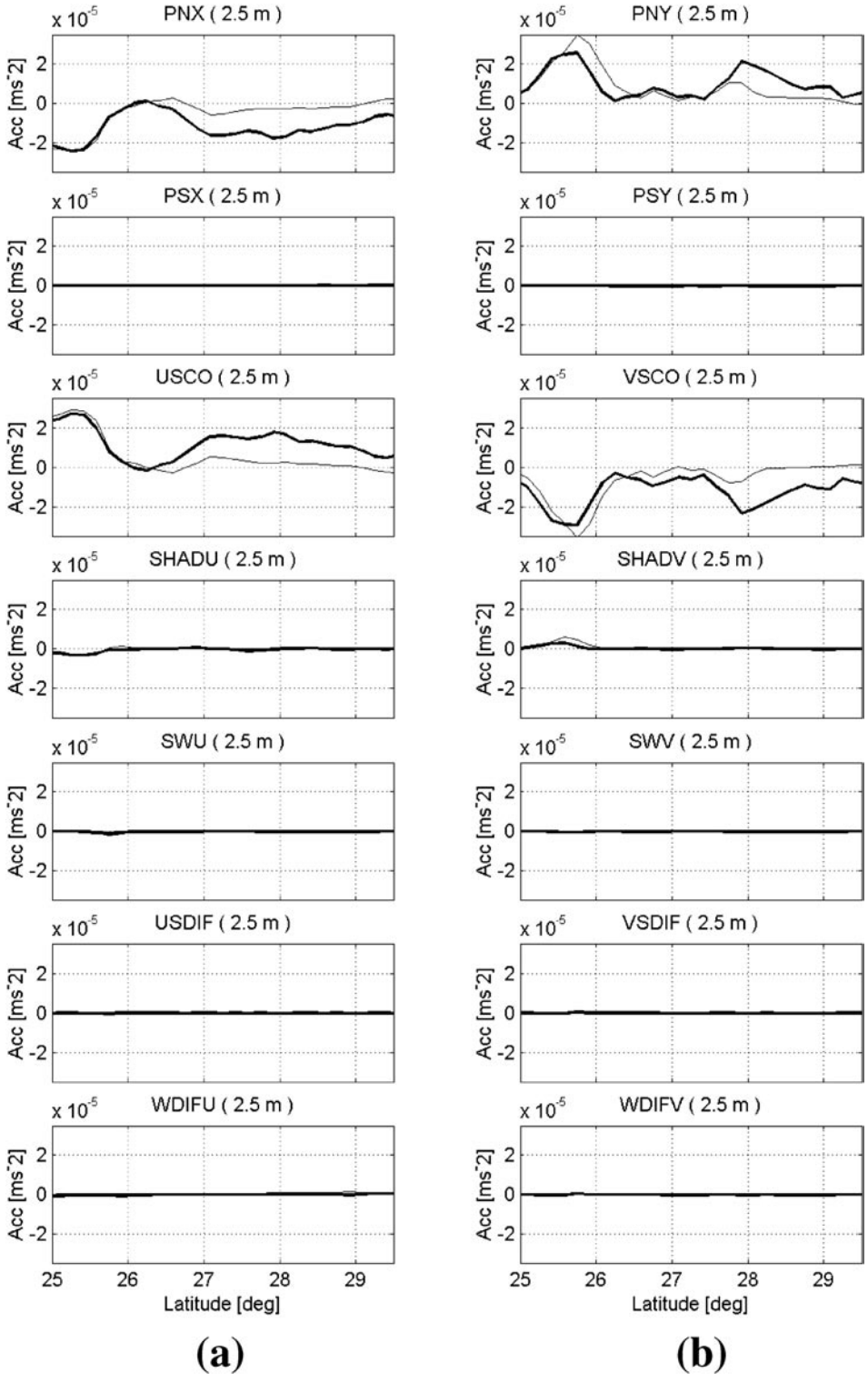

Fig. 5.12 Momentum components along 122.58°E at 2.5 m depth in summer (thick solid line) and winter (thin solid line) (a) in the x-direction and (b) in the y-direction of momentum equation. (pp.41)

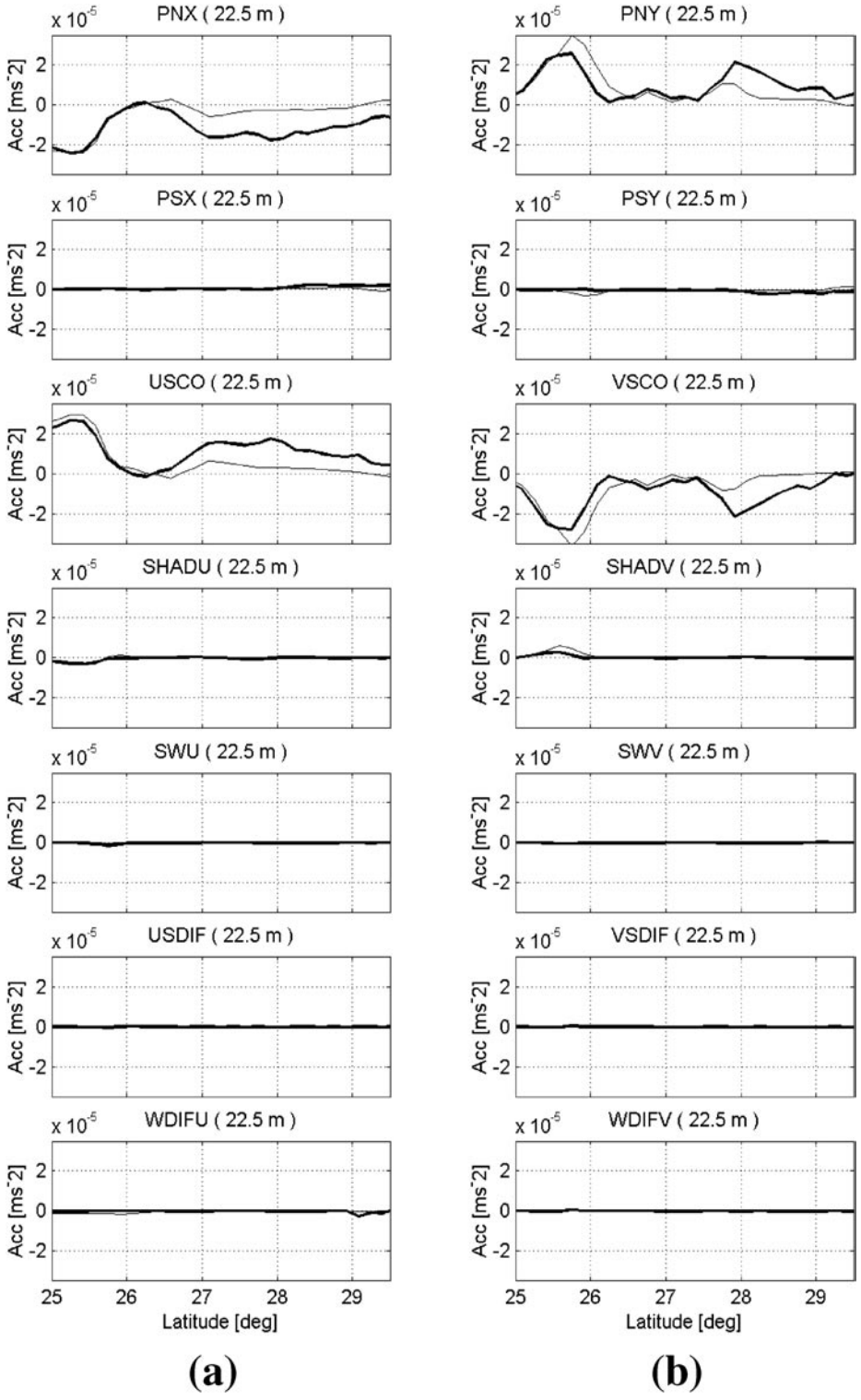

Fig. 5.13 Momentum components along 122.58° E at 22.5 m depth in summer (thick solid line) and winter (thin solid line) (a) in the x-direction and (b) in the y-direction of momentum equation. (pp.41)

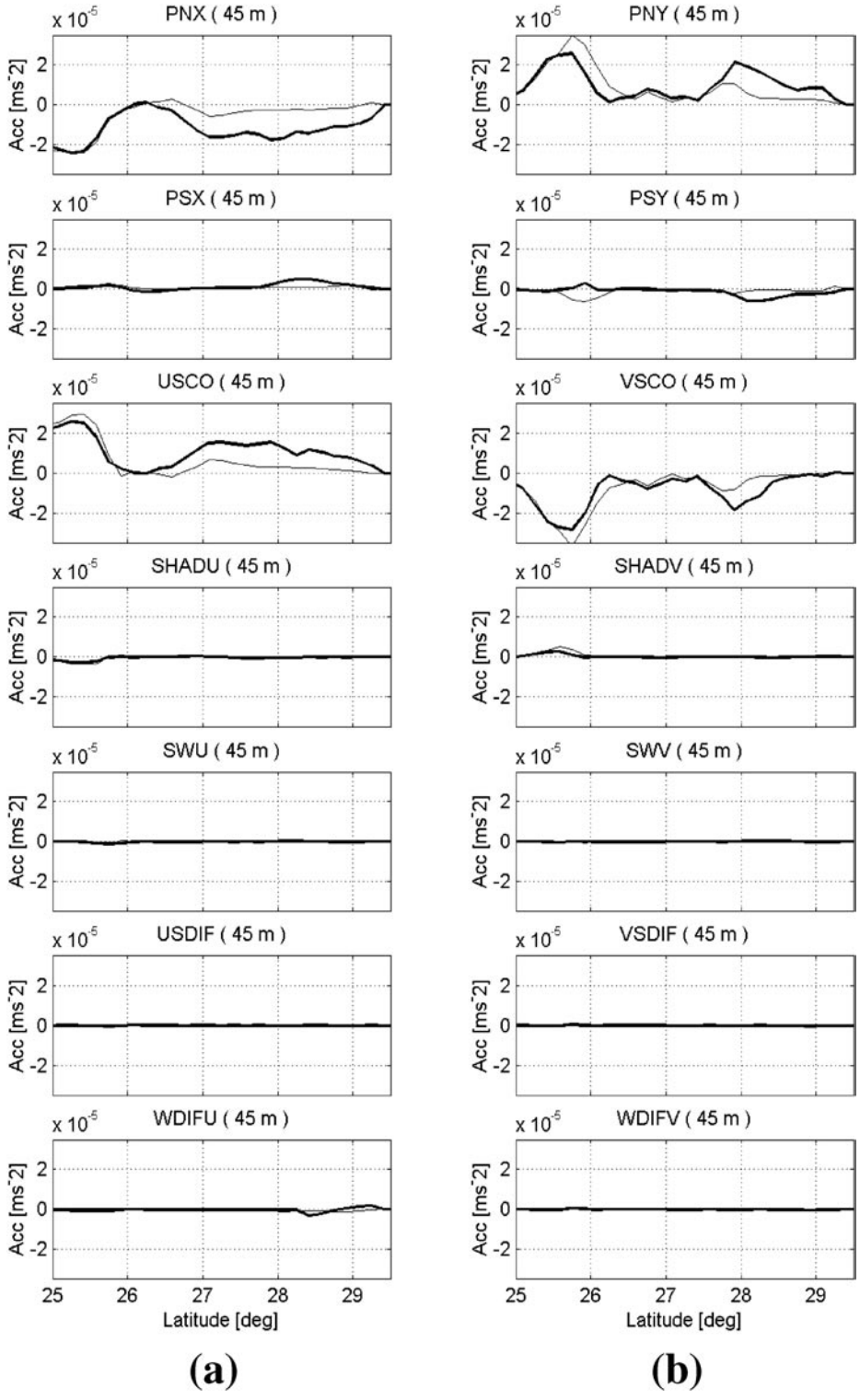

Fig. 5.14 Momentum components along 122.58°E at 45 m depth in summer (thick solid line) and winter (thin solid line) (a) in the x-direction and (b) in the y-direction of momentum equation. p (p.41)

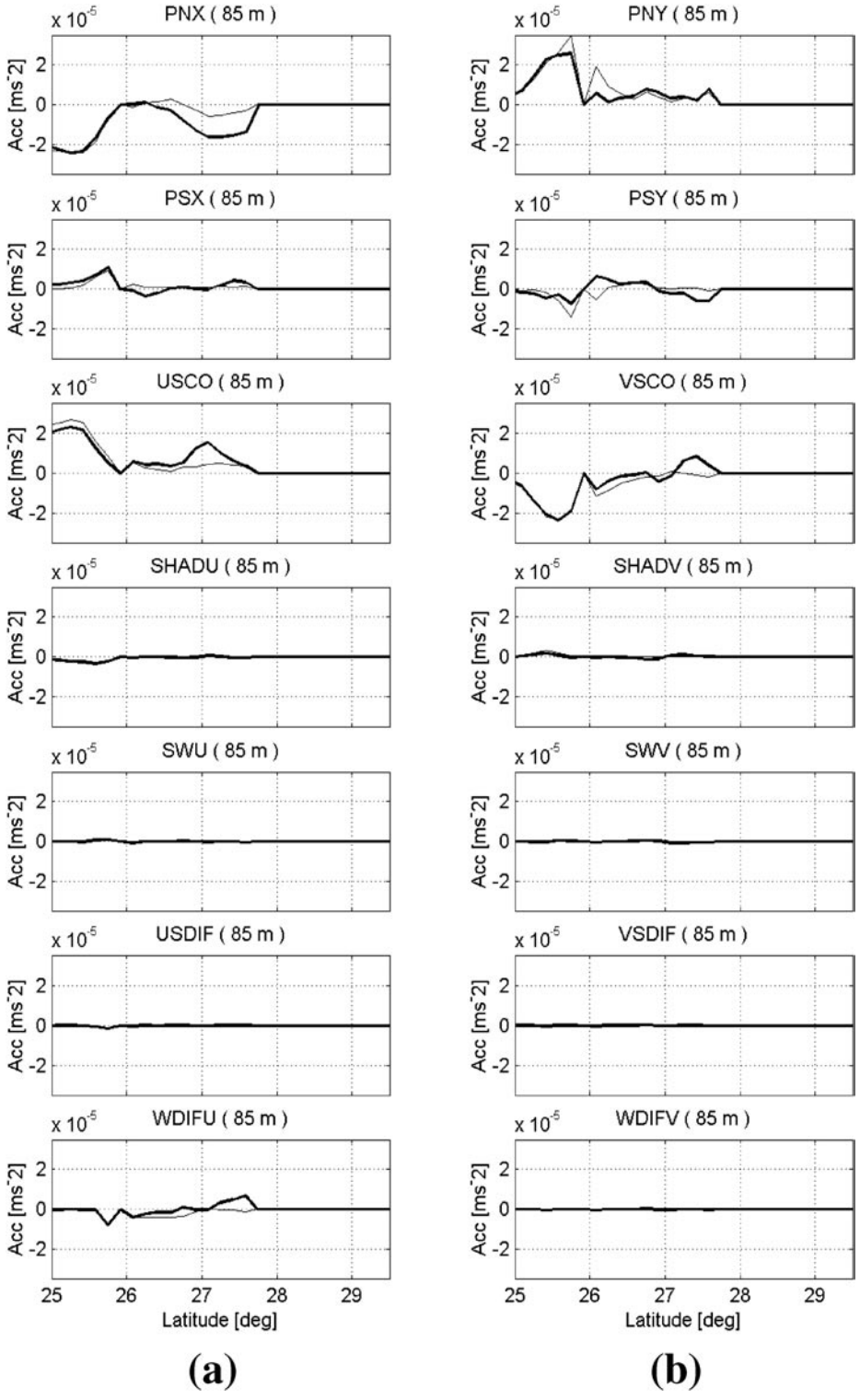

Fig. 5.15 Momentum components along 122.58°E at 85 m depth in summer (thick solid line) and winter (thin solid line) (a) in the x-direction and (b) in the y-direction of momentum equation. (pp.41)

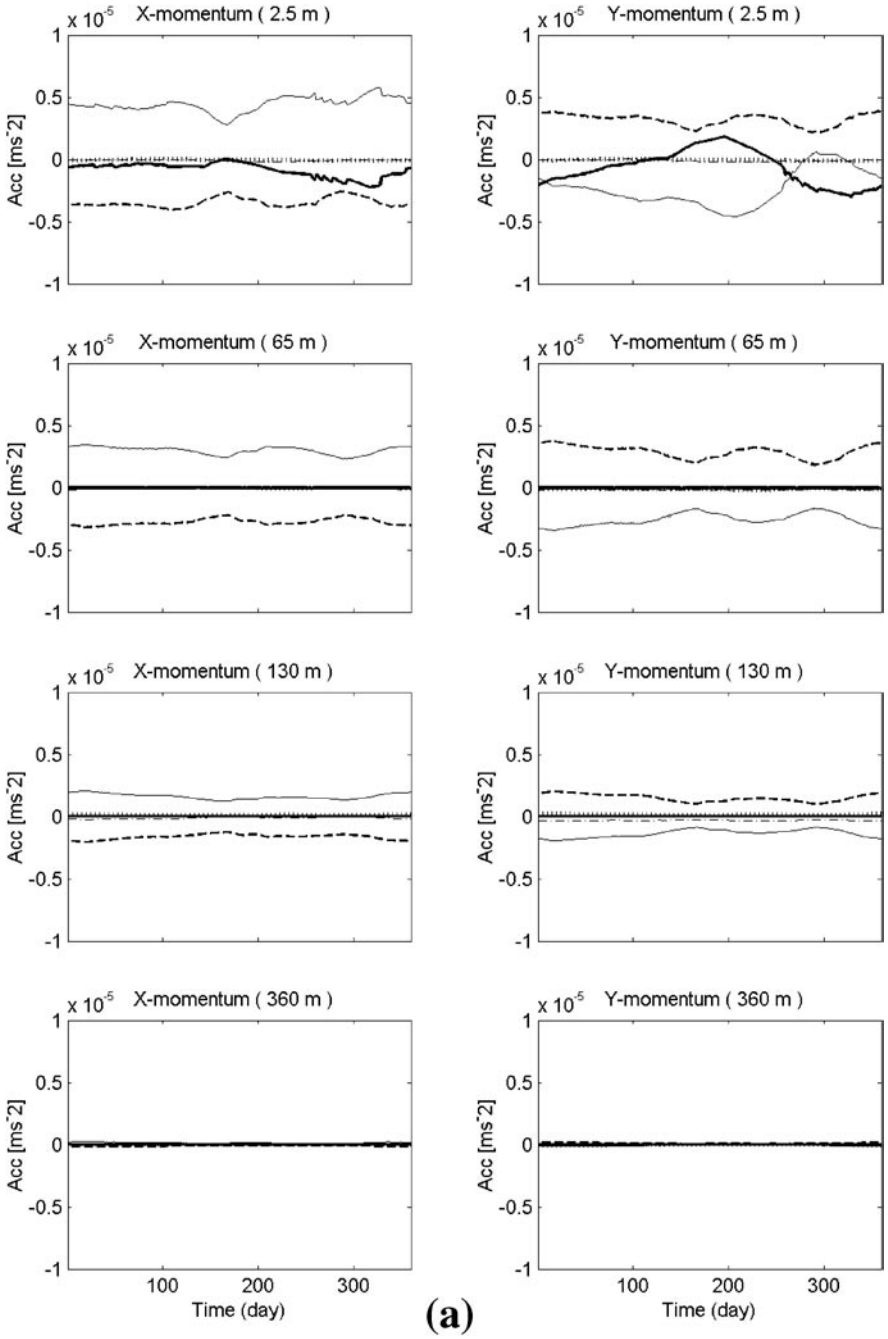

Fig. 5.16 Momentum components (a) at point-A, (b) point-B, and (c) point-C. Thin solid line represents the magnitude of ageostrophic component (GEOX, GEOY), thick solid line the vertical eddy viscosity (WDIFU, WDIFV), thick dashed line the horizontal advection (SHADU, SHADV), dotted line the vertical advection (SWU, SWV), and dashed-dotted line the horizontal eddy viscosity (USDIF, VSDIF). (pp.42)

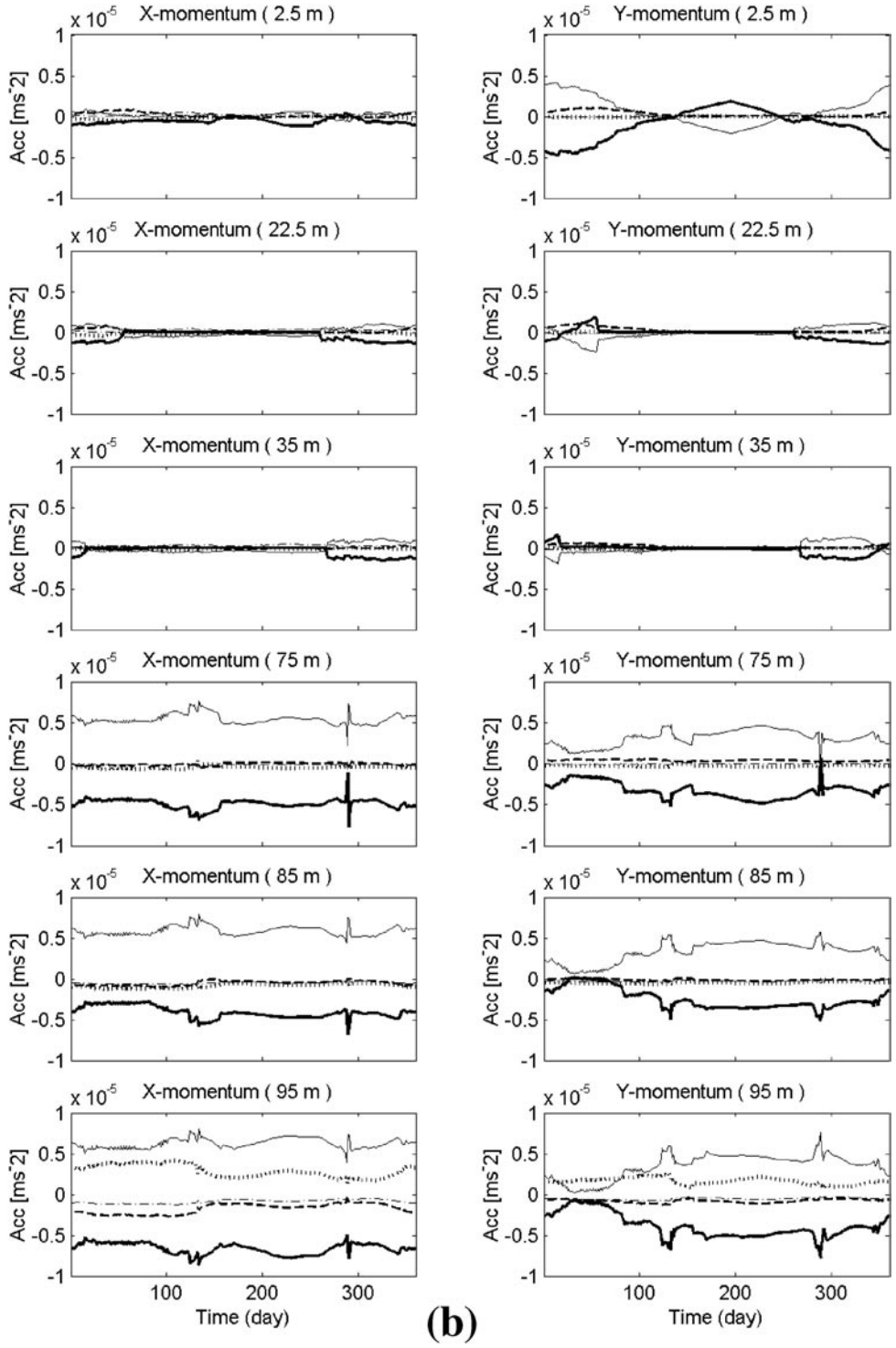

Fig. 5.16 (Continued)

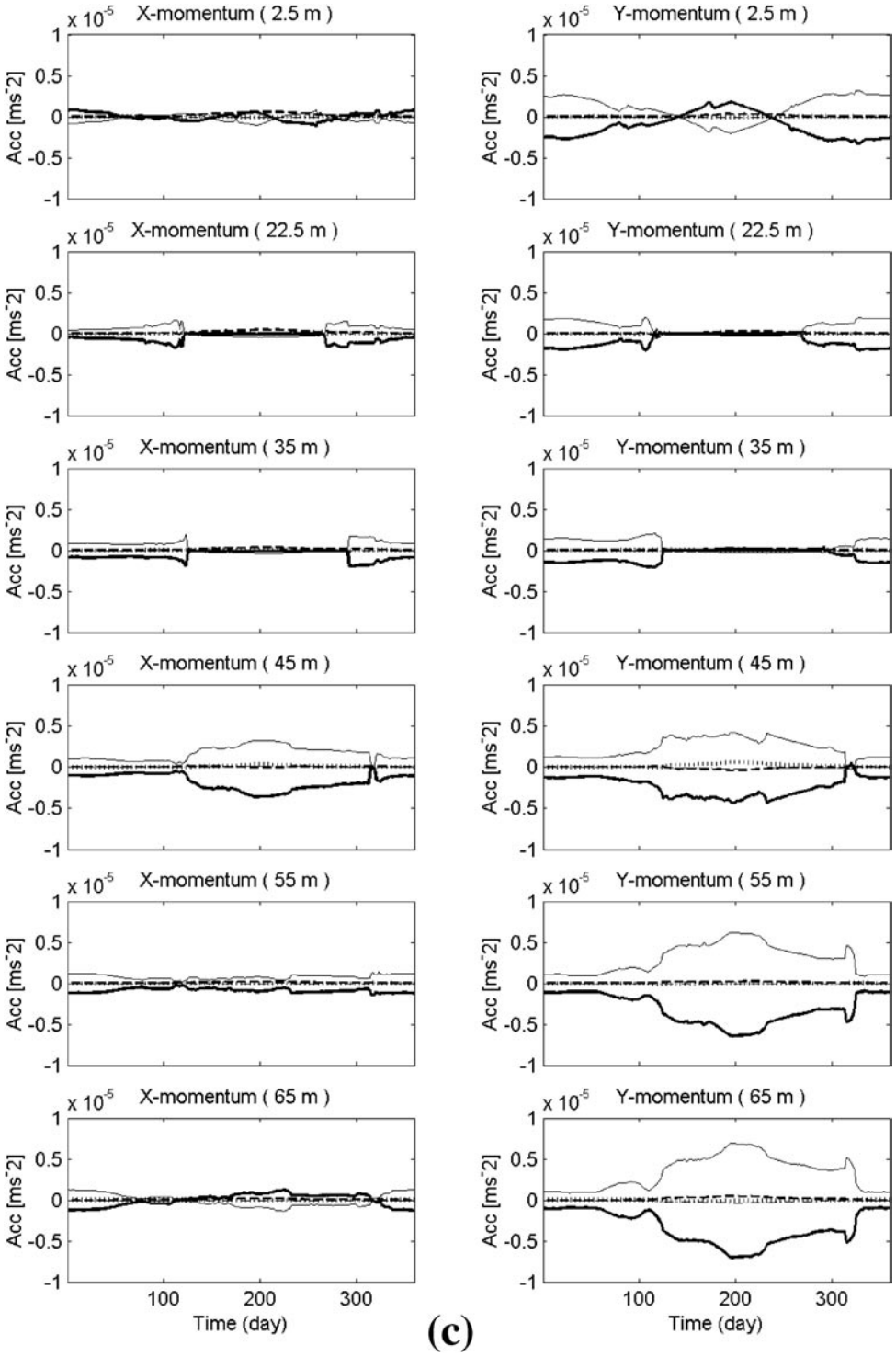

Fig. 5.16 (Continued)

A is the horizontal advection term in all year round, point B the vertical friction and the vertical advection near bottom in all year round, and point C the vertical friction term near bottom only in the summer season.

It represents the main mechanisms of the Kuroshio behavior on the ECS. The momentum balance on point A is mainly maintained by the geostrophic components and the nonlinear horizontal advection components. The vertical friction by local wind stress also affects the balance at the surface with seasonal variation. Horizontal advection terms represents the right turn (north to east) of velocity field in this point, and the effect is maintained all year round. It possibly shows the change of velocity field by topography. On point B, the vertical friction near bottom is formed all year round, and the vertical advection affects the momentum balance at the bottom layer. This represents the year-round upwelling in this place. Point C is the place where the current from the Taiwan Strait in summer flows northeastward. In summer, the upper layer (upper 40 m depth) is in geostrophic balance, except the surface layer where vertical friction by wind stress is dominant. However, at the lower layer (below 40 m depth), vertical friction becomes strong in the summer season with a maximum value in July when the transport from the Taiwan Strait also becomes maximum. It represents the intensification of the bottom friction in summer is induced by the increase of volume transport from the Taiwan Strait.

The current fields are determined as a result of the momentum balance. Fig. 5.17 and Fig. 5.18 represent the winter and the summer current fields for the case including tide effect (Case.1). Each figure shows the current fields at the fourth grids (a), the third grids (b), the second grids from bottom (c), and the bottom grids (d).

Comparing Fig. 5.17 and Fig. 5.18, a large difference between winter and summer emerged from the place near 28°N north of Taiwan where the current from the Taiwan Strait passes rapidly northeastward. Fig. 5.18 confirms that the currents at the bottom grids in summer are considerably weaken compared with the current at the fourth grids from the bottom, and its direction turns anticlockwise when approaching the bottom, at the place where the Kuroshio water intruded onto the shelf area in summer north of 28°N. And, as analyzed in Fig. 5.16c (point C), the northward bottom current is formed by the balance between the geostrophic momentum components and the vertical friction.

Considering the tide effect in Case.1, the vertical friction component near the bottom is increased compared with that in Case.2 (the case excluding tide effect). Fig. 5.19 and Fig. 5.20 show the winter and summer current fields for Case.2. Current field of Case.2 shows that the current velocity near bottom is considerably larger than Case.1. Meanwhile, the northward current near 28°N north of Taiwan, which is below the northeastward current originated from the Taiwan Strait, mainly exists just at the bottom layer in Case.2 (Fig. 5.20). However, though the northward current near bottom in Case.1 (Fig. 5.18) is slower than that in Case.2 (Fig. 5.20), the current also exists partly at the second grid from the bottom, i.e., the northward current in Case.1 is slower but thicker than that in Case.2. This explains why the volume transport of the Kuroshio intrusion onto the shelf area was not very different for both cases including (Case.1) and excluding tide effect (Case.2) in Section 5.2.1.

The vertical friction terms in summer for Case.1 and Case.2 are shown in Fig. 5.21. When considering the tide effect, vertical friction near the bottom was considerably increased at the north of 28°N and also on the Yellow Sea (YS). The consideration of the tide significantly affects on the circulation of both the ECS and the YS.

5.4 Residence time in the Yellow Sea (Tracer experiment 3)

A residence time is defined as the time it takes to replace all except 1/e (~37%) of the original material. Nozaki *et al.* (1991) estimated the residence time to be 5~6 years for YS waters using the Ra isotopes.

In this section, by means of the tracer experiments which release the tracer at the inflow open boundaries (the Taiwan Strait and the east of Taiwan), residence time in the YS was estimated in both cases with and without consideration of tide effect (Case.C, D). The tracer concentration was

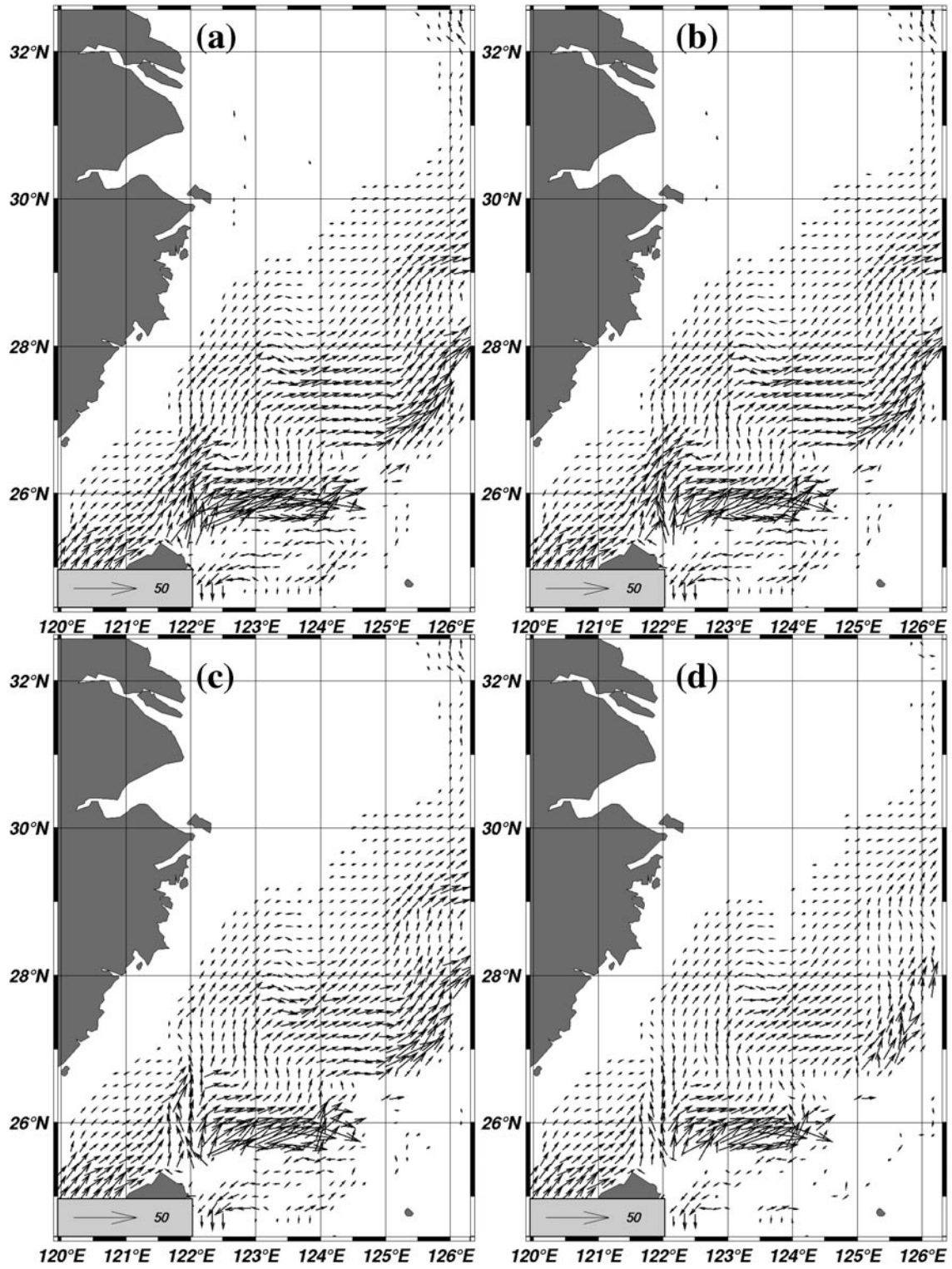

Fig. 5.17 Winter velocity fields of the case including tide effect (Case.1): (a) fourth grids from the bottom, (b) third grids from the bottom (c) second grids from the bottom, and (d) bottom grid. (pp.43)

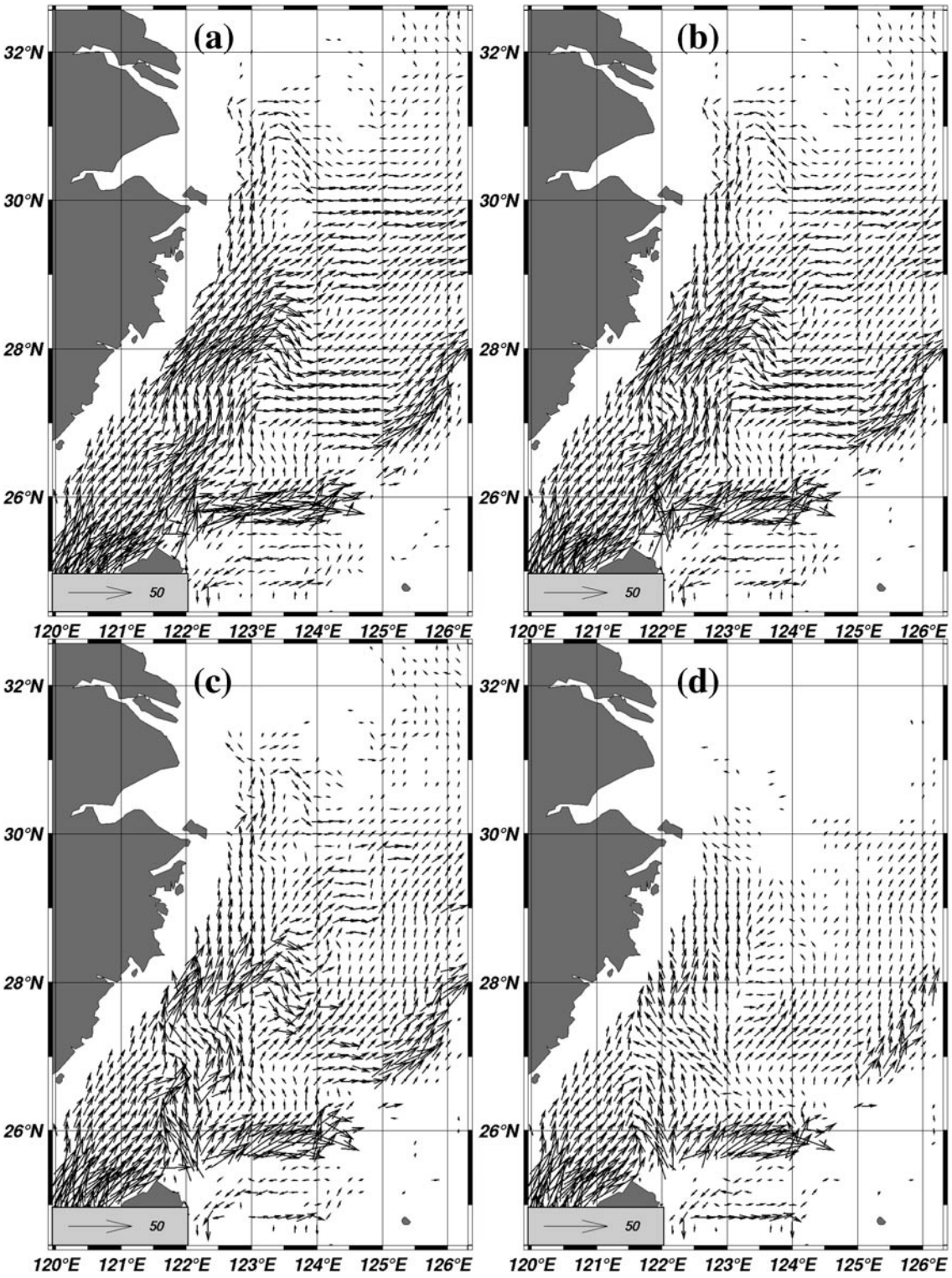

Fig. 5.18 Summer velocity fields of the case including tide effect (Case.1): (a) fourth grids from the bottom, (b) third grids from the bottom (c) second grids from the bottom, and (d) bottom grid. (pp.43)

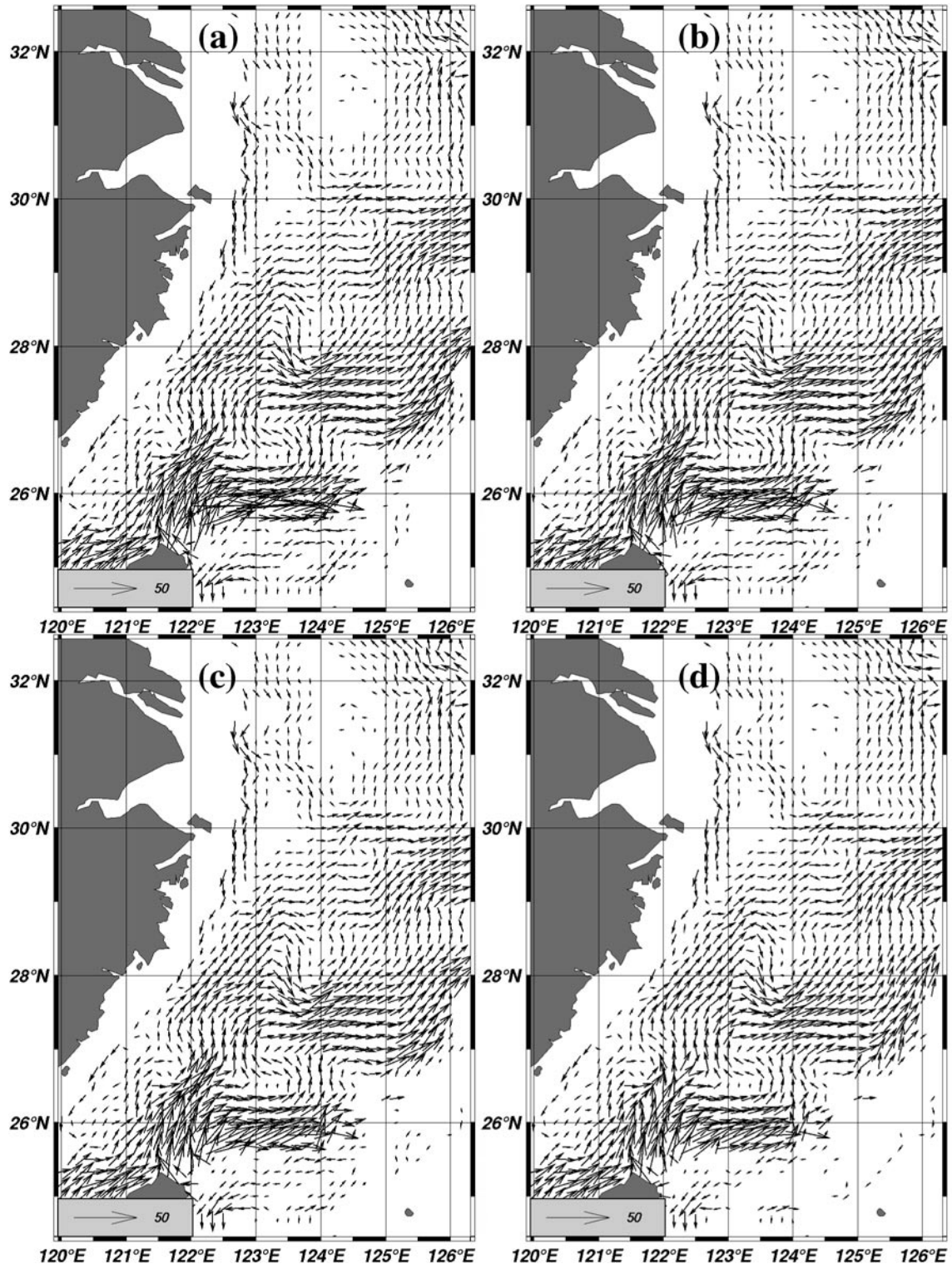

Fig. 5.19 Winter velocity fields of the case excluding tide effect (Case.2): (a) fourth grids from the bottom, (b) third grids from the bottom (c) second grids from the bottom, and (d) bottom grid. (pp.43)

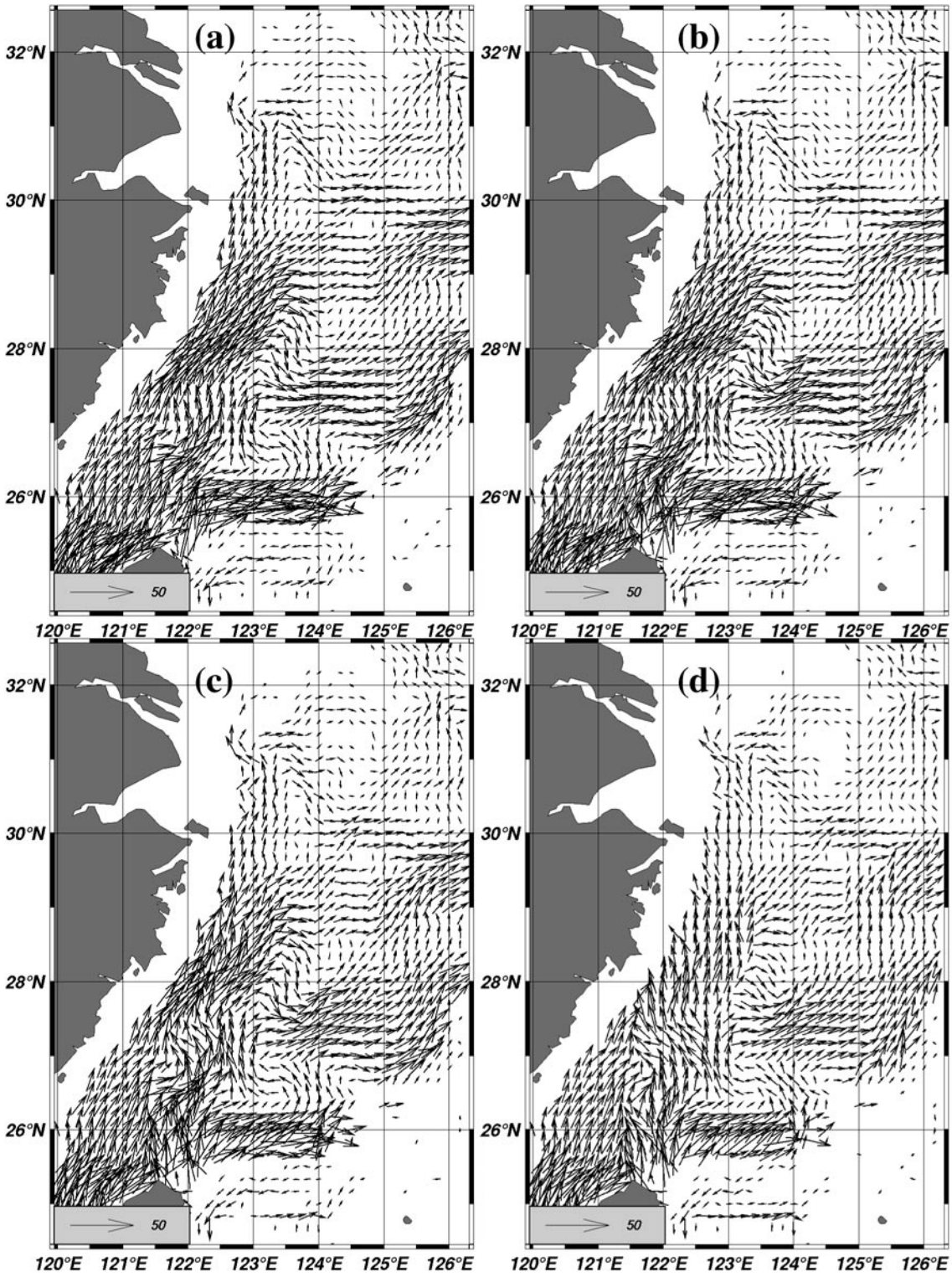

Fig. 5.20 Summer velocity fields of the case excluding tide effect (Case.2): (a) fourth grids from the bottom, (b) third grids from the bottom (c) second grids from the bottom, and (d) bottom grid. (pp.43)

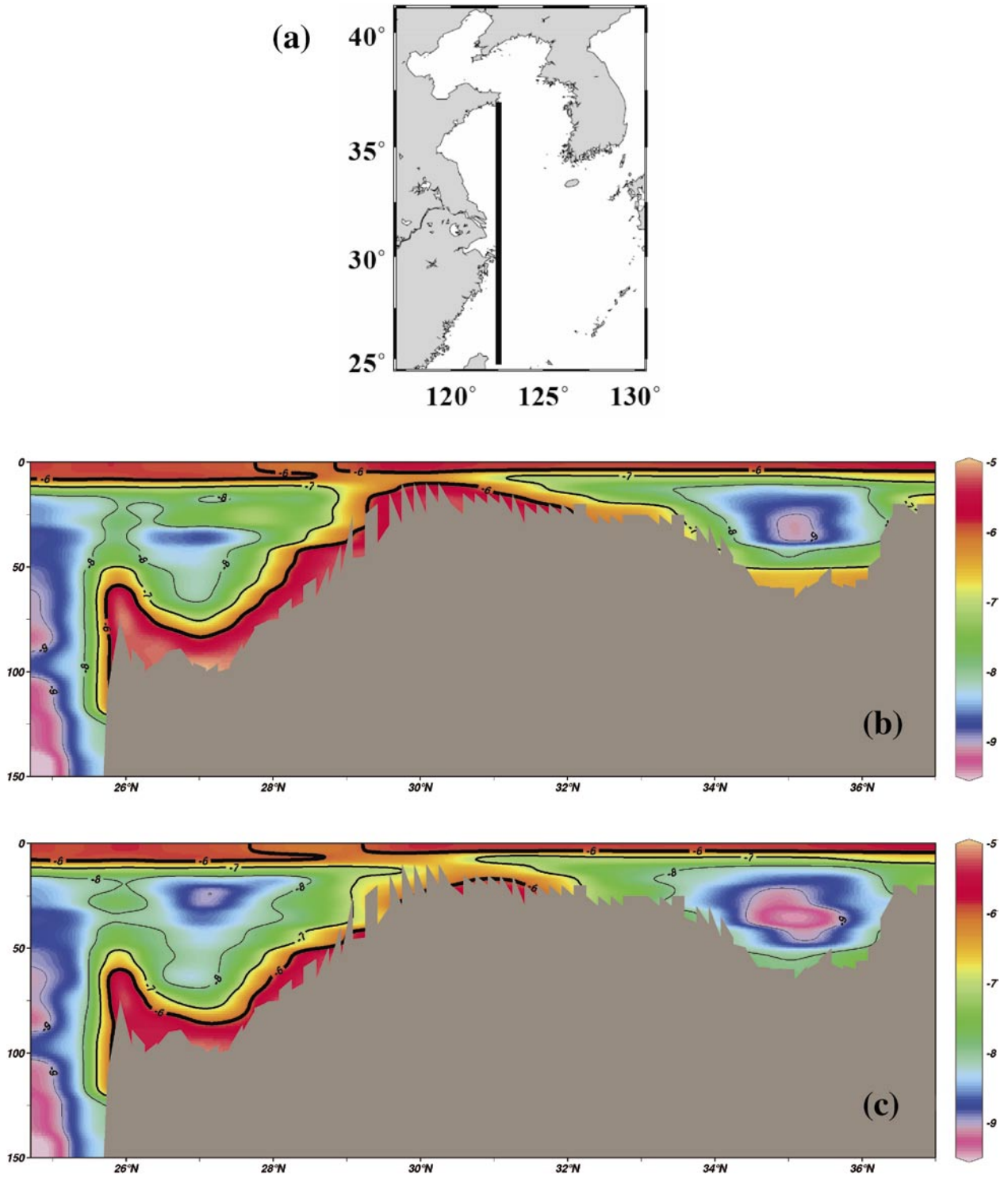

Fig. 5.21 (a) A line along the 122.58°E for vertical profile. Vertical profile of vertical friction term on a logarithmic scale (units: m/s^2) in summer along the 122.58°E line (b) including (Case.1) and (c) excluding tide effect (Case.2). (pp.44)

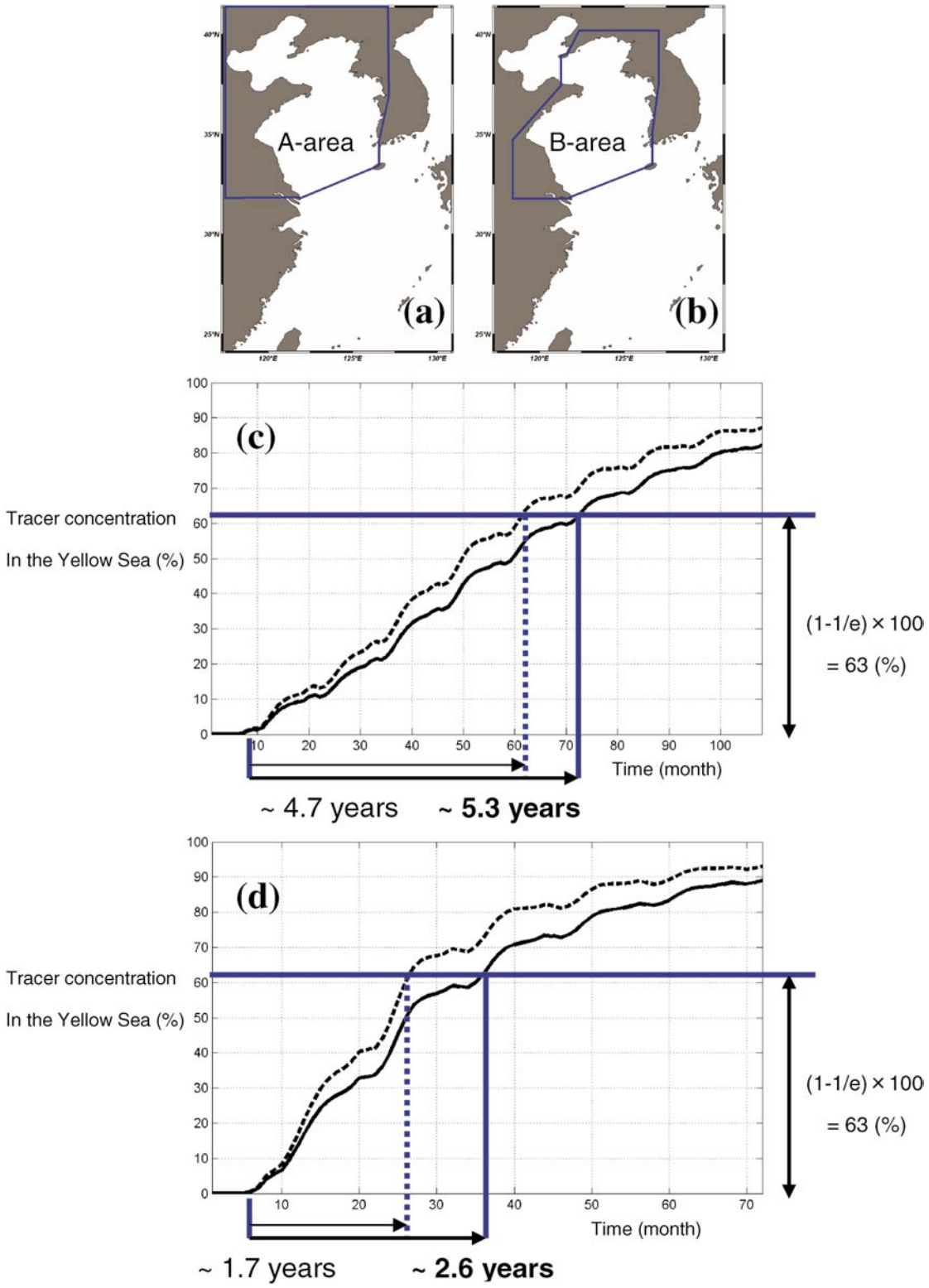

Fig. 5.22 Area for estimation of the residence time of the Yellow Sea: (a) including the Bohai Sea and (b) excluding the Bohai Sea. Changes of tracer concentration with time in A-area (solid line) and B-area (dashed line): (c) Case. C and (d) Case. D. (pp.44)

governed by the same advection-diffusion equation in the same manner as the Preliminary experiment. The results showed remarkable difference indicating that the numerical simulation without the tide effect could greatly reduce the residence time in the YS, making the circulation strong. In the case with consideration of tide (Case.C), the residence time was estimated as 5.3 years (solid line in Fig. 5.22c) and 4.7 years (dashed line in Fig. 5.22c) for inclusion (Fig. 5.22a) and exclusion of the Bohai Sea (Fig. 5.22b), respectively. Meanwhile, in the case without consideration of tide (Case.D), the results showed 2.6 years (solid line in Fig. 5.22d) and 1.7 years (dashed line in Fig. 5.22d), respectively. As shown in Fig. 5.21, the tide parameterization enhanced the vertical friction near bottom, thus the current speed was decreased at the lower layer, and the water exchange between the YS and the ECS also reduced. The estimated residence time considering the tide effect agrees well with the result of Nozaki *et al.* (1991). This result emphasizes that the consideration of tide effect is indispensable to the numerical simulation in the Yellow and East China Seas.

5.5 Origin of the Taiwan Warm Current in summer

The passive tracer experiments and the momentum balance analysis in this study include some clues about the origin of the TWC in summer. Fig. 4.9a and 4.9b in the Preliminary Experiment showed that the tracer released from the Taiwan Strait in summer flowed northeastward at the upper layer, while another tracer released from the east of Taiwan flowed northward along the bottom layer and upwelled near the Chinese coast north of 29°N being mixed with the water originated from the Taiwan Strait. Fig. 4.12d in Exp. 1 further represented that the upwelled Kuroshio water was originated from the lower layer of the northeast of Taiwan in the summer season. These tracer experiments explain that upper water of the TWC in summer originates in the Taiwan Strait and deep water of the TWC in the east of Taiwan.

As for the mechanism how the Kuroshio water forms the deep water of the TWC, it was proved by the momentum balance analysis that increase of the geostrophic flow from the Taiwan Strait in summer induces the Kuroshio water at the bottom Ekman layer to flow northward across the isobath line into the submerged river valley off the Changjiang.

Some observational evidences have been suggested in the previous studies. Su and Weng (1994) classified the Taiwan Warm Current Water (TWCW) into the upper water and the deep water by analysis of water masses, so that they determined the summer characteristic values of upper water to be 27.0℃, 33.7 psu (23.0～29.0℃ and 33.3～34.2 psu), and those of deep water 19.0℃, 34.4 psu (16.0～23.0℃ and 34.1～34.7 psu). The appearance of the deep water was suggested only in the warm half of the year (from April to September), approximately along 123°E in an area north of 28°N. Based on analysis of water masses, they concluded that the upper water of TWCW is formed by the mixing of Kuroshio surface water flowing northward with the Taiwan Strait water, but the deep water originated from the Kuroshio subsurface water east of Taiwan.

In recent studies, appearance of cold, saline Kuroshio subsurface water (below 23.0℃ and over 34 psu) in summer also have been detected near Zhejiang province south of Changjiang estuary and at the submerged river valley off Changjiang (Fig. 5.23, after Chen *et al.*, 2006; Fig. 5.24, after Zhu *et al.* 2001). Considering the Taiwan Strait water in spring and summer is warmer (over 22℃) and less saline (below 34.2 psu) even at the lower layer (Fig. 5.25, after Jan *et al.* 2006), the TWC deep water in the summer season can be regarded to be originated from the Kuroshio subsurface water.

Hu (1994) showed a chart of summer residual currents in the upper layer and the bottom layer (Fig. 5.26), and presumed it to be caused by bottom Ekman layer. As a model study, Jacobs *et al.* (2000) simulated the circulation of the Yellow and the East China Seas (YECS) using Princeton Ocean Model (POM) and explained the possible mechanism for the appearance of the Kuroshio water in the Yangtze Relict River valley (Submerged valley off Changjiang) as bottom Ekman layer, by means of passive tracer experiment and comparison between the bottom velocities and the velocities averaged over the total depth. Guo *et al.* (2006) also supported their idea by the same kind of passive tracer experiment using a numerical model.

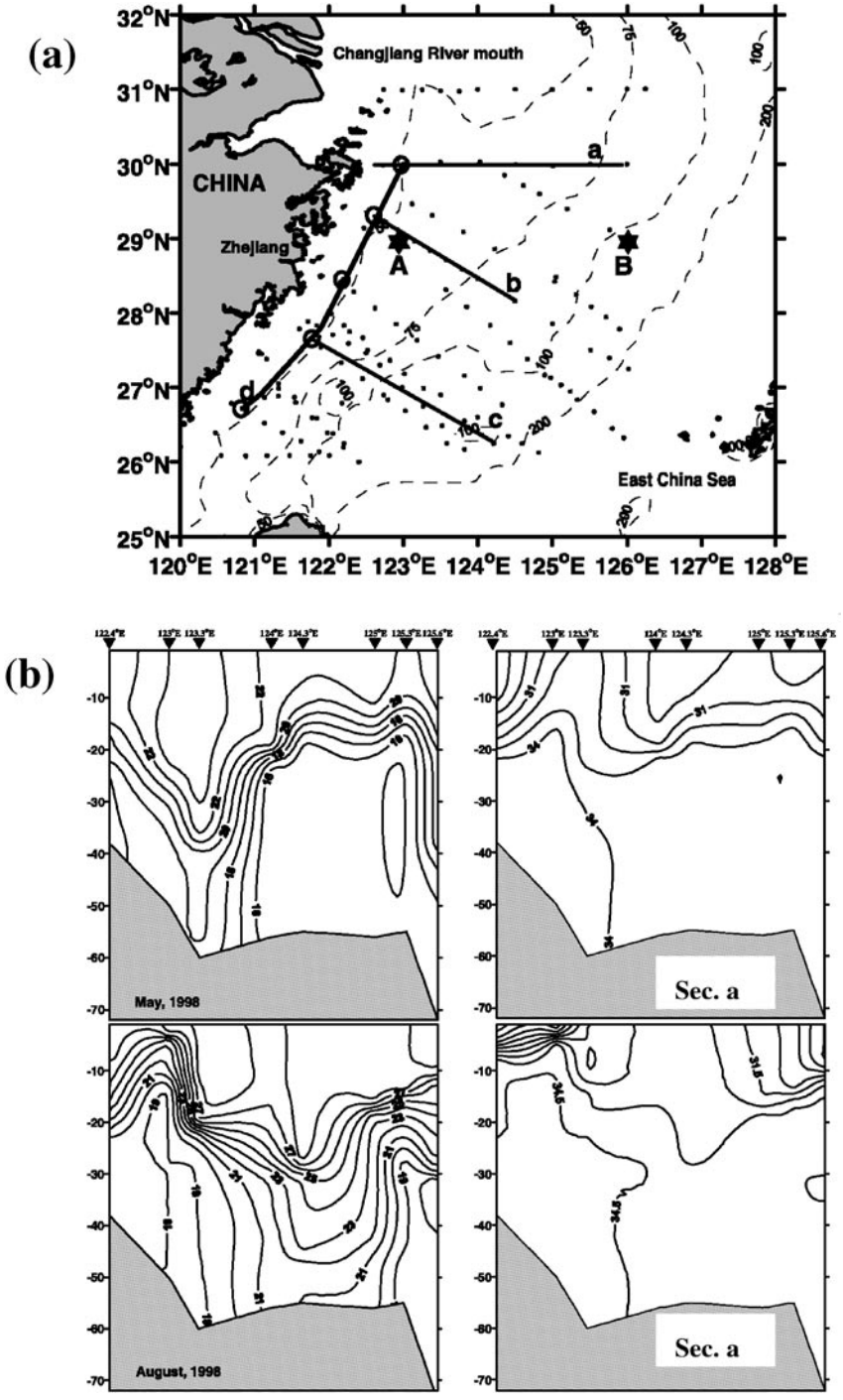

Fig. 5.23 (a) Map of three hydrographic Sections a, b, and c from eight cruises during 1997-2002. Season variation of vertical temperature (left) and salinity (right) distributions along the Section a (b), b (c), and c (d). (after Chen et al., 2006) (pp.46)

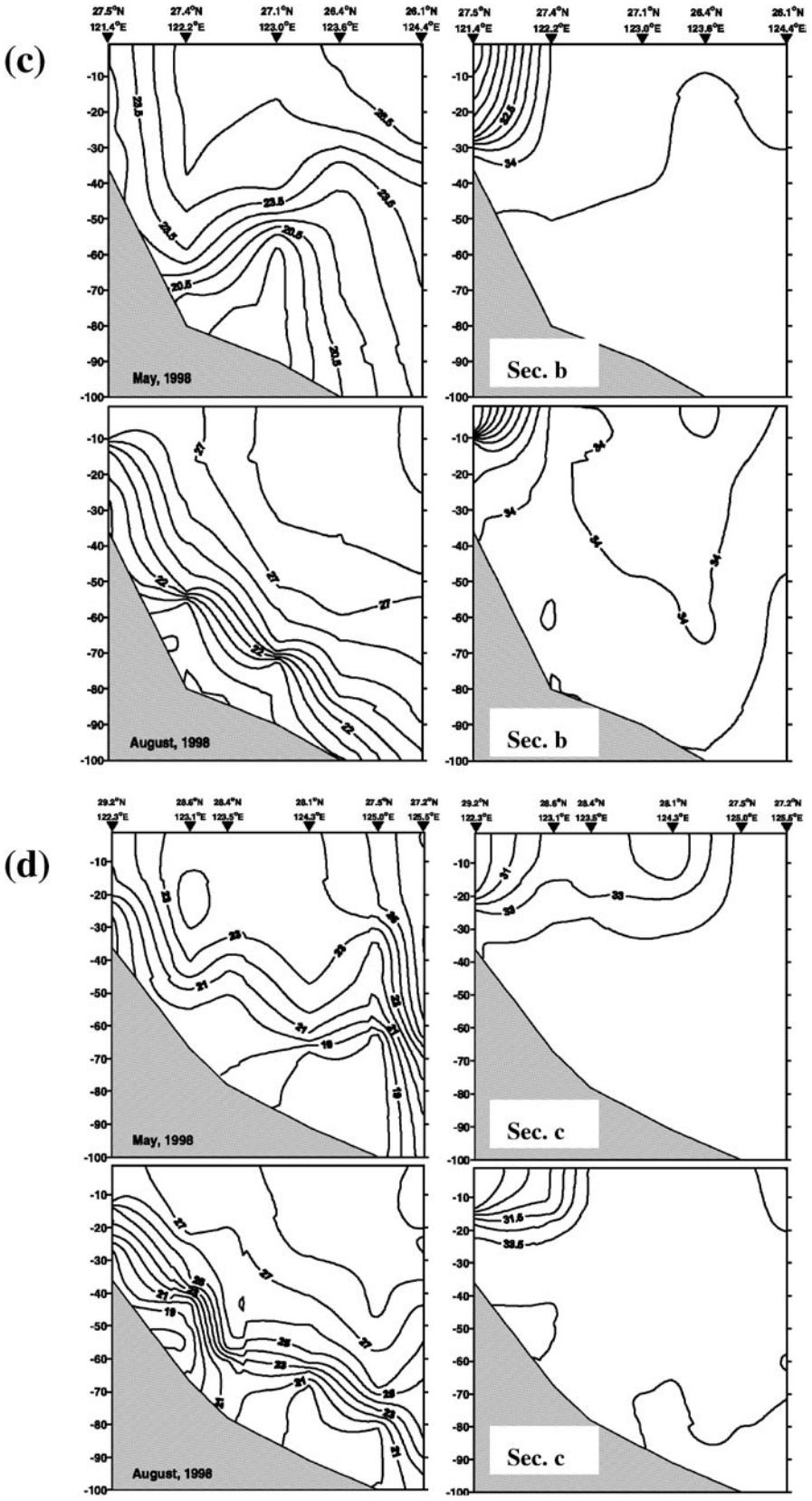

Fig. 5.23 (Continued)

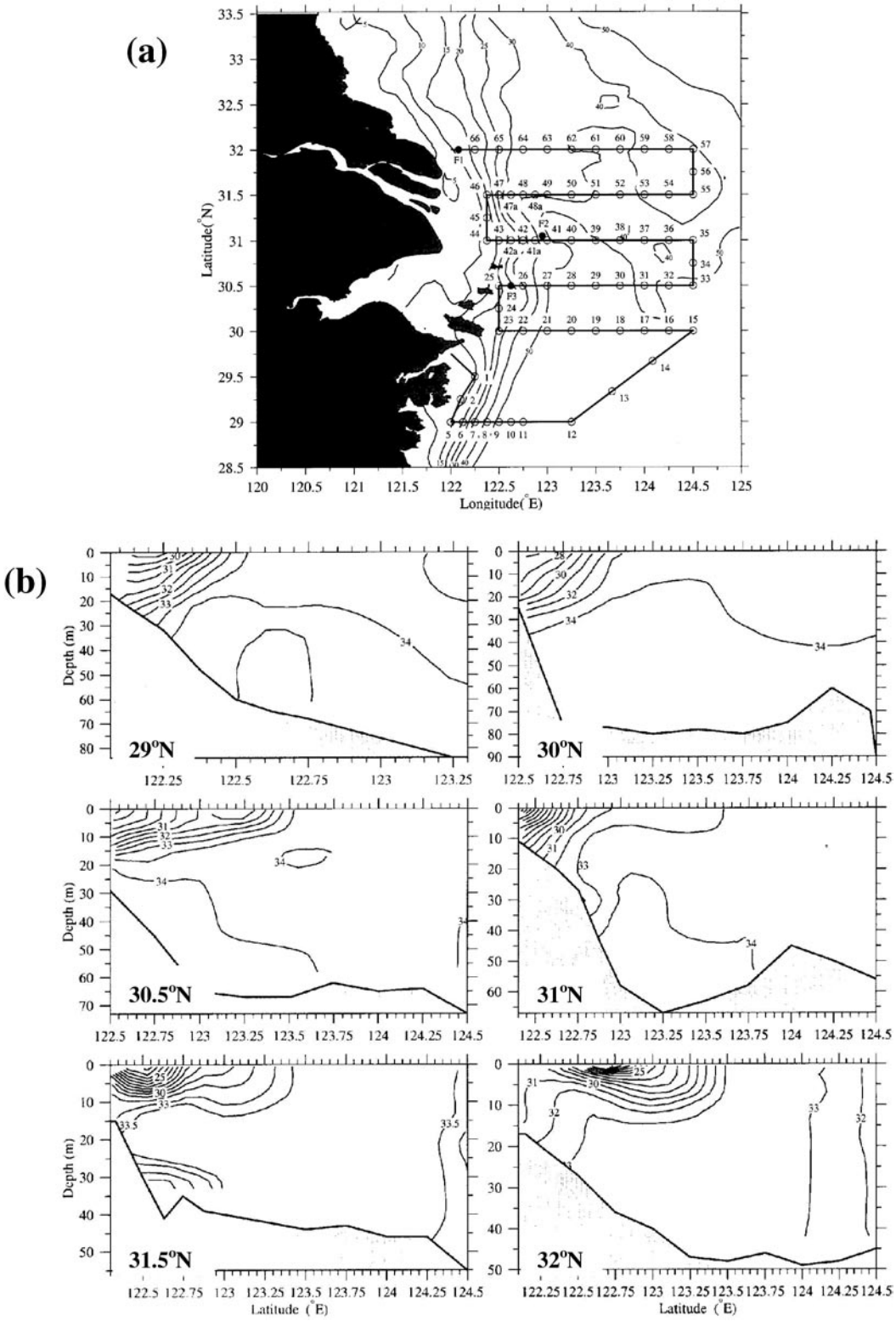

Fig. 5.24 (a) Observation line during August in 2000. Vertical distributions of salinity (b) and temperature (c) (after Zhu *et al.*, 2001) (pp.46)

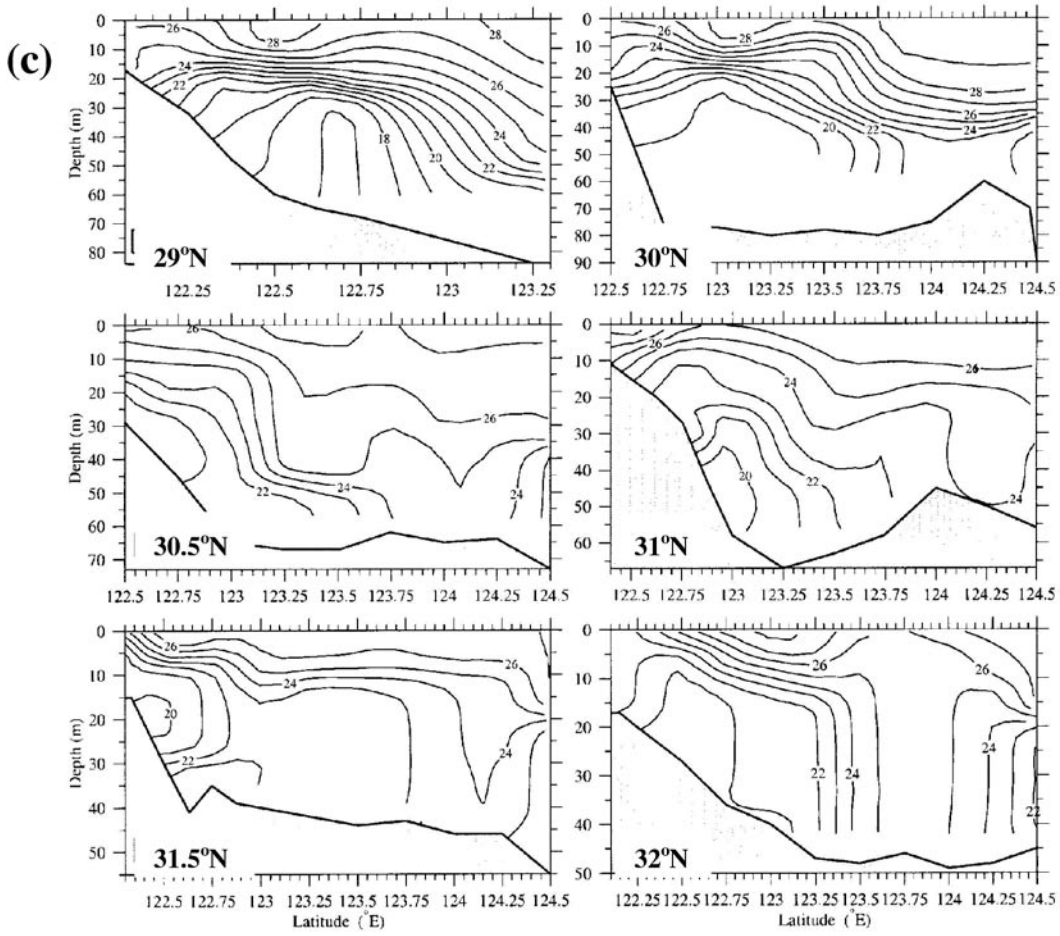

Fig. 5.24 (Continued)

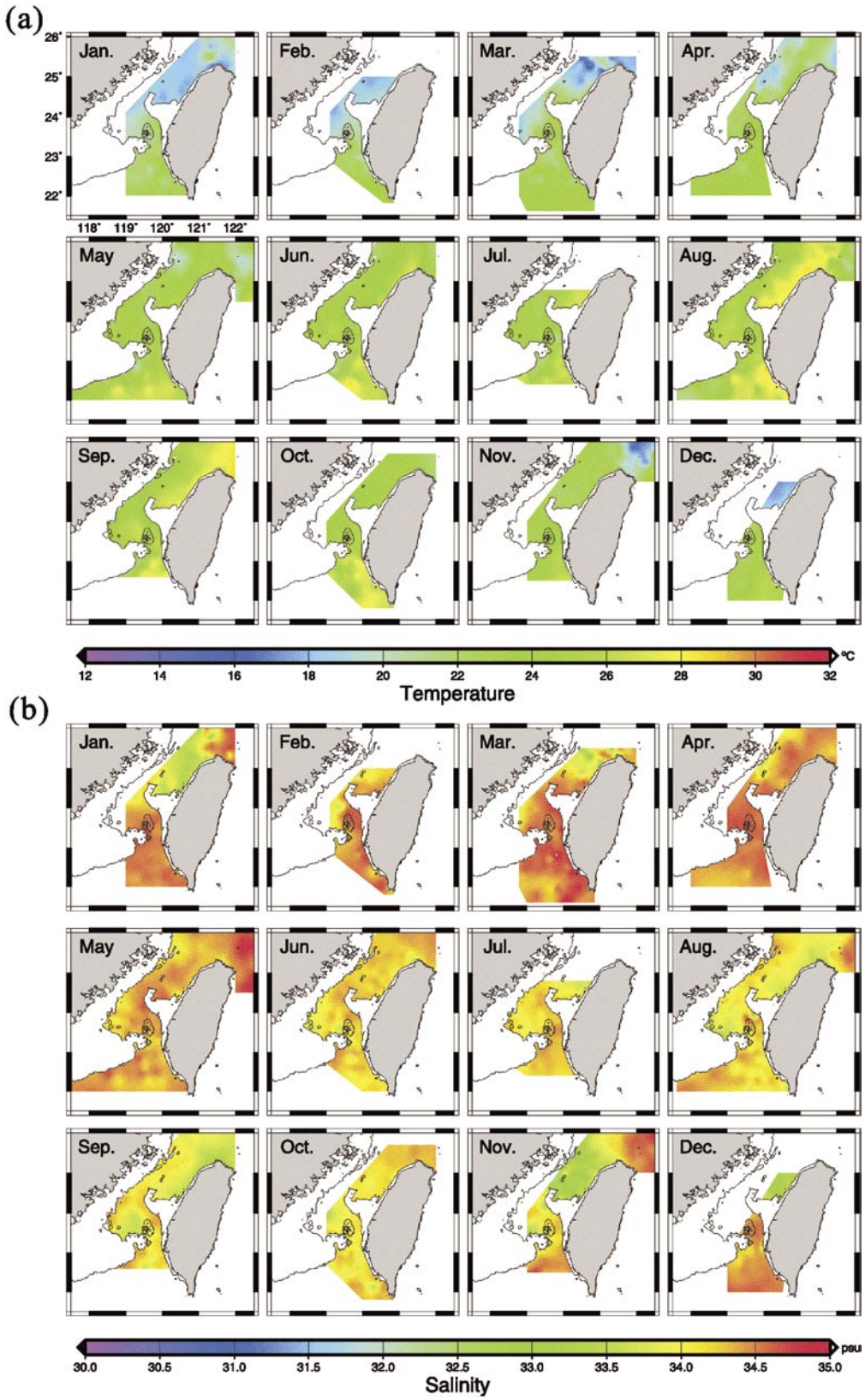

Fig. 5.25 Distributions of (a) temperature and (b) salinity at depth of 50 m for each month (after Jan *et al.*, 2006). (pp.46)

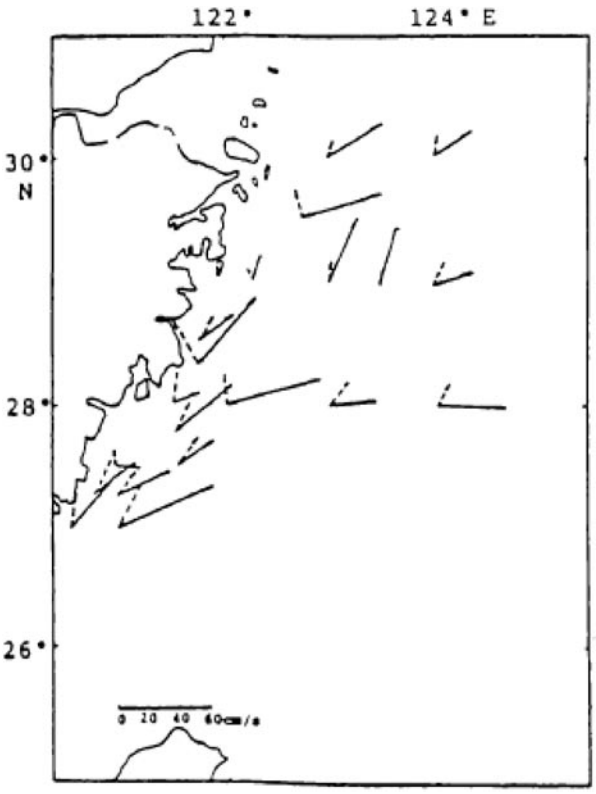

Fig. 5.26 Residual currents in the ECS in summer. Solid line-at 5 m level; dashed line-near bottom (after Hu, 1994) (pp.46)

This study also supports the idea that the TWC deep water is originated from the Kuroshio by the bottom Ekman layer flow. In addition, this study considered the tide effect, and showed that the intrusion northeast of Taiwan, south of 28°N deeper than 100 m, is year-round phenomena possibly due to the difference of water depth between the Taiwan Strait and the northeast of Taiwan where the Kuroshio intrudes. The momentum balance analysis further showed that the intensification of vertical friction near bottom due to the increase of the geostrophic current from the Taiwan Strait, north of 28°N, induced the northward bottom Ekman layer flow which forms the deep water of the TWC.

5.6 Summary

This chapter investigated the mechanisms of the Kuroshio intrusion.

Case studies by tracer experiments were carried out for the effect of tide, transport from the Taiwan Strait, and transport from east of Taiwan. It revealed that the consideration of tide effect considerably decreased the intrusion from the Kuroshio across the 200 m isobath line, in large part east of Taiwan (122～123°E). Except during winter when the shelf water is well-mixed vertically, transport from the Taiwan Strait mainly affects the intrusion from the upper layer of the Kuroshio region, and the intrusion below 80 m did not change greatly in spite of the large transport difference from the Taiwan Strait. Transport variation from the Kuroshio directly exerted an influence on the volume transport of the Kuroshio intrusion in both upper and lower layers.

Momentum balance analysis along 122.58°E northeast of Taiwan, where the Kuroshio water mainly intrudes onto the ECS shelf, described the behavior of the Kuroshio. Basically local wind forcing affects on the surface layer of the ECS with seasonal variation by means of the vertical friction. The Kuroshio, flows into the ECS along the eastern Taiwan coast, is in a geostrophic balance by the westward pressure gradient force by surface elevation and the eastward Coriolis force. The northward Kuroshio turns to the east by curved topography in the balance of the geostrophic components and the horizontal advection. And some of the Kuroshio flows into the ECS shelf or upwells along the bottom layer over the steep topography in the balance of the geostrophic components, the horizontal advection, the vertical advection and the vertical friction components. The intruded Kuroshio water occupies the lower layer northeast of Taiwan south of 28°N all the year round. When summer comes, the northeastward strong current from the Taiwan Strait in geostrophic balance passes through north of 28°N, and near the bottom layer, northward current occurs in the balance of the geostrophic components and the vertical friction component. The northward current at the bottom layer north of 28°N allows the Kuroshio water to intrude onto the shelf area shallower than 80 m.

The momentum balance analysis further showed that the intensification of vertical friction near bottom due to the increase of the geostrophic current from the Taiwan Strait, north of 28°N, induced the northward bottom Ekman layer flow which forms the deep water of the TWC.

The consideration of tide effect by

parameterization increased the vertical friction term in the momentum equation at the lower layer, so that the current velocity at the lower layer was considerably decreased, and thus the water exchange between the YS and the ECS also reduced. The residence time between the YS and the ECS, when considering the tide effect, was estimated as about 5 years which is close to the result of Nozaki *et al.* (1991): 5～6 years.

The passive tracer experiments and the momentum balance analysis supported the idea that the TWC deep water is originated from the Kuroshio in the form of the bottom Ekman layer flow.

Chapter 6. Conclusion and Discussion

Intrusion from the Kuroshio onto the continental shelf of the ECS was investigated using a 3-D numerical model (RIAMOM). The tide effect is additionally considered to intensify the linear bottom friction by Hunter's (1975) formula and the vertical eddy diffusivity and viscosity by James' (1977, 1978) method using M_2 tidal velocity. The main objectives of this study were to understand the behavior of the intruded Kuroshio water, to estimate the volume transport of the intrusion with seasonal variations, and to elucidate the mechanisms of the intrusion from the Kuroshio.

As a method for evaluating the intrusion, passive tracer experiments were carried out. In the Preliminary Experiment, each tracer was released in the Taiwan Strait or the east of Taiwan, and from the vertical profile of the tracer, two vertical sections along the 200 m isobath line were determined for the release of tracers: 0～80 m and 80～200 m. In Exp. 1 and Exp. 2, the tracers were released at local sections along the 200 m isobath line for 30 days. Using the vertically integrated mass of the tracer, the horizontal distributions of the tracer for the control case were compared. In addition, the intruded volume transports for each case was calculated using the time derivative of the total amount of water including the passive tracer. In Exp. 3, the tracer was deployed for six years through the Taiwan Strait and the east of Taiwan at the same time after a spin up time of six years, for the cases with and without consideration of the tide effect.

The tracer experiments for Case.1 (a control case) were discussed in Chapter. 4 and clearly showed two main regions of the Kuroshio intrusion: northeast of Taiwan and west of Kyushu. From additional experiments for Case.1, which released the tracer for 90 days at the 200 m isobath line of 122～123°E, 123～124°E, and 124～125°E, it is realized that the tracer, intruded from 122°E to 123°E through 80 ～ 200 m, shows the largest seasonal difference of the horizontal distribution. In winter, the tracer intrudes solely south of 28°N though intrudes farther northward and flows into the small valley on the western ECS in summer. The spatial distribution with the 10-day interval of the tracer intruded from 122°E to 123°E shows that the intrusion flows downstream along the shelf edge or joins the Kuroshio in winter. On the other hand, the intrusion is divided into two paths in summer: northward flow along the small valley on the western ECS and a northeastward flow along the shelf edge. At the central part of the continental shelf edge (123～127°E), intrusion also takes place, but it does not affect the central ECS, and flows along the shelf break or is confined only to the shelf edge.

The total intruded volume transport through the 200 m isobath line was evaluated as 2.74 Sv in winter, 2.43 Sv in spring, 2.47 Sv in summer, and 2.84 Sv in autumn, while the intruded transport below 80 m was 1.32, 1.51, 1.64, and 1.54 Sv, respectively. The detailed tracer experiments shows that the Kuroshio water affecting the shelf area shallower than 80 m mainly originates east of Taiwan (122 ～ 123°E), especially through the lower layer below 80 m. The intrusion into the shelf region is pushed actively in spring and in summer though does not reach the shelf area in winter and flows down along the shelf break. In summer, a part of the intruded Kuroshio water with a volume transport of 0.19 Sv flows into the shelf area. The transport is approximately three times greater than the volume transport of 0.06 Sv in summer from the Changjiang River. This suggests that the intruded Kuroshio water can be a nutrient source in the shelf area in summer.

From the comparative studies in Exp. 2, several components that affect the intrusion from the

Kuroshio are investigated. Tide effect decreases the current velocity northeast of Taiwan and over the shelf, and the intrusion from the Kuroshio region is decreased in comparison to a case disregarding the tide effect. The transport from the Taiwan Strait has a significant effect on the intrusion of the Kuroshio. However, the transport mainly affects the upper layer (0 ~ 80 m) and the effect on the lower layer is relatively small. The transport of the Kuroshio also has an important role as the Kuroshio water intrudes into the ECS. In this study, the Kuroshio intrusion varied ~ 10% inflow difference between two cases: an increased Kuroshio transport and a decreased transport. The volume transport of the Kuroshio was set to increase or decrease with the same vertical gradient calculated from the density structure itself to discount the effect of the vertical structure variation when the Kuroshio transport is changed. The contribution of the variation of vertical density gradient will be studied in a future experiment.

The Kuroshio intrusion across the 200 m isobath line takes place all year round but the intrusion into the shelf area shallower than 80 m only starts in spring and ends in autumn. In spite of the larger intrusion volume transport across the 200 m isobath line in winter, the intruded Kuroshio water across the 200 m isobath line was not transported into the shelf area shallower than 80 m. On the other hand, it intruded into the shelf area through the lower layer in summer, even though the intruded total volume transport across the 200 m isobath line was decreased in comparison with that in winter. What is the mechanism of summer season intrusion into the shelf area? The answer to this question was obtained from the momentum balance analysis.

Analysis of components in the momentum equations indicated that the momentum balance along 122.58°E northeast of Taiwan, where the Kuroshio mainly intruded onto the shelf area of the ECS, was highly dominated by a geostrophic balance between the pressure gradient by surface elevation and the Coriolis terms. In addition, the vertical friction terms induced by the wind stress in the meridional direction at the surface and that by the tide effect near bottom, especially shallow area north of 28°N, also contributed the momentum balance considerably. The horizontal and vertical advection terms became significant near the shelf break where the Kuroshio turns to the east and some of it upwells onto the shelf.

After all, the characteristic intrusion from the Kuroshio to the shelf area of the ECS north of 28° N in summer was mainly forced by the dominant northeastward geostrophic current, i.e., the transport from the Taiwan Strait increasing in summer, balancing the pressure gradient force by surface elevation and the Coriolis force. Meanwhile, near bottom, northward transport in the bottom Ekman layer, formed by strong vertical friction, effectively allowed the Kuroshio-originated water to intrude onto the shelf area of the ECS through lower layer in summer. The intruded water would be upwelled by the several mechanisms such as bottom friction layer, bottom topography, encroachment of the Taiwan Warm Current, and density gradient by the Changjiang discharge (Hu, 1994; Zhu, 2003; Lü *et al.*, 2006) near the Chinese coast, or by horizontal divergence of the Changjiang Dilute Water (CDW) on the central ECS (Matsuno *et al.*, 2006). Thus, as suggested by Matsuno *et al.* (2006), it is expected that, due to the vertical process, the intruded Kuroshio water could contribute to increase the salinity of the CDW and also provide the nutrients into the euphotic zone resulting in biological production in the shelf region of the ECS.

By means of Exp. 3 which released the tracer at the inflow open boundaries simultaneously, residence time of the Yellow Sea water was estimated for both cases with and without consideration of tide effect. The results showed remarkable difference indicating that the numerical simulation without tide effect could greatly reduce the residence time in the Yellow Sea, making the circulation in the Yellow Sea too strong. In the case with consideration of tide, the residence time was 5.3 years and 4.7 years for inclusion and exclusion of the Bohai Sea, respectively. Meanwhile, in the case without consideration of tide, the results showed 2.6 years and 1.7 years, respectively. The results emphasized that the consideration of tide effect is indispensable to the numerical simulation in the Yellow and East China Seas.

The passive tracer experiments revealed that, all

the year round, the Kuroshio water intrudes onto the ECS shelf northeast of Taiwan deeper than 100 m; through both upper and lower layers in winter and through just lower layer in summer. Moreover, in spite of increasing volume transport from the Taiwan Strait in summer, transport of intrusion through the lower layer did not change greatly. The basic causes of the Kuroshio intrusion across 200 m isobath line are possibly due to the following reasons,

1. Difference of water depth between the Taiwan Strait and the northeast of Taiwan.

: The Taiwan Strait is generally shallower than 60 m, while a broad area deeper than 100 m is located at the northeast of Taiwan.

2. Density difference between the Taiwan Strait water and the Kuroshio subsurface water, and the seasonal variation of the volume transport from the Taiwan Strait.

: In winter, the Taiwan Strait water becomes dense by strong cooling, so that it may flow into the deeper area (over 100 m) northeast of Taiwan. However, the volume transport from the Taiwan Strait is reduced, so that the Taiwan Strait water can not occupy the northeast of Taiwan, and instead, the Kuroshio water intrudes onto the deeper area northeast of Taiwan. In summer, even though the transport from the Taiwan Strait is increased, its density become light due to inflow of the fresh South China Sea water and surface heating, so that the light Taiwan Strait water can not also occupy the deeper area of northeast of Taiwan.

Due to these reasons, the Kuroshio water occupies the lower layer northeast of Taiwan all the year round. Thus, when the current from the Taiwan Strait is increased in the summer season, the intruded Kuroshio water is forced to flow northward into the submerged river valley off Changjiang in the bottom Ekman layer. In this way, the cold, saline Kuroshio water forms the TWC deep water.

In this study, the intrusion pattern from the Kuroshio was confirmed by passive tracer experiments using a numerical model. The model only considered the local tide effect by simple parameterization which excludes the effect of the tidal residual current. In order to implement several cases, the model resolution was kept relatively low compared with previous studies, such as Guo *et al.* (2003, 2006) and Isobe and Beardsley (2006). However, this model has the advantage of simulating realistic motion on steep topography and the results have similar patterns to previous model studies and observations. In order to verify the model results, more observations at the lower layer of the shelf region of ECS are needed.

Acknowledgement

I would like to express my deepest gratitude to my supervisor, Prof. Takeshi Matsuno for his continuous advice and encouragement.

Great thanks go to the members of the committee, Prof. Tetsuo Yanagi, Prof. Naoki Hirose and Prof. Yuji Ohya for their helpful comments on this thesis.

I also wish to thank Professor Jong-Hwan Yoon in Research Institute for Applied Mechanics (RIAM), Kyushu University, for providing me with the 3-D ocean model, RIAMOM. Thanks are also due to Prof. Tomoharu Senjyu, Prof. Atsuhiko Isobe (Kyushu University, Japan), Prof. Ho-Jin Lee (Korea Maritime University, Korea), and Prof. Xinyu Guo (Ehime University, Japan) for their valuable comments on this study.

My appreciation also goes to my fellow Ph.D. students and previous researchers in RIAM who shared a lot of time with me.

Special thanks are due to Drs. Kosei Komatsu, Manabu Shimizu, Hideki Akiyama and Kuniaki Miyaji in Fisheries Research Agency (FRA) for giving me a chance to work and extend my knowledge. My thanks go to everyone else in the group for their careful concern and encouragement.

Finally, I am deeply grateful to my family.

References

An H.-S., 1977: A numerical experiment of the M2 tide in the Yellow Sea. *J. Oceanogr. Soc. Jpn.*, **33**, 103-110.

Baines B. G., 1982: On internal tide generation models. *Deep-Sea Res.*, **29**, 307-338.

Barnier B., Siefridt L., and Marchesiello P., 1995: Thermal forcing for a global ocean circulation

model using a three-year climatology of ECMWF analyses. *J. Mar. Sys.*, **6**, 363-380.

Beardsley R. C., Limeburner R., Yu H. and Cannon G. A., 1985: Discharge of the Changjiang (Yangtze River) into the East China Sea. *Cont. Shelf Res.*, **4**, 57-76.

Boyer T. P., Stephens C., Antonov J. I., Conkright M. E., Locarnini R. A., O'Brien T. D., and Garcia H. E., 2002: *World Ocean Atlas 2001*, vol. 2, *Salinity, Tech. Rep., Atlas NESDIS*, **50**, 165 pp., Natl. Oceanic and Atmos. Admin., Washington, D.C.

Chang K.-I., Suk M.-S., Pang I.-C., and Teague W.J., 2000: Observations of the Cheju Current. *J. Korean Soc. Oceanogr.*, **35**, 129-152.

Chang P.-H. and Isobe A., 2003: A numerical study on the Changjiang Diluted Water in the East and Yellow China seas, *J. Geophys. Res.*, **108**, No. C9, 3299, doi:10.1029/2002JC001749.

Chang P.-H. and Isobe A., 2005: Interannual variation of freshwater in the Yellow and East China Seas: Roles of the Changjiang discharge and wind forcing. *J. Oceanogr.*, **61**, 817-834.

Chao S.-Y., 1990: Circulation of the East China Sea, a numerical study. *J. Oceanogr. Soc. Japan*, **46**, 273-295.

Chen C., Beardsley R. C., Limeburner R., and Kim K., 1994: Comparison of winter and summer hydrographic observations in the Yellow and East China Seas and adjacent Kuroshio during 1986. *Cont. Shelf Res.*, **14**, 909-929.

Chen C.-T. A., 1996: The Kuroshio intermediate water is the major source of nutrients on the East China Sea continental shelf, *Oceangol. Acta*, **19**, 523-527

Chen C.-T. A., 2005: Tracing tropical and intermediate waters from the South China Sea to the Okinawa Trough and beyond, *J. Geophys. Res.*, **110**, No. C5, C05012, doi:10.1029/2004JC002494.

Chen C.-T. A., Ruo R., Pai S. C., Liu C. T., and Wong G. T. F., 1995: Exchange of water masses between the East China Sea and the Kuroshio off northeastern Taiwan. *Cont. Shelf Res.*, **15**, 19-39.

Chen C.-T. A. and Huang M.-H., 1996: A mid-depth front separation the South China Sea water and the West Philippine Sea water. *J. Oceanogr.*, **52**, 17-25

Chen C.-T. A. and Wang S.-L., 1998: Influence of intermediate water in the western Okinawa Trough by the outflow from the South China Sea, *J. Geophys. Res.*, **103**, No. C6, 12,683-12,688.

Chen C.-T. A. and Wang S.-L., 1999: Carbon, alkalinity and nutrient budgets on the East China Sea continental shelf. *J. Geophys. Res.*, **104**, No. C9, 20675-20686.

Chen C.-T. A. and Sheu D. D., 2006: Does the Taiwan Warm Current originate in the Taiwan Strait in wintertime?, *J. Geophys. Res.*, **111**, C04005, doi:10.1029/2005JC003281.

Chen X., 2004: Analysis of the circulation on the East-Chinese Shelf and the adjacent Pacific Ocean. PhD. Thesis, Hamburg University

Chen X., Qiao F., Ge R., Xia C., and Yuan Y., 2006: Development of subsurface warm water in the East China Sea in fall, *J. Geophys. Res.*, **111**, C11S10, doi:10.1029/2005JC003163.

Chern C.-S. and Wang J., 1990: On the Kuroshio branch current north of Taiwan. *Acta Oceanogr. Taiwan.*, **25**, 55-64.

Chern C.-S., Wang J., and Wang D.-P., 1990: The exchange of Kuroshio and East China Sea shelf water. *J. Geophys. Res.*, **95**, 16017-16023.

Chern C.-S. and Wang J., 1992: The influence of Taiwan Strait waters on the circulation of the southern East China Sea. *La Mer*, **30**, 223-228.

Choi B.-H., 1980: A tidal model of the Yellow Sea and the Eastern China Sea. *KORDI Rep.* 80-02, 72 pp., Korea Ocean Res. and Dev. Inst. Seoul

Choi B.-H., 1990: Development of fine-grid numerical tidal models of the Yellow Sea and the East China Sea. *J. Korean Soc. Coast. Ocean Eng.*, **2 (4)**, 231-234.

Chuang W.-S., 1985: Dynamics of subtidal flow in the Taiwan Strait. *J. Oceanogr. Soc. Japan*, **41**, 65-72.

Chuang W.-S., 1986: A note on the driving mechanisms of current in the Taiwan Strait. *J. Oceanogr. Soc. Japan*, **42**, 355-361.

Chuang W. S. and Liang W. D., 1994: Seasonal variability of intrusion of the Kuroshio water across the continental shelf northeast of Taiwan, *J. Oceanogr*, **50**, 531-542.

Fan K.-L., 1980: On upwelling off northeastern shore of Taiwan. *Acta Oceanogr. Taiwan.*, **11**, 105-117.

Fang G., Zhao B., and Zhu Y., 1991: Water volume

transport through the Taiwan Strait and the continental shelf of the East China Sea measured with current meters, in *Oceanography of Asian Marginal Seas*, edited by K. Takano, 345-358.

Gong G.-C., Liu K.-K., and Pai S.-C., 1995: Prediction of nitrate concentration from two end member mixing in the southern East China Sea. *Cont. Shelf Res.*, **15**, 827-842.

Grist J. P. and Josey S. A., 2003: Inverse analysis adjustment of the SOC air-sea flux climatology using ocean heat transport constraints, *Journal of Climate*, **16**, No. 20, 3274-3295.

Guan B. X., 1994: Patterns and structures of the currents in Bohai, Huanghai and East China Seas, In *Oceanology of China Seas, Volume 1*, ed. by D. Zhou *et al.*, Kluwer Academic Publishers, 17-26.

Guo X. and Yanagi T., 1998: Three dimensional structure of tidal current in the East China Sea and the Yellow Sea. *J. Oceanogr.*, **54**, 651-668.

Guo X., Hukuda H., Miyazawa Y., and Yamagata T., 2003: A triply nested ocean model for simulating the Kuroshio-Roles of horizontal resolution on JEBAR. *J. Phys. Oceanogr.*, **33**, 146-169.

Guo X., Miyazawa Y., and Yamagata T., 2006: The Kuroshio onshore intrusion along the shelf break of the East China Sea: the origin of the Tsushima Warm Current. *J. Phys. Oceanogr.*, **36**, 2205-2231.

Han I. S., Kamio K., Matsuno T., Manda A., and Isobe A., 2001: High frequency current fluctuations and cross-shelf flows around the pycnocline near the shelf break in the East China Sea. *J. Oceanogr.*, **57**, 235-249.

Hirose N., Fukumori I., Kim C. H., and Yoon J.-H., 2005: Numerical simulation and satellite altimeter data assimilation of the Japan Sea circulation, *Deep-Sea Res. II*, **52**, 1443-1463.

Hsu M.-K., Liu A. K., and Liu C., 2000: A study of internal waves in the China Seas and Yellow Sea using SAR. *Cont. Shelf Res.*, **20**, 389-410.

Hsueh Y., Wang J., and Chern C. S., 1992: The intrusion of the Kuroshio by the continental shelf northeast of Taiwan. *J. Geophys. Res.*, **97**, 14323-14330.

Hsueh Y., Lie H.-J., and Ichikawa H., 1996: On the branching of the Kuroshio west of Kyushu. *J. Geophys. Res.*, **101**, 3851-3857.

Hu D. X., 1994: Some striking features of circulation in Huanghai Sea and East China Sea, In *Oceanology of China Seas, Volume 1*, ed. by D. Zhou *et al.*, Kluwer Academic Publishers, 27-38.

Hu J., Kawamura H., Hong H., and Qi Y., 2000: A Review on the Currents in the South China Sea: Seasonal Circulation, South China Sea Warm Current and Kuroshio Intrusion. *J. Oceanogr.*, **56**, 607-624

Huang Q. Z., Wang W. Z., Li Y. S., and Li C. W., 1994: Current characteristics of the South China Sea, In *Oceanology of China Seas, Volume 1*, ed. by D. Zhou *et al.*, Kluwer Academic Publishers, 113-122.

Huh O. K., 1982: Spring season flow of the Tsushima Current and its separation from the Kuroshio: Satellite evidence. *J. Geophys. Res.*, **87**, 9687-9693.

Hunter J. R., 1975: A note on quadratic friction in the presence of tides. *Estuar. Coast. Mar. Sci.*, **3**, 473-475.

Hur H. B., Jacobs G. A., and Teague W. J., 1999: Monthly water mass analyses in the Yellow and East China Seas. *J. Oceanogr.*, **55**, 171-184.

Ichikawa H. and Beardsley R. C., 1993: Temporal and spatial variability of volume transport of the Kuroshio in the East China Sea. *Deep-Sea Res.*, **40**, 583-605.

Inoue N., 1975: Bottom current on the continental shelf of the East China Sea. *Mar. Sci. Mon.*, **7**, 12-18 (in Japanese with English abstract).

Ishizaki H. and Motoi T., 1999: Reevaluation of the Takano-Oonishi scheme for momentum advection of bottom relief in ocean models. *J. of Atmos. and ocean. Tech.*, **16**, 1994-2010.

Isobe A., 1999a: On the origin of the Tsushima Warm Current and its seasonality. *Cont. Shelf Res.*, **19**, 117-133.

Isobe A., 1999b: The Taiwan-Tsushima Warm Current System: Its path and the transformation of the water mass in the East China Sea. *J. Oceanogr.*, **55**, 185-195.

Isobe A., Fujiwara E., Chang P.-H., Sugimatsu K., Shimizu M., Matsuno T., and Manda A., 2004: Intrusion of less saline shelf water into the

Kuroshio subsurface layer in the East China Sea. *J. Oceanogr.*, **60**, 853-863.

Isobe A. and Beardsley R. C., 2006: An estimate of the cross-frontal transport at the shelf break of the East China Sea with the Finite Volume Coastal Ocean Model. *J. Geophys. Res.*, **111**, C03012, doi:10.1029/2005JC003290

Ito T., Kaneko A., Tsubota H. and Gohda N., 1994: The characteristic distribution of silica over the East China Sea shelf slope. *J. Oceanogr.*, **50**, 465-477.

Jacobs G. A., Hur H. B., and Riedlinger S. K., 2000: Yellow and East China Seas response to winds and currents, *J. Geophys. Res.*, **105**, 21,947-21,968.

James I.D., 1977: A model of the annual cycle of temperature in the frontal region of the Celtic Sea. *Estuar. Coast. Mar. Sci.*, **5**, 339-353.

James I.D., 1978: A note on the circulation induced by a shallow-sea front. *Estuar. Coast. Mar. Sci.*, **7**, 197-202.

James C., Winbush M., and Ichikawa H., 1999: Kuroshio meanders in the East China Sea. *J. Phys. Oceanogr.*, **29**, 259-272.

Jan S., Sheu D. D., and Kuo H.-M., 2006: Water mass and throughflow transport variability in the Taiwan Strait, *J. Geophys. Res.*, **111**, C12012, doi:10.1029 /2006JC003656.

Kang S. K., Lee S. R., Yum K. D., and Jung K. T., 1991: Tidal computation of the East China Sea, the Yellow Sea and the East Sea. in *Oceanography of Asian Marginal Seas*, edited by K. Takano, Ed., 25-48.

Kang S. K., Foreman M. G. G., Lie H., Lee J., Cherniawsky J., and Yum K., 2002: Two-layer tidal modeling of the Yellow and East China Seas with application to seasonal variability of the M_2 tide, *J. Geophys. Res.*, **107**, No. C3, doi:10. 1029/2001JC000838.

Katoh O., Teshima K., Kubota K. and Tsukiyama K., 1996a: Downstream transition of the Tsushima Current west of Kyushu in summer. *J. Oceanogr.*, **52**, 93-108.

Katoh O., Teshima K., Abe O., Fujita H., Miyaji K., Morinaga K., and Nakagawa N., 1996b: Process of the Tsushima Current formation revealed by ADCP measurements in summer. *J. Oceanogr.*, **52**, 491-507.

Katoh O., Morinaga K., and Nakagawa N., 2000: Current distributions in the southern East China Sea in summer. *J. Geophys. Res.*, **105**, No. C4, 8565-8573.

Kuroda Y. and Mitsudera H., 1995: Observation of internal tides in the East China Sea with an Underwater Sliding Vehicle. *J. Geophys. Res.*, **100**, 10801-10816.

Large W. G. and Pond S., 1981: Open ocean momentum flux measurement in moderate to strong winds. *J. Phys. Oceanogr.*, **11**, 324-336.

Larsen L. H., Cannon G. A., and Choi B. H., 1985: East China Sea tide currents. *Cont. Shelf Res.*, **4**, 77-103.

Lee H. J., Jung K. T., Foreman M. G. G., and Chung J. Y., 2000: A three-dimensional mixed finite-difference Galerkin function model for the oceanic circulation in the Yellow and the East China Sea. *Cont. Shelf Res.*, **20**, 863-895.

Lee H. J., Yoon J. H., Kawamura H., and Kang H. W., 2003: Comparison of RIAMOM and MOM in modelling the East Sea/Japan Sea circulation, *Ocean Polar Res.*, **25**, 287-302.

Lee H.-C., Rosati A. and Spelman M. J., 2006: Barotropic tidal mixing effects in a coupled climate model: Oceanic conditions in the Northern Atlantic. *Ocean Modell.*, **11**, 464-477.

Lee J. H., Lozovatsky I., Jang S.-T., Jang C. J., Hong C. S., and Fernando H. J. S., 2006: Episodes of nonlinear internal waves in the northern East China Sea, *Geophys. Res. Lett.*, **33**, L18601, doi: 10.1029/2006GL027136.

Lee S.-H. and Beardsley R. C., 1999: Influence of stratification on residual tidal currents in the Yellow Sea. *J. Geophys. Res.*, **104**, 156679-156701.

Lee T. N., Johns W. E., Liu C.-T., Zhang D., Zantopp R., and Yang Y., 2001: Mean transport and seasonal cycle of the Kuroshio east of Taiwan with comparison to the Florida Current. *J. Geophys. Res.*, 106, No. C10, 22143-22158.

Liang W. D., Tang T. Y., Yang Y. J., Ko M. T., and Chuang W. S., 2003: Upper-ocean currents around Taiwan. *Deep Sea Res. II*, **50**, 1085-1105.

Lie H.-J. and Cho C.-H., 1994: On the origin of the Tsushima Warm Current. *J. Geophys. Res.*, **99**, 25081-25091.

Lie H.-J., Cho C.-H., Lee J.-H., Niller P., and Hu J.-H., 1998: Separation of the Kuroshio water and its penetration onto the continental shelf west of Kyushu. *J. Geophys. Res.*, **103**, No. C2, 2963-2976.

Lie H.-J., Cho C.-H., Lee J.-H., Lee S., Tang Y., and Zou E., 2001: Does the Yellow Sea Warm Current really exist as a persistent mean flow?, *J. Geophys. Res.*, **106**, No. C10, 22,199-22,210.

Lie H.-J., Cho C.-H., Lee J.-H., and Lee S., 2003: Structure and eastward extension of the Changjiang River plume in the East China Sea, *J. Geophys. Res.*, **108**, No. C3, 3077, doi:10.1029/2001 JC001194.

Lin C.-Y., Shyu C.-Z., and Shih W.-H., 1992: The Kuroshio fronts and cold eddies off northeastern Taiwan observed by NOAA-AVHRR imageries. *Terr. Atmos. Oceanic Sci.*, **3**, 225-242.

Liu A. K., Chang Y. S., Hsu M.-K., and Liang N. K., 1998: Evolution of nonlinear internal waves in the East and South China Seas, *J. Geophys. Res.*,**103**, 7995-8008.

Liu K.-K., Gong G.-C., Shyu C.-Z., Pai S.-C., Wei C.-L., and Chao S.-Y., 1992a: Response of Kuroshio upwelling to the onset of the northeast monsoon in the sea north of Taiwan: Observations and a numerical simulation. *J. Geophy. Res.*, **97**, No. C8, 12511-12526.

Liu K. K., Gong G. C., Lin S., Shyu C. Z., Yang C. Y., Wei C. L., Pai S. C., and Wu C. K., 1992b: The year-round upwelling at the shelf break near the northern tip of Taiwan as evidenced by chemical hydrography, *Terr. Atmos. Oceanic Sci.*, **3**, 234- 276.

Liu K.-K., Tang T.-Y., Gong G.-C., Chen L.-Y., and Shiah F.-K., 2000: Cross-shelf and along-shelf nutrient fluxes derived from flow fields and chemical hydrography observed in the southern East China Sea off northern Taiwan. *Cont. Shelf Res.*, **20**, 493-523.

Lü X., Qiao F., Xia C., Zhu J., and Yuan Y., 2006: Upwelling off Yangtze River estuary in summer. *J. Geophys. Res.*, **111**, C11S08, doi:10.1029/2005JC 003250.

Mao H. L., Ren Y. W. and Wan K. M., 1964: A preliminary investigation on the application of using *T-S* diagrams for the quantitative analysis of the water masses in the shallow water area, *Oceanologia et Limnologia Sinica*, **6**, 1-22

Matsumoto K., Takanezawa T., and Ooe M., 2000: Ocean tide models developed by assimilating TOPEX/POSEIDON altimeter data into hydrodynamical model: a global model and a regional model around Japan. *J. Oceanogr.*, **56**, 567-581.

Matsuno T., Hibiya T., Kanari S., and Kobayashi C., 1997: Small scale internal waves and turbulent fluctuations near the continental shelf break in the East China Sea. *J. Oceanogr.*, **53**, 259-269.

Matsuno T, Shimizu M., Morii Y., Nishida H., and Takaki Y., 2005: Measurements of the Turbulent Energy Dissipation Rate around the Shelf Break in the East China Sea. *J. Oceanogr.*, **61**, 1029-1037.

Matsuno T., Lee J.-S., Shimizu M., Kim S.-H., and Pang I.-C., 2006: Measurements of the turbulent energy dissipation rate ε and an evaluation of the dispersion process of the Changjiang Diluted Water in the East China Sea. *J. Geophys. Res.*, **111**, C11S09, doi:10.1029/2005JC003196.

Mellor G. L., 1991: An equation of state for numerical models of oceans and estuaries. *J. Atmos. Oceanic Technol.*, **8**, 609-611.

Mertz G. and Wright D. G., 1992: Interpretations of the JEBAR Term. *J. Phys. Oceanogr.*, **22**, 301-305.

Munk W. H. and Anderson E. R., 1948: Notes on a theory of the thermocline. *J. Mar. Res.*, **7**, No. 3, 276-295.

Na J. Y. and Seo J. W., 1998: The sea surface winds and heat fluxes in the East Asian marginal seas (a booklet for the data contained in the CD-ROM, pp. 53).

Nitani H., 1972: Beginning of the Kuroshio, In *Kuroshio, Its Physical Aspects*, ed. by H. Stommel and K. Yoshida, Univ. Tokyo Press, Tokyo, 129-163.

Noh Y., Jang C. J., Yamakata T., Chu P. C., and Kim C.-H., 2002: Simulation of more realistic upper-ocean processes from an OGCM with a new ocean mixed layer model. *J. Phys. Oceanogr.*, **32**, 1284-1307.

Nozaki Y., Tsubota H. and Kasemsupaya V., 1991: Residence time of surface water and particule reactive 210Pb and 210Po in the East China and

Yellow Seas. *Geochim. Cosmochim. Acta*, **55**, 1265-1272.

Oka E. and Kawabe M., 1998: Characteristics of variations of water properties and density structure around the Kuroshio in the East China Sea. *J. Oceanogr.*, **54**, 605-617.

Pang I.-C., Hong C.-S., Chang K.-I., Lee J.-C., and Kim J.-T., 2003: Monthly variation of water mass distribution and current in the Cheju Strait. *J. Korean Soc. Oceanogr.*, **38**, 87-100.

Pohlmann T., 1999: Discussion of the JBAR term — Derivation, Interpretation and Application to the Northeastern Atlantic Shelf. *Report of European Communities*.

Qiu B. and Imasato N., 1990: A numerical study on the formation of the Kuroshio Counter Current and the Kuroshio Branch Current in the east China Sea. *Cont. Shelf Res.*, **10**, 165-184.

Sarkisyan A. S. and Ivanov V. F., 1971: The combined effect of baroclinicity and bottom relief as an important factor in the dynamics of ocean currents (AGU translation). *Izv. Acad. Sci. USSR, Atmos. Oceanic Phys.*, 173-188.

Seung Y. H., 1999: A geostrophic adjustment model of shelfward intrusion of oceanic upper water across a depth discontinuity: implication to the Kuroshio region. *Cont. Shelf Res.*, **19**, 247-269.

Shaw P. T. and Chao S. Y., 1994: Surface circulation in the South China Sea. *Deep Sea Res., I*, **41**, 1663-1683.

Stephens C., Antonov J. I., Boyer T. P., Conkright M. E., Locarnini R. A., O'Brien T. D., and Garcia H. E., 2002: *World Ocean Atlas 2001*, vol. 1, *Temperature, Tech. Rep., Atlas NESDIS*, **49**, 167 pp., Natl. Ocean and Atmos. Admin., Washington, D.C.

Su J.-L., Pan Y.-Q., and Liang X.-S., 1994: Kuroshio intrusion and Taiwan warm current, In *Oceanology of China Seas, Volume 1*, ed. by D. Zhou *et al.*, Kluwer Academic Publishers, 59-70.

Su Y. S. and Weng X. C., 1994: Water masses in China Seas, In *Oceanology of China Seas, Volume 1*, ed. by D. Zhou *et al.*, Kluwer Academic Publishers, 3-16.

Sugimoto Y., Kimura S., and Miyaji K., 1988: Meander of the Kuroshio front and current variability in the East China Sea. *J. Oceanogr. Soc. Japan*, **44**, 125-135.

Takikawa T. and Yoon J.-H., 2005: Volume transport through the Tsushima Straits estimated from sea level difference. *J. Oceanogr.*, **61**, 699-708.

Tang T. Y. and Yang Y. J., 1993: Low frequency current variability on the shelf break northeast of Taiwan. *J. Oceanogr.*, **49**, 193-210.

Tang T. Y., Hsueh Y., Yang Y. J., and Ma J. C., 1999: Continental slope flow northeast of Taiwan. *J. Phys. Oceanogr.*, **29**, 1353-1362.

Tang T. Y., Tai J. H., and Yang Y. J., 2000: The flow pattern north of Taiwan and the migration of the Kuroshio. *Cont. Shelf Res.*, **20**, 349-371.

Teague W. J., Jacobs G. A., Ko D. S., Tang T. Y., Chang K. I., and Suk M. S., 2003: Connectivity of the Taiwan, Cheju, and Korea Straits. *Cont. Shelf Res.*, **23**, 63-77.

Uda M., 1934: Hydrographical researches on the normal monthly conditions in the Japan Sea, the Yellow Sea, and the Okhotsk Sea. *J. Imp. Fish. Exp. Sta.*, **5**, 191-236 (in Japanese).

Wang Y. H., Jan S., and Wang D. P., 2003: Transports and tidal current estimates in the Taiwan Strait from the shipboard ADCP observations (1999-2001). *Estuarine, Coastal and Shelf Sci.*, **57**, 193-199.

Webb D. J., Cuevas B. A., and Richmond C. S., 1998: Improved advection schemes for ocean models. *J. of Atmos. and Ocean. Tech.*, **15**, 1171-1187.

Wyrtki K., 1961: Physical oceanography of the southeast Asia waters. Scientific results of marine investigations of the South China Sea and Gulf of Thailand. 1959-1961. Naga Report, 2, 195 pp.

Yanagi T., Morimoto A. and Ichikawa K., 1997: Co-tidal and co-range charts for the East China Sea and the Yellow Sea derived from satellite altimetric data. *J. Oceanogr.*, **53**, 303-310.

Yanagi T., Shimizu T., and Lie H.-J., 1998: Detailed structure of the Kuroshio frontal eddy along the shelf edge of the East China Sea. *Cont. Shelf Res.*, **18**, 1039-1056.

You S.-H. and Yoon J.-H., 2004: Modeling of the Ryukyu Current along the Pacific side of the Ryukyu Islands. *Pacific Oceanology*, **2**, 44-51.

Zhu J., 2003: Dynamic mechanism of the upwelling on the west side of the submerged river valley

off the Yangtze mouth in summertime. *Chin. Sci. Bull.*, **48**, 2754-2758.

Zhu J., Chen C., Ding P., Li C., and Lin H., 2004: Does the Taiwan warm current exist in winter?, *Geophys. Res. Lett.*, **31**, L12302, doi:10.1029/2004 GL019997.

Zhu J., Ding P., Hu S., and Yang L., 2001: Observation of the Changjiang diluted water, plume front and upwelling off the Changjiang mouth during August 2000. In *Proceedings of the 11th PAMS/JECSS Workshop*, Cheju, Korea.